

CU-CSSC-90-27

CENTER FOR SPACE STRUCTURES AND CONTROLS

10/21/90
P. 217

A COMPUTATIONAL PROCEDURE FOR THE DYNAMICS OF FLEXIBLE BEAMS WITHIN MULTIBODY SYSTEMS

by

Janice Diane Downer

(NASA-CR-187667) A COMPUTATIONAL PROCEDURE
FOR THE DYNAMICS OF FLEXIBLE BEAMS WITHIN
MULTIBODY SYSTEMS Ph.D. Thesis Final
Technical Report (Colorado Univ.) 217 p

N91-13760

Unclass
CSCL 20K 63/39 0319218

November 1990

COLLEGE OF ENGINEERING
UNIVERSITY OF COLORADO
CAMPUS BOX 429
BOULDER, COLORADO 80309

A COMPUTATIONAL PROCEDURE FOR
THE DYNAMICS OF FLEXIBLE BEAMS
WITHIN MULTIBODY SYSTEMS

by

JANICE DIANE DOWNER

B. S., University of Michigan, 1982

M. S., University of Colorado, 1985

A dissertation submitted to the
Faculty of the Graduate School of the
University of Colorado in partial fulfillment
of the requirement for the degree of
Doctor of Philosophy
Aerospace Engineering Sciences

1990

This dissertation for the Doctor of Philosophy degree by

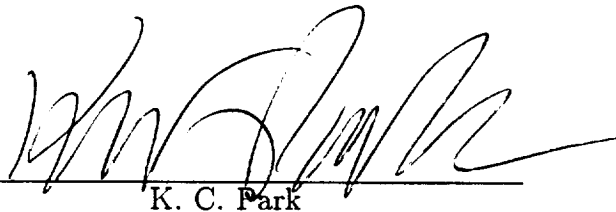
Janice Diane Downer

has been approved for the

Department of

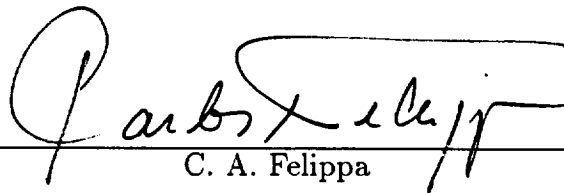
Aerospace Engineering Sciences

by



A handwritten signature in black ink, appearing to read 'K. C. Park', written over a horizontal line.

K. C. Park



A handwritten signature in black ink, appearing to read 'C. A. Felippa', written over a horizontal line.

C. A. Felippa

Date 11-13-90

Downer, Janice Diane (Ph.D., Aerospace Engineering Sciences)

A Computational Procedure for the Dynamics of Flexible

Beams within Multibody Systems

Dissertation directed by Professor K. C. Park

This dissertation is concerned with the dynamic analysis of three-dimensional elastic beams which experience large rotational and large deformational motions. To this end, the beam motion is modeled using an inertial reference for the translational displacements and a body-fixed reference for the rotational quantities. Finite strain rod theories are then defined in conjunction with the beam kinematic description which account for the effects of stretching, bending, torsion, and transverse shear deformations. A convected coordinate representation of the Cauchy stress tensor and a conjugate strain definition is introduced to model the beam deformation. Due to the inertial reference of the beam kinematics and the convected reference of the beam stresses, the present formulation is easily interfaced with general multibody dynamics methodologies as well as software modules for active control simulations.

The numerical treatment of the beam formulation is considered in detail. A procedure to compute the beam internal force is derived from the continuum formulation. The procedure is proven to be invariant to arbitrary rigid motions of the beam while accurately modeling the beam strain. To treat the beam dynamics, a two-stage modification of the central difference algorithm is presented to integrate the translational coordinates and the angular velocity vector. The angular orientation is then obtained from the application of an implicit integration algorithm to the Euler param-

ter/angular velocity kinematical relation. The combined developments of the objective internal force computation with the dynamic solution procedures result in the computational preservation of total energy for undamped systems.

The present methodology is also extended to model the dynamics of deployment/retrieval of the flexible members. A moving spatial grid corresponding to the configuration of a deployed rigid beam is employed as a reference for the dynamic variables. A transient integration scheme which accurately accounts for the deforming spatial grid is derived from a space-time finite element discretization of a Hamiltonian variational statement. The computational results of this general deforming finite element beam formulation are compared to reported results for a planar inverse-spaghetti problem.

To my parents for their love and support.

“ BREAK A LEG !! ”

ACKNOWLEDGEMENTS

With sincere pleasure, I acknowledge the contributions of my advisor Professor K. C. Park. His keen interest and enthusiasm toward the research effort as well as his outstanding technical support enabled the author to complete this work. I am indebted to Professor Park for making possible this opportunity to experience and explore exciting technical horizons.

In addition, I acknowledge the support and guidance of the additional members of my thesis committee: Professor Carlos Felippa, Professor Charbel Farhat, Professor Kaspar Willam, Adjoint Professor Jerry Housner serving as the NASA technical supervisor, and Adjoint Professor Eric Schmitz. I gratefully acknowledge the interest and financial support of the NASA Graduate Students Research Program through grant number NGT-50254. Additional support of the NASA/Langley Research Center through grant NAG-1-756 and the Air Force Office of Scientific Research through grant F49620-87-C-0074 is also acknowledged.

I wish to thank Dr. Felippa, Dr. Farhat, and the many other colleagues within the Center for Space Structures and Control for their efforts in making the center a stimulating and enjoyable research environment. Finally, I acknowledge the support of the friends and fellow sports fans in Boulder, especially E.J.R., who stood by me rooting through all the extra innings.

CONTENTS

CHAPTER

I.	INTRODUCTION	1
II.	FLEXIBLE BEAM DYNAMICS FORMULATION	10
2.1	Introduction	10
2.2	Large Rotation Beam Kinematics	13
2.3	Nonlinear Equations of Motion	18
2.3.1	Inertia Operator	20
2.3.2	Internal Force Operator	21
2.3.3	External Force and Traction Operator	28
2.4	Constitutive Equations	28
2.5	Consistent Linearization	37
2.5.1	Tangent Mass	38
2.5.2	Tangent Stiffness	40
2.6	Concluding Remarks	44
III.	COMPUTATIONAL TREATMENT OF THE DISCRETE INTERNAL FORCE	45
3.1	Introduction	45
3.2	Finite Rotation Representations	49
3.3	Finite Element Discretization	56
3.3.1	Discrete Equations of Motion	58
3.3.2	Discrete Rotation Matrix Computations	61
3.3.3	Discrete Curvature Computation	63
3.4	Incremental Strain Computations	67
3.4.1	Membrane Strain Increments	70

3.4.2	Transverse Shear and Curvature Strain Increments	...	74
3.5	Static Solutions	77
3.5.1	Discrete Tangent Stiffness Matrices	78
3.5.2	Example Problems	82
3.6	Concluding Remarks	90
IV.	MULTIBODY DYNAMICS SOLUTION PROCEDURES	89
4.1	Introduction	91
4.2	Multibody System Equations	95
4.3	Integration of Generalized Coordinates	98
4.3.1	Implicit Integration Techniques	100
4.3.2	Explicit Integration Techniques	104
4.3.2.1	Standard Central Difference Implementation	105
4.3.2.2	Modified Central Difference Implementation	110
4.4	Rotational Orientation Update Procedure	112
4.5	Constraint Force Solution Procedure	116
4.6	Numerical Examples	118
4.7	Concluding Remarks	123
V.	DEPLOYMENT DYNAMICS OF BEAM STRUCTURES	149
5.1	Introduction	149
5.2	Deployment Kinematics	153
5.3	Hamiltonian Equations of Motion	160
5.4	Space-Time Discretization	164
5.4.1	Discrete Equations of Motion	165
5.4.2	Consistency Analysis	169
5.4.3	Nonlinear Solution Strategy	173

5.5 Results	178
5.6 Concluding Remarks	181
VI. CONCLUSIONS	182
6.1 Summary of Work	182
6.2 Directions for Further Research	185
REFERENCES	188
APPENDIX A	200
APPENDIX B	203

Tables

Table

3.1	Comparison of results for the cantilever subjected to an end moment	88
3.2	Comparison of results for the cantilever 45-degree bend	89

Figures

Figure

2.1	Spatial beam kinematics: floating frame approach	14
2.2	Spatial beam kinematics: nonlinear continuum approach	17
2.3	Spatial beam kinematics: convected reference frame	22
3.1	Euler-Chasles rotation representation	50
3.2	Convected reference frame	62
3.3	Pure bending of beam element	65
3.4a	Cantilever beam subjected to end moment: problem data	84
3.4b	Cantilever beam subjected to end moment: deformed shapes	85
3.5a	Cantilever 45-degree bend subjected to end load: problem data	86
3.5b	Cantilever 45-degree bend subjected to end load: deformed shapes	87
4.1a	Spin-up maneuver: problem data	124
4.1b	Spin-up maneuver: motion history, tip deflection history relative to floating reference	125
4.2a	Planar motion of pinned beam (1): problem data	126
4.2b	Planar motion of pinned beam (1): motion history, energy history	127
4.2c	Planar motion of pinned beam (2): problem data	128
4.2d	Planar motion of pinned beam (2): motion history, energy history	129
4.3a	Closed-loop chain in free flight: problem data	130

4.3b	Closed-loop chain in free flight: motion history, close-up deformations	131
4.4a	Spatial motion of pinned beam (1): problem data	132
4.4b	Spatial motion of pinned beam (1): motion history	133
4.4c	Spatial motion of pinned beam (1): motion history	134
4.4d	Spatial motion of pinned beam (2): problem data	135
4.4e	Spatial motion of pinned beam (2): motion history	136
4.4f	Spatial motion of pinned beam (2): motion history	137
4.4g	Spatial motion of pinned beam: energy history (1)	138
4.4h	Spatial motion of pinned beam: energy history (2)	139
4.5a	Spatial motion of double pendulum: problem data	140
4.5b	Spatial motion of double pendulum: projected trajectories	141
4.5c	Spatial motion of pinned beam: energy history (1)	142
4.5d	Spatial motion of pinned beam: energy history (2)	143
4.5e	Spatial motion of pinned beam: energy history (3)	144
4.5f	Spatial motion of pinned beam: energy history (4)	145
4.6a	Spatial motion of double pendulum: problem data	146
4.6b	Spatial motion of double pendulum: motion history	147
4.6c	Spatial motion of double pendulum: energy history	148
5.1	Axial deployment subject to gravity	154
5.2	Fixed vs. variable grid approaches	155
5.3	Deployment kinematics	156
5.4	Dispersion relations	173
5.5	Extrapolation of displacement coordinates	176
5.6	End orbits for various deployment speeds (V)	179
5.7	Motion history for various deployment speeds (V)	180

CHAPTER I

INTRODUCTION

The simulation of flexible multibody systems is becoming an increasingly important tool for the design and operation of many engineering applications. The interest in modeling the dynamics of multibody systems has emerged in the distinct fields of space dynamics, mechanisms, and robotics. Typical examples of these systems include elastic linkages, high precision machine dynamics and robot manipulator arms, aircraft propellers, helicopter or turbine rotor blades, and flexible satellites and other types of deployable space structures. The articulated structures are thus comprised of flexible components which undergo large relative displacements and rotations in order to carry out the intended operations. To perform the desired kinematic motions, various types of mechanical joints are introduced to constrain the relative motion between the various components.

New technology needs of both the space and robotics industries have increased the demand for accurate numerical simulations of the performance of multibody systems. The design trend of newly developed mechanisms is toward the use of very lightweight structural components. Likewise, equipment performance requirements are being emphasized which dictate the high speed operation and a greater positioning accuracy of these highly flexible components. Under these circumstances, a significant coupling can be experienced between the gross rigid body motion and the elastic vibrations of the mechanism. To accurately simulate this phenomenon and study the effect of component flexibility on the overall system performance, a realistic

mathematical model of the flexible components that can readily be incorporated into a general multibody dynamics methodology is necessary. To this end, this dissertation addresses the computational analysis of the dynamics of a flexible beam undergoing arbitrary spatial motions and experiencing large elastic deformations.

The development of accurate methods to model the geometric nonlinearities of structural components has been the subject of numerous investigations. One approach considers the small elastic deformations of components which undergo large overall rigid body motions. The two effects are modeled separately by introducing a *floating reference frame* which follows some overall mean rigid body motion of the beam; the elastic deformation of the beam is then described relative to this moving reference frame [1-13]. In this manner, computer codes for analysis of multi-rigid body systems were extended to include structural flexibility by superposing existing linear deformation descriptions onto the rigid motions of the floating reference frame [11-13].

The resulting equations of motion of the above approach are in terms of a set of reference coordinates representing the motion of the floating reference frame and a set of relative elastic coordinates representing the deformation. For structures consisting of a rigid main body to which flexible appendages are attached, the floating reference frame coincides with the rotation of the main body [1-2]. For arbitrary configurations in which the choice is not obvious, the floating reference frame is constructed to follow some mean rigid motion of the flexible body such that the relative deformation is minimized [3-6]. To determine this frame, constraint conditions must be introduced to offset the additional unknown variables of the mov-

ing reference; these constraints can be satisfied through a proper choice of deformation modes [3-4]. The construction of this mean axis system and the appropriate deformation modes has been presented within the context of general finite element structural representations [7]. For multibody dynamics applications, the research effort has been toward the construction of elastic coordinates which accurately represent the deformation of these joint-dominated constrained systems [8-11]. The proper selection of the floating reference frame and the consistent set of elastic coordinates is crucial to the success of this approach as the component can deform only as dictated by the selected modes. The accurate prediction of a proper representation remains a difficult challenge in the modeling of flexible multibody systems.

The initial floating frame approach is limited by an inherent assumption of linear deformation theory. However, the use of nonlinear theories becomes necessary when current space and robotics industry applications are considered due to the emphasis toward lightweight and highly flexible components. Another instance mandating the use of nonlinear deformation theories is the high speed rotation of a flexible component. In this case, the rotation gives rise to centrifugal forces which affects the bending stiffness in a manner not predicted by the linear deformation theories [14-15]. For these purposes, the initial approach was extended to model nonlinear effects by including nonlinear strain measures [16-17].

An alternative method based on *convected* coordinate systems has been developed to provide the capability of modeling large deformations within the context of overall rigid body motions. Instead of modeling the entire structural component with a *single* floating reference frame and an appropriate set of deformational coordinates, this method employs finite

element based deformational theories by introducing an element-attached convected reference frame [18-23]. The convected reference frame is defined to represent the overall rigid motion of the individual finite element. Standard finite element methodologies are then incorporated to describe the deformations with respect to the convected coordinate system. This method was employed to model large deformations of beam elements using updated or total Lagrangian formulations of large deformation continuum mechanics [24-27]. A similar concept, termed the element-independent corotational formulation, was introduced as a method for upgrading existing finite elements to allow for large rotations [28-29]. In this method, rigid body motions are extracted from the total element displacements prior to computing element deformations. Another approach partitioned the component into substructures such that linear elasticity theory referred to a local frame was adequate to capture nonlinear effects [30].

Recently, a different approach has been adopted to describe the dynamics of a flexible beam which departs from the use of floating or convected reference frames [31-36]. The approach introduces finite-deformation rod theories from the outset such that the effects of both finite rotation kinematics and large deformations are taken into account [37-43]. The beam kinematics are described with respect to the inertial reference frame such that the motion due to rigid rotations of the beam is not distinguished from that due to deformations. As such, the introduction of a moving frame as a reference for elastic deformations is unnecessary. The advantage to this is that a natural representation for dynamic systems results such that the beam inertia is identical in form to that of rigid body dynamics. In addition, large deformations are accurately represented as these formulations incorpo-

rate strain measures modeling the combined effects of stretching, transverse shear, torsion, and bending deformations. The resulting structure of the equations of motion is simpler due to the use of the inertial frame kinematic description as opposed to the floating frame or convected frame descriptions. These latter approaches result in a complex coupling of the moving reference coordinates and the elastic deformation coordinates within the inertia terms, whereas the former approach results in a greatly simplified inertia operator. In exchange for this simplicity, a nonlinear internal force expression which is invariant to rigid body motions must be derived, as existing linear deformation descriptions referenced with respect to a fixed coordinate system become invalid for systems exhibiting large rotational motions.

The development of a computational procedure capable of real-time simulations of space and robotic applications requires further research involving both the model formulation and computational solution procedures. To this end, the present work is focused on achieving effective and accurate computational methods for the simulation of multibody systems in which flexible components may be conceptualized as spatial beams. For a computationally effective formulation, an automatic derivation of the equations of motion is necessary which includes a realistic modeling of the flexible members and a streamlined incorporation of system constraints. Likewise, robust and efficient time integration procedures which exploit inherent characteristics of the formulation are required. Finally, it is desirable to be able to incorporate additional analysis capabilities such as the deployment and/or retrieval of the flexible member, active control and state estimation, thermal and environmental effects, and other specialized fields into the present formulation. As each of these computational elements are best formulated

by specialists of the various fields, it is advantageous to conduct a modular solution approach toward the software development rather than embedding several analysis capabilities into a single monolithic program.

To this end, separate software modules have been developed which are easily interfaced to form an attractive multibody dynamics simulation package. First, a computer-oriented formulation of flexible spatial beams has been developed to constitute an integral kernel of the multibody dynamics methodology. The flexible beam model accounts for both finite rotations and large deformations, and can be incorporated into general multibody dynamics systems in a straightforward manner. The beam kinematics are referenced directly to the inertial frame. As such, the equations of motion for an arbitrary configuration of flexible beams and rigid bodies can automatically be generated in terms of an identical set of physical coordinates. The structure of the equations, aside from an expression for the nonlinear internal force, is identical for both the rigid and flexible components. Numerical strategies developed for the solution of equations representing spatial kinematic systems are thus applicable for the entire flexible multibody system. Such a unified treatment is not applicable for equations formulated within the context of the floating frame approach. In this case, the reference and elastic coordinate definitions are of highly different character and thus require separate numerical treatment.

A multibody dynamics solution procedure, originally demonstrated on rigid body systems in previous studies [44], has been adopted for the present flexible multibody formulation. For multibody dynamics applications, time integration algorithms must include a proper treatment of three-dimensional finite rotations and also a method to satisfy the kinematic con-

straint conditions. In the present work, an attractive partitioned solution procedure has been developed such that the generalized coordinates are solved in a separate module from the constraint forces. The generalized coordinate solution procedure is based on the application of an improved variation of the explicit central difference algorithm to the translational coordinates and the angular velocity. To update the configuration orientation from the angular velocity, a separate numerical procedure based on the Euler parameter representation of finite rotations is introduced. This overall solution of the spatial dynamics is successfully interfaced with a separate module which enforces the multibody system constraints. The constraint force solver implicitly integrates a stabilized companion differential equation for Lagrange multipliers.

The application of these multibody dynamics solution procedures to systems including spatial beam components relies on an accurate computation of the beam internal force. As the degrees of freedom implicitly contain information of both rigid motion and strain deformation, the internal force computation depends on a judicious procedure which filters out the rigid body motions embedded within these variables. For this purpose, an objective strain increment/stress update procedure has been developed which remains invariant to arbitrary rigid body motions occurring in finite increments of time. The combined developments of this internal force computation with the multibody dynamics solution procedures results in a computational preservation of total energy for undamped systems. This distinct feature of the present work will be demonstrated with several examples.

Simulations of active control/vibration suppression or controlled slewing maneuvers can easily be performed using the present beam for-

mulation. This is due to the use of a convected coordinate representation of the Cauchy stress tensor to describe the beam deformation. The physically appealing description of stress as related to the surface of the deformed configuration has been recast into a coordinate system moving with the beam in a manner which provides conceptual and computational simplifications of the deformation representation. As such, the actual strains measured by sensors located and operating on the deformed structure correspond to those with which the present multibody dynamics formulation is based. Control software modules may thus be interfaced with the present multibody dynamic solution modules in a straightforward manner.

The present methodology is also extended to include the dynamics of deployment and/or retrieval of the flexible members. Hamilton's law of varying action is used to formulate the equations of motion for this three-dimensional moving boundary value problem. A moving node reference for the beam dynamics is employed within the present formulation to account for the changing spatial volume. The reference, which previously was fixed, now corresponds to the configuration of a deployed beam as if it were rigid. A transient integration scheme is derived from a space-time discretization of the Hamiltonian formulation, effectively accounting for the changing spatial reference. The methodology is successfully interfaced with the internal force computational procedure, thus retaining the large rotation/large deformation modeling capabilities of the present work. The formulation and the computational procedure are then specialized to a planar inverse-spaghetti problem for illustrative purposes.

The rest of the thesis is organized as follows. Necessary mathematical preliminaries are presented in Chapter II in deriving the equations

of motion for a flexible spatial beam. The numerical treatment of a discrete form of the equations is then considered in detail in the remaining chapters. A computational procedure for the internal force is derived from the continuum formulation in Chapter III. Special care has been taken to achieve a computation which remains invariant to arbitrary finite rigid rotations while accurately representing the strain of the beam. The formulation is then extended into the multibody dynamics framework in Chapter IV. The solution techniques for multibody systems, including the orientation update procedure and the treatment of constraints, are presented in this chapter. The combined effort of these techniques with the invariant internal force computation results in successful simulations of flexible multibody dynamic systems as shown in several examples. The extension to model deployment/retrieval dynamics of the beam member is presented in Chapter V. The methodology developed to simulate the dynamics of the changing spatial volume is presented in this chapter. Chapter VI then summarizes the major contributions of this work.

CHAPTER II

FLEXIBLE BEAM DYNAMICS FORMULATION

2.1 Introduction

The formulation of the equations of motion for a flexible spatial beam is presented in this chapter. The formulation accounts for the effects of both finite rotations and large deformations of the beam component. To model these geometric nonlinearities, a relevant description of the spatial kinematics must be introduced. The equations of motion of the beam as governed by the basic principles of continuum mechanics are then derived from these kinematic definitions. A complete understanding of this continuum formulation is necessary prior to the development of effective computational techniques for a finite strain beam theory.

To formulate the equations, the beam kinematics are described with reference to the inertial frame as in [31-36]. With this approach, the motion due to rigid rotations of the beam is not distinguished from that due to deformations. The beam configuration is defined by a position vector locating the centroid of a typical cross-section and an orthogonal matrix designating the orientation of this cross-section, both of which are referenced to a fixed inertial frame. As a consequence, the beam inertia operator is identical in form to that of rigid body dynamics. This procedure fully departs from the traditional approach discussed in the preceding chapter in which a floating reference frame is introduced to separate the rigid body motions from the elastic deformations.

As the kinematics are referred to a fixed inertial coordinate system, the present formulation relies on the use of strain measures which are invariant to rigid body motion. Applicable invariant strain measures which model stretching, transverse shear, torsion, and bending deformations of rod-type structures have been developed in the literature. The classical Kirchhoff-Love rod theory modeling large bending and torsion deformations was extended to include stretching and transverse shear strains in [37]. Other formulations derive similar rod theories from an appropriate version of the principle of virtual work [38-40] and from kinematical considerations including the effect of warping which induces torsion-bending coupling [41-43]. The use of these rod-type theories within dynamics problems involving large spatial rotations was initiated in [31-33] and further pursued in [34-36]. These and other works modeling the finite rotations and deformations of beam components employ the Piola-Kirchhoff stress representations in which traction forces acting on a deformed surface element are referenced back to the undeformed configuration [24-27,31-36]. Although these formulations are mathematically consistent, the stresses transmitted in the instantaneous state are referred to the initial state in a way that is physically artificial [45]. Transformations must then be made to relate the stresses back to the actual deformed configuration. In addition, the use of the unsymmetric first Piola-Kirchhoff stress tensor as employed in [31-36] leads to complexities in subsequent computations and linearizations.

A desire for a beam formulation which can easily be interfaced with active feedback control schemes has motivated a more physically-based interpretation of the spatial beam formulations. To achieve real-time software simulations, the computed deformation representations must correspond to

the actual stress/strain measurements of the sensors located and operating on the deformed structure. For this purpose, the present formulation employs the Cauchy stress and a corresponding strain tensor, which are related to the true deformed beam configuration, to describe the elastic deformations. To implement this physical representation, a convected frame which follows the rigid motion of the beam is introduced as the reference for the Cauchy stress and corresponding strain components. Thus the present formulation combines this convected reference for the stress representation with the inertial reference for the beam dynamics. As such, the present formulation is easily adapted within general multibody dynamics methodologies; this advantage will be illuminated in Chapter IV. The formulation can also be readily extended to model the dynamics of deployment and retrieval of the beam as will be shown in Chapter V. The key to the success of the present formulation within these applications is a procedure developed for the computation of the internal force. This algorithmic development, presented in Chapter III, guarantees that the physical stress representation computationally remains invariant to arbitrary rigid-body motions.

The rest of this chapter is organized as follows. Section 2.2 will detail the beam kinematics in which the total motion is referred directly to the inertial reference frame. The description is compared to the kinematic formalisms of the floating frame approach, thus illuminating advantages to the former description. The equations of motion are formulated in Section 2.3 by specializing the principle of virtual work of a continuum solid to the spatial beam kinematic assumptions. The convected frame decomposition of the Cauchy stresses is introduced, and virtual strain-displacement relationships are identified from the virtual work expression. The convected

coordinate stress/strain representation provides conceptual simplifications in the derivation and subsequent computations of the internal force. To complete the formulation, a constitutive law relating the convected frame stress and strain rates is presented in Section 2.4. Consistent linearization procedures employed to obtain linearized weak forms of the equations of motion are then presented in Section 2.5. Using a natural continuum based approach for the linearization procedure, the present formulation inherently based on stresses referred to a deformed configuration results in symmetric tangent matrices. A summary of the present formulation is then given in Section 2.6.

2.2 Large Rotation Beam Kinematics

The inherent difference of the floating frame approach and the inertial reference approach to describe the dynamics of spatial beams is illuminated as follows. As stated in Chapter I, the floating frame approach introduces a reference frame to follow an overall mean rigid-body motion of the beam; the elastic deformations of the beam are then described relative to this moving reference. In this manner the motion due to the rigid rotation of the beam is separated from the local deformation of the beam. The position vector describing the location of an arbitrary particle point on the beam from the inertial origin, as shown below in Figure 2.1, is given by

$$\mathbf{r} = z^T \mathbf{e} + (X + u_f)^T \mathbf{f} \quad . \quad (2.2.1)$$

The following notation is introduced in (2.2.1) to describe these kinematics: $\mathbf{e} = \{ \mathbf{e}_1, \mathbf{e}_2, \mathbf{e}_3 \}^T$ represents the orthogonal basis vectors of the inertial reference frame; $\mathbf{f} = \{ \mathbf{f}_1, \mathbf{f}_2, \mathbf{f}_3 \}^T$ represents the orthogonal basis vectors

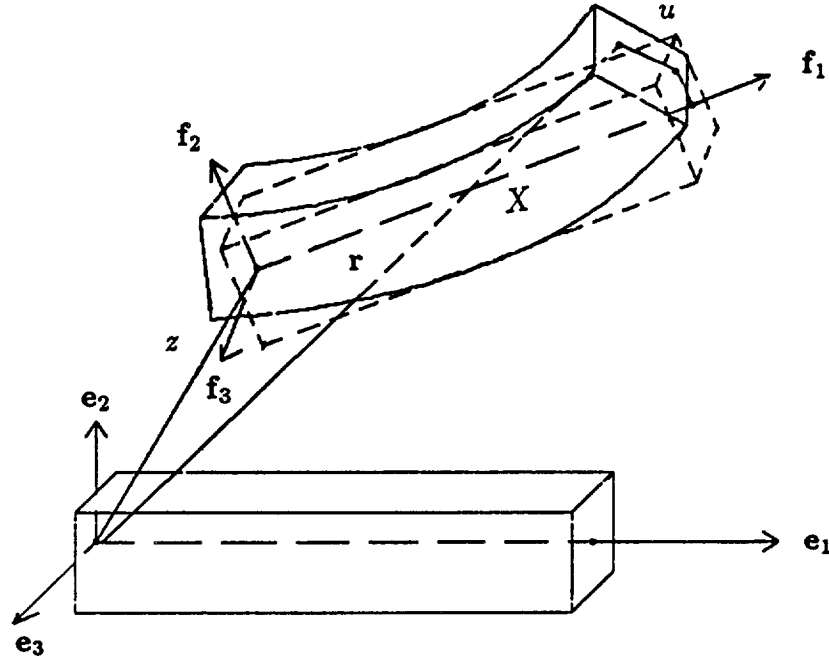


Figure 2.1 Spatial Beam Kinematics: Floating Frame Approach

of floating reference frame; $z^T = \{ z_1, z_2, z_3 \}$ represents the inertial components of the origin of this moving reference frame; $X = \{ X_1, X_2, X_3 \}^T$ represents the moving frame components of the undeformed beam position, and $u_f = \{ u_{f_1}, u_{f_2}, u_{f_3} \}^T$ represents the moving frame components of the relative deformational displacement of the beam from the undeformed position. The terms $z^T \mathbf{e}$ and $X^T \mathbf{f}$ represent the rigid-body motion of the beam, while the terms $u_f^T \mathbf{f}$ represent the small deformational displacements relative to the rigid-body reference frame.

The 3×3 orthogonal transformation matrix \mathbf{A} is introduced to orient the \mathbf{f} -basis from the \mathbf{e} -basis as $\mathbf{f} = \mathbf{A} \mathbf{e}$. The angular velocity of the moving

frame is thus given by [47-48]

$$\tilde{\omega}_f = -\frac{d\mathbf{A}}{dt} \mathbf{A}^T, \quad \tilde{\omega} \equiv \begin{bmatrix} 0 & -\omega_3 & \omega_2 \\ \omega_3 & 0 & -\omega_1 \\ -\omega_2 & \omega_1 & 0 \end{bmatrix} \quad (2.2.2)$$

in which the tensor components are referred to the moving basis and the notation $[\sim]$ represents skew-symmetric matrices. A conjugate virtual rotation tensor is defined analogous to the angular velocity tensor as

$$\delta\tilde{\theta} = -\delta\mathbf{A}\mathbf{A}^T. \quad (2.2.3)$$

The time differentiation of (2.2.1) is obtained from the well known formula applicable for rotating coordinate systems [47]

$$\frac{d}{dt} \equiv \frac{d^e}{dt} = \frac{d^b}{dt} + \boldsymbol{\omega} \times \quad (2.2.4)$$

in which $\boldsymbol{\omega}$ is the angular velocity vector and the superscripts e and b indicate that the derivatives are to be those observed in the inertial and moving system of axes respectively. The above relation is expressed in the following matrix form as

$$\frac{d}{dt} = \frac{d^b}{dt} + \tilde{\omega} \quad (2.2.5)$$

which acts on the moving frame components of a given vector. The velocity, acceleration, and variation of the position vector (2.2.1) are thus given as

$$\dot{\mathbf{r}} = \dot{z}^T \mathbf{e} + \dot{u}^T \mathbf{f} + (X^T + u^T) \tilde{\omega}_f^T \mathbf{f} \quad (2.2.6a)$$

$$\begin{aligned} \ddot{\mathbf{r}} = & \ddot{z}^T \mathbf{e} + \ddot{u}^T \mathbf{f} + 2\dot{u}^T \tilde{\omega}_f^T \mathbf{f} + (X^T + u^T) \\ & \tilde{\dot{\omega}}_f^T \mathbf{f} + (X^T + u^T) \tilde{\omega}_f^T \tilde{\omega}_f^T \mathbf{f} \end{aligned} \quad (2.2.6b)$$

$$\delta\mathbf{r} = \delta z^T \mathbf{e} + \delta u^T \mathbf{f} + (X^T + u^T) \delta\tilde{\theta}^T \mathbf{f}. \quad (2.2.6c)$$

The major drawback of the floating frame approach is immediately seen in the above acceleration expression. The terms \dot{u}_f and u_f representing

the elastic deformations are coupled with the terms ω_f and $\dot{\omega}_f$ representing the angular velocity and acceleration of the floating reference frame. This coupling between the rigid body motion and the elastic deformation requires the development of specialized numerical procedures for the solution of the equations of motion formulated from this kinematic description.

The present formulation adopts an inertial reference frame for describing the translational motions and a body-fixed reference frame for describing the rotational motions. The consequence of this description is that the translational and rotational variables embody information due to both rigid-body motions and deformations of the beam. The configuration of the beam is completely characterized using a position vector locating the neutral axis of the beam from the inertial origin and a body-fixed reference frame representing the orientation of the cross-section with respect to the inertial reference frame. The position vector describing the location of an arbitrary particle point on the beam from the inertial origin, as shown below in Figure 2.2, is given by

$$\mathbf{r} = (X + u)^T \mathbf{e} + \ell^T \mathbf{b} \quad . \quad (2.2.7)$$

In the above equation, the notation $\mathbf{e} = \{ \mathbf{e}_1, \mathbf{e}_2, \mathbf{e}_3 \}^T$ represents the orthogonal basis vectors of the inertial reference frame; $\mathbf{b} = \{ \mathbf{b}_1, \mathbf{b}_2, \mathbf{b}_3 \}^T$ represents the orthogonal basis vectors of the body-fixed reference frame attached to the beam cross section; $X = \{ X_1, X_2, X_3 \}^T$ represents the inertial components of the original neutral axis position; $u = \{ u_1, u_2, u_3 \}^T$ represents the inertial components of the subsequent total translational displacement of the neutral axis, and $\ell^T = \{ 0, \ell_2, \ell_3 \}$ represents the body-fixed components of the distance from the beam neutral-axis to the ma-

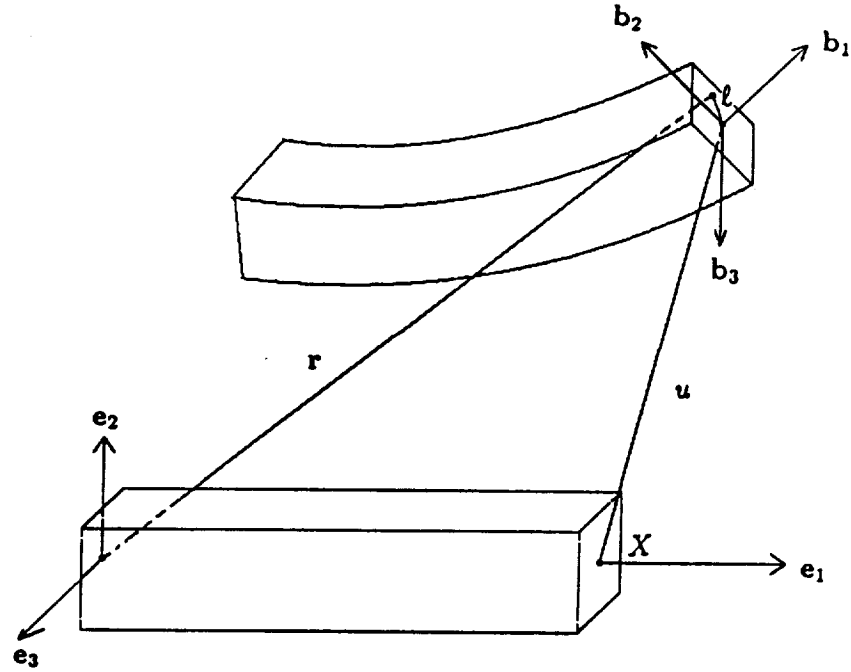


Figure 2.2 Spatial Beam Kinematics: Nonlinear Continuum Approach

terial point located on the deformed beam cross-section. Thus the total large rotation motions are modeled by a combination of the translational displacements u and the moving reference frame \mathbf{b} . It is noted that the beam cross-section is allowed to rotate with respect to the neutral axis of the beam. In this manner, transverse shear deformations are modeled as the orientation of the beam cross-section is not necessarily perpendicular to the beam neutral axis. Warping deformation of the cross-section is not taken into consideration in the present formulation.

The orientation of the body-fixed reference frame is expressed with

respect to the inertial reference frame as

$$\mathbf{b} = \mathbf{R} \mathbf{e} \quad (2.2.8)$$

where \mathbf{R} is a 3×3 orthogonal transformation matrix. The body frame components of the angular velocity tensor and the virtual rotation tensor of the cross-section orientation are given by

$$\tilde{\omega} = -\frac{d\mathbf{R}}{dt} \mathbf{R}^T, \quad \delta\tilde{\alpha} = -\delta\mathbf{R} \mathbf{R}^T, \quad (2.2.9)$$

respectively. The velocity, acceleration, and variation of (2.2.7) are thus

$$\frac{d\mathbf{r}}{dt} = \frac{du^T}{dt} \mathbf{e} + \ell^T \tilde{\omega}^T \mathbf{b} \quad (2.2.10a)$$

$$\frac{d^2\mathbf{r}}{dt^2} = \frac{d^2u^T}{dt^2} \mathbf{e} + \ell^T \left(\frac{d^b\tilde{\omega}^T}{dt} + \tilde{\omega}^T \tilde{\omega}^T \right) \mathbf{b} \quad (2.2.10b)$$

$$\delta\mathbf{r} = \delta u^T \mathbf{e} + \ell^T \delta\tilde{\alpha}^T \mathbf{b} \quad (2.2.10c)$$

It is seen in this acceleration expression, in contrast to (2.2.6b), that the translational displacements of the neutral axis are completely decoupled from the angular orientations of the cross-section. The acceleration is of the same form as in the Euler equations for rigid body motion. This leads to an effective partitioned numerical solution procedure which is equally applicable to both rigid and flexible components of a multibody system. The derivation of the equations of motion are discussed next. The numerical techniques for the solution of these equations of motion are discussed in Chapter IV.

2.3 Nonlinear Equations of Motion

The conditions for the equilibrium of a solid continuum are given by Cauchy's equations of motion. These differential equation of motions are

stated as [45-46]

$$\begin{aligned}\frac{\partial \sigma_{ji}^e}{\partial x_j} + \rho (f_i - \dot{v}_i) &= 0 \\ \sigma_{ij}^e &= \sigma_{ji}^e\end{aligned}$$

to be satisfied through the interior of the continuum V subject to displacement and traction boundary conditions

$$x_i = \bar{x}_i \quad \text{on} \quad S_u, \quad t_i = \sigma_{ji}^e n_j \quad \text{on} \quad S_\sigma$$

on the respective displacement and traction surfaces S_u , S_σ . The Cartesian coordinates x_i represent the particle position after the deformation, v_i the particle velocity, f_i the external force per unit mass, and ρ the mass per unit volume. Likewise, σ_{ij}^e represents the Cartesian components of the Cauchy stress tensor and t_i the stress vector acting on a surface with outward normal components n_i .

The *weak* or variational form of Cauchy's differential equations are employed to deduce a conjugate set of Cauchy stress/virtual strain-displacement relations as well as to provide a basis for the displacement based finite element method. The variational form of Cauchy's equations is the principle of virtual work given as [45]

$$\int_V \delta r_i \rho \ddot{r}_i dV + \int_V \sigma_{ij}^e \frac{\partial \delta r_i}{\partial x_j} dV = \int_V \delta r_i f_i dV + \int_S \delta r_i t_i dS. \quad (2.3.1)$$

The Cartesian coordinates δr_i represent a kinematically admissible virtual displacement. This virtual work expression is tailored to the continuum beam by incorporating the kinematic relations (2.2.7), (2.2.10b), and (2.2.10c) for the components x_i , \ddot{r}_i , and δr_i , respectively. For notational

convenience and subsequent finite element discretization, the principle of virtual work is expressed in the following operator form:

$$\delta F^I + \delta F^S = \delta F^E + \delta F^T \quad (2.3.2)$$

where the inertia operator δF^I , internal force operator δF^S , external force operator δF^E , and traction operator δF^T are identified from (2.3.1). Explicit expressions for the various operators are given in the following Sections 2.3.1 to 2.3.3.

2.3.1 Inertia Operator

The inertia operator defined in (2.3.1)

$$\delta F^I = \int_V \rho \delta \mathbf{r}_i \ddot{\mathbf{r}}_i dV = \int_V \rho \delta \mathbf{r} \cdot \ddot{\mathbf{r}} dV \quad (2.3.3)$$

is tailored to the present problem with the kinematic equations (2.2.10). The following simple expression results for δF^I if the origin of the body-fixed basis is located at the centroid of the cross-section:

$$\delta F^I = \int_s \left\{ \delta u^T \quad \delta \alpha^T \right\} \left\{ J \frac{d^2 \omega}{dt^2} + \tilde{\omega} J \omega \right\} ds, \quad (2.3.4)$$

where

$$m = \int_A \rho dA, \quad J = \int_A \rho \tilde{\ell} \ell^T dA$$

represents the area and inertia properties of the beam cross-section and s represents a length parameter to be taken along the beam neutral axis. It is seen that the translational inertia is completely decoupled from the rotary inertia and is of the same form as the classic Euler equations of rigid body dynamics. This is due to the dual choice of the translational displacements measured in the inertial basis and the angular velocity measured in the body-fixed basis located at the center of mass of the cross-section.

2.3.2 Internal Force Operator

The internal force operator is defined from (2.3.1) as

$$\delta \mathbf{F}^S = \int_V \frac{\partial \delta r_i}{\partial x_j} \sigma_{ij}^e dV \quad (2.3.5)$$

identifying as conjugate quantities the virtual displacement gradient and the Cauchy stress tensor. An explicit expression for the internal force is then derived from the beam kinematics (2.2.10). A set of virtual strain-displacement relations that are invariant to rigid body motions are deduced from this virtual work expression as in [38-40]. To complete the formulation, a suitable constitutive relation is chosen to relate the strain rates, which are of identical form as the virtual strain relations, to an appropriate stress rate tensor. An objective incremental procedure is then derived from this rate-type constitutive law.

To provide conceptual simplifications in the derivation and subsequent computations, the Cauchy stress tensor and the virtual strain tensor are decomposed with respect to an alternative beam reference frame which lies tangent to the deformed neutral axis. The virtual strain tensor contains three independent, non-zero components when referenced to this convected coordinate system. In addition, the task of stress update is accomplished with a much simpler computation when convected frame as opposed to inertial frame stress components are considered. When inertial frame components are employed within problems exhibiting large rigid body motions, an appropriate nonlinear constitutive relation is required to obtain an objective stress update from strain measures. When expressed using convected frame stress and strain tensor components, the constitutive law leads to a simple additive update procedure.

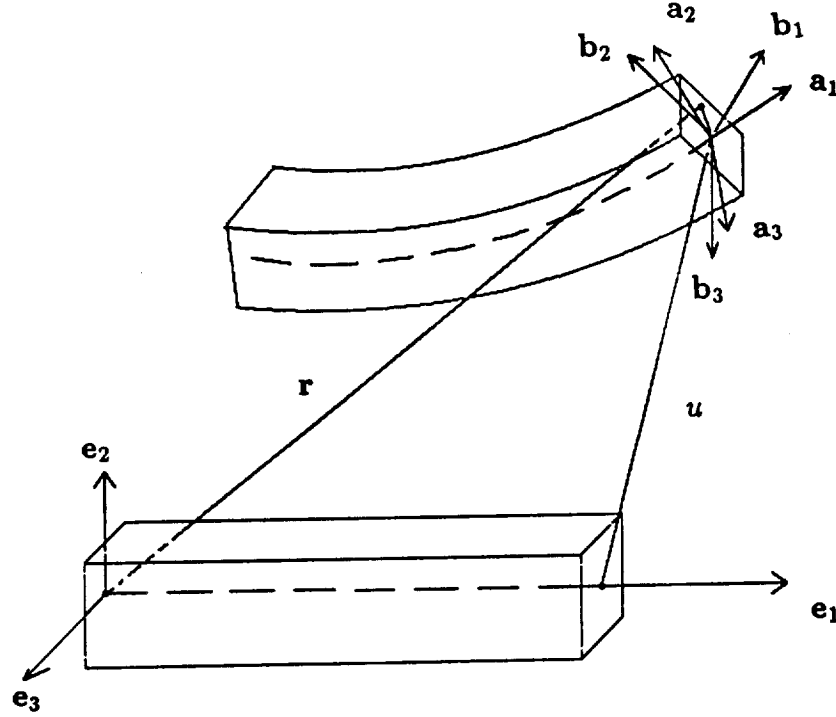


Figure 2.3 Spatial Beam Kinematics: Convected Reference Frame

For this purpose, we introduce a convected reference frame which lies tangent to the deformed neutral axis. The convected reference frame $\mathbf{a} = \{ \mathbf{a}_1, \mathbf{a}_2, \mathbf{a}_3 \}^T$, as shown above in Figure 2.3, is related to the inertial reference frame \mathbf{e} by $\mathbf{a} = \mathbf{T} \mathbf{e}$. For present implementation purposes within the context of a constant-strain finite element, the convected frame will be approximated as a straight line connecting the two element nodes. As such, the reference frame is constant on the element level and is similar in concept to that introduced in [19-20]. It is noted that this reference frame does not coincide with the body frame \mathbf{b} attached to the cross-section. The relative difference between these two frames is represented by the ro-

tation matrix \mathbf{S} which models the effects of transverse shear and torsion deformations as

$$\mathbf{b} = \mathbf{S} \mathbf{a} , \quad \mathbf{R} = \mathbf{S} \mathbf{T} . \quad (2.3.6)$$

As will be shown, the interdependence between \mathbf{R} , \mathbf{S} , and \mathbf{T} plays a key role in the algorithmic implementation of the present formulation.

The internal force operator, originally characterized by inertial frame components of the Cauchy stress tensor σ_{ij}^e and conjugate virtual displacement gradient, can equivalently be expressed in terms of the convected frame stress tensor components σ_{ij}^a and a corresponding convected virtual displacement gradient. As the rotational tensor T_{ij} maps the inertial coordinates x_i to the convected coordinates ξ_i , the following tensor transformations

$$\frac{\partial}{\partial x_j} = T_{kj} \frac{\partial}{\partial \xi_k} \quad \sigma_{ij}^e = T_{ki} \sigma_{kl}^a T_{lj} \quad (2.3.7)$$

are incorporated into (2.3.5) to yield

$$\delta F^S = \int_V T_{mi} \frac{\partial \delta r_i}{\partial \xi_k} \sigma_{mk}^a dV . \quad (2.3.8)$$

The virtual strain tensor $\delta \varepsilon_{mk}^a$ is defined from the symmetric portion of the transformed deformation gradients as

$$\delta \varepsilon_{mk}^a \equiv \frac{1}{2} \left(T_{mi} \frac{\partial \delta r_i}{\partial \xi_k} + T_{ki} \frac{\partial \delta r_i}{\partial \xi_m} \right) . \quad (2.3.9)$$

The virtual strain definition (2.3.9) vanishes during a rigid body rotation. As the virtual displacements of a rigid-body rotation are $\delta \mathbf{r} = \delta \tilde{\alpha} \mathbf{r}$, the virtual deformation gradient reduces to the skew-symmetric matrix $\delta \tilde{\alpha}$ in this instance. As such, the symmetric virtual strain definition (2.3.9) is

invariant to rigid body motions and is thus classified as an objective rate-type tensor.

Due to the symmetry of the Cauchy stress tensor, the virtual work of the internal force is given as

$$\delta F^S = \int_V \delta \varepsilon_{mk}^a \sigma_{mk}^a dV . \quad (2.3.10)$$

This expression is rewritten in the following vector product format as

$$\delta F^S = \int_V \{ \sigma_{\xi\xi} \quad \hat{\sigma}_{\xi\eta} \quad \hat{\sigma}_{\xi\zeta} \} \begin{Bmatrix} \delta \varepsilon_{\xi\xi} \\ \delta \hat{\varepsilon}_{\xi\eta} \\ \delta \hat{\varepsilon}_{\xi\zeta} \end{Bmatrix} dV . \quad (2.3.11)$$

In the above equation, the notations

$$\xi_i = \{ \xi_1, \xi_2, \xi_3 \} = \{ \xi, \eta, \zeta \} , \quad (\hat{\cdot})_{ij} = (\cdot)_{ij} + (\cdot)_{ji}$$

denote the coordinates of the convected reference frame and the engineering shear strain definitions respectively. The remaining convected frame strain components $\delta \varepsilon_{\eta\eta}$, $\delta \varepsilon_{\zeta\zeta}$, $\delta \hat{\varepsilon}_{\eta\zeta}$ are identically equal to zero due to the original assumptions of the beam kinematics. From (2.3.9), the three non-zero virtual strain components are given as

$$\delta \varepsilon_{\xi\xi} = T_{1i} \frac{\partial \delta r_i}{\partial \xi} \quad (2.3.12a)$$

$$\delta \hat{\varepsilon}_{\xi\eta} = T_{2i} \frac{\partial \delta r_i}{\partial \xi} + T_{1i} \frac{\partial \delta r_i}{\partial \eta} \quad (2.3.12b)$$

$$\delta \hat{\varepsilon}_{\xi\zeta} = T_{3i} \frac{\partial \delta r_i}{\partial \xi} + T_{1i} \frac{\partial \delta r_i}{\partial \zeta} \quad (2.3.12c)$$

The above definitions are rewritten terms of the virtual translations and virtual rotations by performing the parametric differentiation of the variation of the position vector (2.2.10c) with respect to the convected frame coordinates. As the convected reference frame has been constructed to be

constant over the element domain where the differentiation is performed, it becomes convenient to express the variation of the position vector as

$$\begin{aligned}\delta \mathbf{r} &= \delta u^T \mathbf{e} + \delta \beta^T \tilde{\ell}_a^T \mathbf{a} \\ &= (\delta u^T + \delta \beta^T \tilde{\ell}_a^T T) \mathbf{e} .\end{aligned}\quad (2.3.13)$$

In the above equation, the components $\delta \beta$ and ℓ_a are defined as

$$\delta \beta = S^T \delta \alpha , \quad \ell_a = S^T \ell = \begin{Bmatrix} \xi_l \\ \eta \\ \zeta \end{Bmatrix} \quad (2.3.14)$$

to represent convected frame decompositions of the cross-section virtual rotation vector and material position coordinates. The variation (2.3.13) is differentiated with respect to the neutral-axis coordinate ξ to give

$$\frac{\partial \delta \mathbf{r}}{\partial \xi} = \left(\frac{\partial \delta u^T}{\partial \xi} + \frac{\partial \delta \beta^T}{\partial \xi} \tilde{\ell}_a^T T \right) \mathbf{e} \quad (2.3.15)$$

where the approximation

$$\frac{\partial \ell_a}{\partial \xi} \simeq 0$$

is employed as the change in the neutral-axis coordinate of the total position due to a small rotation of the cross-section about the neutral axis is negligible. Likewise, the differentiation of (2.3.13) with respect to the coordinates perpendicular to the neutral-axis yields

$$\frac{\partial \delta \mathbf{r}}{\partial \eta} = \delta \beta^T \tilde{i}_2^T T \mathbf{e} \quad (2.3.16)$$

$$\frac{\partial \delta \mathbf{r}}{\partial \zeta} = \delta \beta^T \tilde{i}_3^T T \mathbf{e} \quad (2.3.17)$$

where \tilde{i}_2 and \tilde{i}_3 are given by

$$\tilde{i}_2 \equiv \begin{bmatrix} 0 & 0 & 1 \\ 0 & 0 & 0 \\ -1 & 0 & 0 \end{bmatrix} = \frac{\partial \tilde{\ell}_a}{\partial \eta}$$

$$\tilde{i}_3 \equiv \begin{bmatrix} 0 & -1 & 0 \\ 1 & 0 & 0 \\ 0 & 0 & 0 \end{bmatrix} = \frac{\partial \tilde{\ell}_a}{\partial \zeta}.$$

It is noted that in the above derivations the assumptions intrinsic to the beam formulation in which the virtual translations δu and virtual rotations $\delta\beta$ are independent of the cross-section variables η and ζ have been effected. Substitutions of the derivatives (2.3.15), (2.3.16), and (2.3.17) into (2.3.12) yield the expression

$$\delta \begin{Bmatrix} \varepsilon_{\xi\xi} \\ \hat{\varepsilon}_{\xi\eta} \\ \hat{\varepsilon}_{\xi\zeta} \end{Bmatrix} = \mathbf{T} \frac{\partial \delta u}{\partial \xi} + \tilde{i}_1 \delta\beta + \tilde{\ell}_a^T \frac{\partial \delta\beta}{\partial \xi} \quad (2.3.18)$$

where

$$\tilde{i}_1 \equiv \begin{bmatrix} 0 & 0 & 0 \\ 0 & 0 & -1 \\ 0 & 1 & 0 \end{bmatrix}.$$

The above equation (2.3.18) is rewritten as

$$\begin{Bmatrix} \delta\varepsilon_{\xi\xi} \\ \delta\hat{\varepsilon}_{\xi\eta} \\ \delta\hat{\varepsilon}_{\xi\zeta} \end{Bmatrix} = \delta\gamma + \tilde{\ell}^T \delta\kappa \quad (2.3.19)$$

where $\delta\gamma$ represents the membrane and two transverse shear virtual strains and $\delta\kappa$ represents the torsion and two bending virtual strains. The definitions

$$\delta\gamma = \mathbf{T} \frac{\partial \delta u}{\partial \xi} + \begin{Bmatrix} 0 \\ -\delta\beta_3 \\ \delta\beta_2 \end{Bmatrix} \quad (2.3.20)$$

$$\delta\kappa = \frac{\partial \delta\beta}{\partial \xi} \quad (2.3.21)$$

are a convected coordinate representation of the virtual strains derived in [39-40].

To determine the stress state, it remains to introduce an appropriate constitutive law. A rate-type constitutive law, as discussed in Section 2.4,

is employed for this purpose. The resulting stress state, as derived in the following section, is written in form similar to (2.3.19) as

$$\begin{Bmatrix} \sigma_{\xi\xi} \\ \sigma_{\xi\eta} \\ \sigma_{\xi\zeta} \end{Bmatrix} = \sigma_\gamma + \tilde{\ell}^T \sigma_\kappa \quad (2.3.22)$$

where σ_γ represents the membrane and two transverse shear stresses and σ_κ represents the torsion and two bending stresses. From this result, the virtual work of the internal force can be written as

$$\delta F^S = \int_\xi \{ \delta \gamma^T N_\gamma + \delta \kappa^T M_\kappa \} d\xi \quad (2.3.23)$$

by substituting (2.3.22) and (2.3.19) into (2.3.11) and integrating over the area coordinates of a symmetric cross section. In the above equation, N_γ represents the axial and transverse shear forces per unit length, and M_κ represents the torsional and bending moments per unit length as

$$N_\gamma = \int_A \sigma dA, \quad M_\kappa = \int_A \tilde{\ell} \sigma dA. \quad (2.3.24)$$

It is necessary to rewrite (2.3.23) in a manner consistent with the inertia operator (2.3.4) as

$$\delta F^S = \int_\xi \{ \delta u^T \quad \delta \alpha^T \} [B]^T \begin{Bmatrix} N_\gamma \\ M_\kappa \end{Bmatrix} d\xi. \quad (2.3.25)$$

To identify the proper strain-displacement matrix $[B]$, a transformation of the virtual strains back to the body frame components of the virtual rotations is required. To effect the change of the body reference frame of the cross-section orientation in space with respect to the constant convected reference frame, we invoke the following relations

$$\frac{\partial^a \delta \beta}{\partial \xi} = S^T \frac{\partial^a \delta \alpha}{\partial \xi} \quad (2.3.26)$$

$$= S^T \left(\frac{\partial^b \delta \alpha}{\partial \xi} + \tilde{\kappa}_S \delta \alpha \right), \quad \tilde{\kappa}_S^T = \frac{\partial^a S}{\partial \xi} S^T \quad (2.3.27)$$

which are completely analogous to the time derivatives of rotating coordinates. The strain operator $[B]$ is then identified as

$$[B] = \begin{bmatrix} \mathbf{T} \frac{\partial^a}{\partial \xi} & \tilde{i}_1 \mathbf{S}^T \\ \mathbf{0} & \mathbf{S}^T (\tilde{\kappa}_S + \mathbf{I} \frac{\partial^b}{\partial \xi}) \end{bmatrix} \quad (2.3.28)$$

To complete the internal force definition, it remains to provide a procedure for updating σ_γ and σ_κ in order to compute N_γ and M_κ . This is accomplished via the numerical integration of an appropriate rate-type constitutive law to be discussed shortly in Section 2.4.

2.3.3 External Force and Traction Operator

The external force operator defined in (2.3.1) as

$$\delta F^E = \int_V \delta r_i f_i dV$$

has the final resultant form

$$\delta F^E = \int_\xi \left\{ \delta u^T \delta \alpha^T \right\} \left\{ \begin{matrix} f^e \\ f^b \end{matrix} \right\} d\xi \quad (2.3.29)$$

where f^e represents the inertial components of a force per unit length acting on the beam neutral axis and f^b represents the body-fixed components of a moment per unit length acting on the beam cross-section. The traction operator defined as

$$\delta F^T = \int_S \delta r_i t_i dS \quad (2.3.30)$$

acts on the exterior surfaces of the beam as natural boundary conditions.

2.4 Constitutive Equations

To complete the description of the nonlinear continuum problem, the derivation of a stress-state from an applicable constitutive equation is necessary. The classical elastic constitutive equations applicable within the

finite deformation context relates the second Piola-Kirchhoff stress components to a linear combination of the Lagrangian finite strain components within a generalized Hooke's Law [45]. This type of deformation description is based on a direct comparison of the the current shape of the continuum back to its original reference configuration. Such a formulation thus asserts that regardless of the extent of the deformation, the material response of the continuum is based solely from the unstressed state without any reference to the history of the deformation. A more natural concept is based on the idea that an increment of stress is a function of the increment of strain from an immediately preceding state [49]. The constitutive law which mathematically generalizes this concept relates the instantaneous rate of stress to the instantaneous rate of deformation. This concept is adopted in the present beam formulation.

When stress and strain rates are used with a constitutive law, the property of objectivity must be taken into consideration. The principle of objectivity requires that intrinsic physical properties of a body be independent of the body's orientation in space. This principle is embodied in constitutive theory by requiring that constitutive equations contain only objective tensor fields. Tensors defined from the material coordinates of the undeformed continuum such as the Piola-Kirchhoff stress tensors automatically possess this property as do time independent tensors. However, the time derivative of the Cauchy stress tensor is not objective, and an alternate rate definition other than the time derivative must be used within a constitutive law based on Cauchy stress rates.

One objective stress rate constructed from the Cauchy stress tensor

is the Truesdell stress rate tensor $\hat{\sigma}_{kl}$ defined as

$$\hat{\sigma}_{kl}^e = \dot{\sigma}_{kl}^e - \sigma_{km}^e v_{l,m}^e - \sigma_{ml}^e v_{k,m}^e + \sigma_{kl}^e v_{m,m}^e , \quad (2.4.1)$$

and an objective constitutive law incorporating this definition is

$$\hat{\sigma}_{kl}^e = c_{ijkl} \dot{\epsilon}_{kl}^e . \quad (2.4.2)$$

The notation

$$v_{l,m}^e = \frac{\partial \dot{u}_l}{\partial x_m} , \quad \dot{\epsilon}_{kl}^e = \frac{1}{2} \left(\frac{\partial \dot{u}_k}{\partial x_l} + \frac{\partial \dot{u}_l}{\partial x_k} \right) ,$$

represents the velocity gradient tensor and the symmetric part of the velocity gradient respectively, and c_{ijkl} is the spatial transformation of the material response tensor C_{ABCD} to be defined shortly. Similar objective stress rates, as the Jauman stress rate tensor, may also be employed within objective constitutive laws. In the present formulation, the Truesdell rate equation is chosen as it leads to symmetric tangent stiffness matrices within the linearization procedure discussed in Section 2.5.

For computational convenience, the Truesdell constitutive equation (2.4.2) is rearranged as

$$\dot{\sigma}_{ij}^e + \sigma_{ik}^e \tilde{w}_{kj}^e - \tilde{w}_{ik}^e \sigma_{kj} = \bar{C}_{ijkl} \dot{\epsilon}_{kl}^e \quad (2.4.3)$$

where

$$\bar{C}_{ijkl} = c_{ijkl} - \delta_{kl} \sigma_{ij} + \frac{1}{2} \left(\delta_{il} \sigma_{jk} + \delta_{jl} \sigma_{ik} + \delta_{ik} \sigma_{jl} + \delta_{jk} \sigma_{il} \right) \quad (2.4.4)$$

corresponds to a stress-dependent constitutive tensor and

$$\tilde{w}_{kl} = \frac{1}{2} \left(\frac{\partial \dot{u}_k}{\partial x_l} - \frac{\partial \dot{u}_l}{\partial x_k} \right) \quad (2.4.5)$$

corresponds to the skew-symmetric spin tensor. This form (2.4.3) is conducive for the development of a computational procedure to update a given stress state. Any stress rate defined from a skew symmetric tensor as

$$\sigma^{<W>} \equiv \dot{\sigma} + \sigma \tilde{\Omega} - \tilde{\Omega} \sigma, \quad \tilde{\Omega} = \dot{\mathbf{W}} \mathbf{W}^T$$

is automatically objective. It is easily shown that when this stress rate is transformed to the basis defined by the orthogonal rotation tensor \mathbf{W} characterizing $\tilde{\Omega}$ as

$$\sigma_W^{<W>} \equiv \mathbf{W}^T (\dot{\sigma} + \sigma \tilde{\Omega} - \tilde{\Omega} \sigma) \mathbf{W},$$

it is precisely the time derivative of the stress tensor also transformed to the \mathbf{W} basis as

$$\sigma_W^{<W>} = \frac{d}{dt} (\mathbf{W}^T \sigma^e \mathbf{W}) \equiv \dot{\sigma}_W.$$

The transformed stress rate tensor can then be directly integrated as

$$\sigma_W^{n+1} = \sigma_W^n + \int_{t_n}^{t_{n+1}} (\bar{C} \dot{\epsilon})_W dt \quad (2.4.6)$$

where the right hand side of the constitutive equation is also transformed to the \mathbf{W} basis. The above equation is accurately approximated with a midpoint integration rule as [50]

$$\sigma_W^{n+1} = \sigma_W^n + \bar{C} \Delta \epsilon_W \quad (2.4.7)$$

where the increment $\Delta \epsilon_W$ is strictly due to deformation and calculated at time $t^{n+\frac{1}{2}}$.

This stress update procedure, as applied to the Truesdell rate definition, requires that the stress and strain tensors originally referred to the

inertial basis be transformed to a basis rotating with the spin tensor. This basis must be calculated from its generating differential equation

$$\dot{\mathbf{W}} = \tilde{\mathbf{w}} \mathbf{W} ,$$

and for this purpose algorithms have been developed which computationally remain objective [51-53]. However, this additional complexity is bypassed within the present beam formulation. The update procedure (2.4.7) can be directly applied to the convected frame tensor components of the Cauchy stresses and strains without the need for further transformations. This is shown as follows by expressing the the Truesdell rate equation (2.4.3) with convected frame tensor components as opposed to inertial frame components.

To derive the appropriate constitutive law for the present beam formulation, the origin of the Truesdell rate equation is first examined. The Truesdell rate equation is based on the classical hyper-elastic constitutive equations [45]

$$\frac{D}{Dt} (S_{KL}) = \dot{S}_{AB} = C_{ABCD} \dot{E}_{CD} \quad (2.4.8)$$

where S_{AB} is the second Piola-Kirchhoff stress tensor, E_{CD} is the Lagrange strain tensor and C_{ABCD} is a material response tensor derived from a prescribed elastic strain energy function. The second Piola-Kirchhoff stress tensor is related to the Cauchy stress tensor σ_{ij}^e by

$$S_{AB} = j X_{A,i} \sigma_{ij}^e X_{B,j} , \quad (2.4.9)$$

and the Lagrange strain tensor is defined as

$$E_{AB} = \frac{1}{2} (x_{i,A} x_{i,B} - \delta_{AB}) .$$

In the above equations, the components X_I denote the material coordinates of the undeformed configuration, x_i the spatial coordinates of the deformed configuration, and

$$x_{i,A} = \frac{\partial x_i}{\partial X_A} \quad , \quad j = \det(x_{i,A}) \quad , \quad X_{A,i} = \frac{\partial X_A}{\partial x_i}$$

denote the deformation gradient, its determinant, and its inverse, respectively. The material time derivative of the second Piola-Kirchoff stress tensor and the Truesdell rate of the Cauchy stress tensor are related in the same manner as the stress tensors themselves (see, e.g. [46]) as

$$\frac{D}{Dt} (S_{KL}) = j X_{K,k} X_{L,l} (\dot{\sigma}_{kl}^e) \quad . \quad (2.4.10)$$

The Truesdell rate equation is derived by transforming (2.4.8) to spatial coordinates as

$$j X_{A,k} X_{B,l} (\dot{\sigma}_{kl}^e) = C_{ABCD} x_{i,C} x_{j,D} \dot{\epsilon}_{ij}^e \quad ,$$

and after further manipulation (2.4.2) results with the definition

$$c_{ijkl} = \frac{1}{j} x_{i,A} x_{j,B} x_{k,C} x_{l,D} C_{ABCD} \quad .$$

In the same manner, a constitutive relation suitable for the present beam formulation which incorporates the convected frame decomposition of the Cauchy stresses is derived. The following relationship similar to (2.4.9)

$$S_{KL} = j \sigma_{pq}^a \frac{\partial X_K}{\partial \xi_p} \frac{\partial X_L}{\partial \xi_q} \quad (2.4.11)$$

is defined by transforming the spatial coordinates from the inertial basis to the convected basis. The convected frame interpretation of the Truesdell

stress rate is derived by taking the material time derivative of the right-hand side of (2.4.11) to yield

$$\frac{D}{Dt} (S_{KL}) = j \frac{\partial X_K}{\partial \xi_k} \frac{\partial X_L}{\partial \xi_l} (\dot{\sigma}_{kl}^a) , \quad (2.4.12)$$

and the objective convected coordinate stress rate tensor becomes

$$\dot{\sigma}_{kl}^a = \dot{\sigma}_{kl}^a - \sigma_{il}^a v_{ki}^a - \sigma_{ki}^a v_{li}^a + \sigma_{kl}^a v_{m,m}^a + \sigma_{il}^a \dot{\beta}_{ik} + \sigma_{ki}^a \dot{\beta}_{il} . \quad (2.4.13)$$

In the above equation, the notation

$$v_{ki}^a = T_{kp} \frac{\partial \dot{u}_p}{\partial \xi_i} , \quad \dot{\beta}_{ik} = \dot{T}_{ij} T_{kj}$$

denotes the transformed velocity gradient tensor and the angular velocity tensor of the convected reference frame respectively. The constitutive law is then derived as

$$\dot{\sigma}_{ij}^a = c_{ijkl} \dot{\epsilon}_{kl}^a \quad (2.4.14)$$

where

$$\dot{\epsilon}_{mp}^a = \frac{1}{2} \left(T_{mk} \frac{\partial \dot{u}_k}{\partial \xi_p} + T_{pk} \frac{\partial \dot{u}_k}{\partial \xi_m} \right)$$

is the symmetric part of the velocity gradient tensor analogous to (2.3.9).

The constitutive law is rewritten in terms of skew-symmetric tensors as

$$\begin{aligned} \dot{\sigma}_{kl}^a + \sigma_{ki}^a (\tilde{\mu}_{il} - \tilde{\beta}_{il}) - (\tilde{\mu}_{ki} - \tilde{\beta}_{ki}) \sigma_{il}^a \\ = (c_{klmp} + \hat{c}_{klmp}) \dot{\epsilon}_{mp}^a \end{aligned} \quad (2.4.15)$$

where

$$\tilde{\mu}_{mp} = \frac{1}{2} \left(T_{mk} \frac{\partial \dot{u}_k}{\partial \xi_p} - T_{pk} \frac{\partial \dot{u}_k}{\partial \xi_m} \right)$$

is the skew-symmetric part of the transformed velocity gradient tensor. It is noted that the skew symmetric tensor of the above constitutive law represents the difference between the convected frame spin tensor and the convected frame angular velocity vector. It can be shown that this difference is approximately the order of magnitude of the incremental rotations of the shear \mathbf{S} rotation matrix. Under the assumption of small shear strains, this skew tensor can be neglected, and the constitutive equation reduces to

$$\dot{\sigma}_{kl}^a \simeq \bar{C}_{klmp} \dot{\varepsilon}_{mp}^a \quad (2.4.16)$$

This equation can then be integrated directly without requiring a transformation of basis as

$$\sigma_{kl}^{a^{n+1}} = \sigma_{kl}^{a^n} + \bar{C}_{klmp} \Delta \varepsilon_{mp}^a \quad (2.4.17)$$

to define the stress update procedure.

The above expression (2.4.17) is then written in terms of the relevant convected frame stress components as

$$\begin{Bmatrix} \sigma_{\xi\xi} \\ \sigma_{\xi\zeta} \\ \sigma_{\xi\eta} \end{Bmatrix}^{n+1} = \begin{Bmatrix} \sigma_{\xi\xi} \\ \sigma_{\xi\zeta} \\ \sigma_{\xi\eta} \end{Bmatrix}^n + \bar{\mathbf{C}} \begin{Bmatrix} \Delta \varepsilon_{\xi\xi} \\ \Delta \varepsilon_{\xi\zeta} \\ \Delta \varepsilon_{\xi\eta} \end{Bmatrix} \quad (2.4.18)$$

The constitutive matrix is subsequently given as

$$\begin{aligned} \bar{\mathbf{C}} &= \begin{bmatrix} \bar{C}_{1111} & \bar{C}_{1112} & \bar{C}_{1113} \\ \bar{C}_{1211} & \bar{C}_{1212} & \bar{C}_{1213} \\ \bar{C}_{1311} & \bar{C}_{1312} & \bar{C}_{1313} \end{bmatrix} \\ &= \text{Diag} \left(E + \sigma_{\xi\xi}, G + \frac{1}{2}\sigma_{\xi\xi}, G + \frac{1}{2}\sigma_{\xi\xi} \right) \end{aligned}$$

by specializing the definition (2.4.4) to the tensor components representative of the beam formulation. Alternative stress-dependent constitutive laws,

as for inelastic material behavior, may also be implemented. The stress components are then written as

$$\sigma = \sigma^0 + \ell_2 \sigma^{\ell_2} + \ell_3 \sigma^{\ell_3} , \quad (2.4.19)$$

illuminating the dependency on the cross-sectional variables ℓ_i . This dependency is immediately seen from (2.4.18) due to the incremental strains which will be of the same form as the virtual strains (2.3.19). Likewise, the stress dependent constitutive matrix is decomposed as

$$\bar{C} = \bar{C}^0 + \ell_2 \bar{C}^{\ell_2} + \ell_3 \bar{C}^{\ell_3} \quad (2.4.20)$$

where

$$\bar{C}^0 = \bar{C}(\sigma^0) , \quad \bar{C}^{\ell_2} = \bar{C}(\sigma^{\ell_2}) , \quad \bar{C}^{\ell_3} = \bar{C}(\sigma^{\ell_3})$$

are defined from the appropriate stress components of (2.4.19). By combining the above with the following incremental analog to the virtual strains (2.3.19)

$$\Delta \varepsilon = \Delta \gamma + \tilde{\ell}^T \Delta \kappa ,$$

the stress update thus takes the form

$$\sigma^0{}^{n+1} = \sigma^0{}^n + \Delta \sigma^0$$

$$\sigma^{\ell_2}{}^{n+1} = \sigma^{\ell_2}{}^n + \Delta \sigma^{\ell_2}$$

$$\sigma^{\ell_3}{}^{n+1} = \sigma^{\ell_3}{}^n + \Delta \sigma^{\ell_3}$$

where

$$\Delta \sigma^0 = \bar{C}^0 \Delta \gamma$$

$$\Delta \sigma^{\ell_2} = \bar{C}^{\ell_2} \Delta \gamma + \bar{C}^0 \tilde{i}_2^T \Delta \kappa$$

$$\Delta \sigma^{\ell_3} = \bar{C}^{\ell_3} \Delta \gamma + \bar{C}^0 \tilde{i}_3^T \Delta \kappa .$$

The evaluation of the strain increments $\Delta\gamma$ and $\Delta\kappa$ will be detailed in Chapter III. The stress resultant forces and moments per unit length N and M defined in (2.3.24) are now given in a more explicit form as

$$\begin{Bmatrix} N_1 \\ N_2 \\ N_3 \end{Bmatrix} = \begin{Bmatrix} \sigma_{\xi\xi}^0 A \\ \sigma_{\xi\eta}^0 A \\ \sigma_{\xi\eta}^0 A \end{Bmatrix}, \quad \begin{Bmatrix} M_1 \\ M_2 \\ M_3 \end{Bmatrix} = \begin{Bmatrix} \sigma_{\xi\xi}^{\ell_2} I_3 - \sigma_{\xi\eta}^{\ell_3} I_2 \\ \sigma_{\xi\xi}^{\ell_3} I_2 \\ -\sigma_{\xi\xi}^{\ell_2} I_3 \end{Bmatrix}.$$

2.5 Consistent Linearization

The derivation of the equations representing the spatial motion of a flexible beam is thus concluded. Inherent in these equations is an inertia force containing a nonlinear rotary acceleration, and a nonlinear internal force expression. To achieve numerical solutions to both static and dynamic problems, it is necessary to work with a linearized set of equations representing the best linear approximation of the nonlinear equations within a small neighborhood of some equilibrium configuration. The term consistent linearization refers to a process of achieving this approximation in a manner that retains the inherent properties of the formulation. Consistent linearization techniques which account for the effect of finite rotations in deriving tangent stiffness matrices have been presented for nonlinear beam formulations [25-27,31-36,54]. In what follows, an intuitive approach is presented to linearize the inertia and internal force terms.

To this end, the displacements and rotations which inherently define the nonlinear functions are represented as a linear perturbation about a known equilibrium state. An incremental displacement Δx represents the linear portion of any possible perturbation of a known displacement x^n and

to an alternative displacement \mathbf{x} as

$$\mathbf{x} \simeq \mathbf{x}^n + \Delta\mathbf{x} \quad . \quad (2.5.1)$$

The equivalent concept which gives the linear portion of any possible excursion between a known orientation represented by the orthogonal rotation matrix \mathbf{R}^n and an alternative rotation \mathbf{R} is given as

$$\mathbf{R} \simeq \mathbf{R}^n + \Delta\mathbf{R} \quad (2.5.2)$$

$$= \mathbf{R}^n + \Delta\tilde{\alpha}^T \mathbf{R}^n \quad . \quad (2.5.3)$$

The definition $\Delta\mathbf{R} = \Delta\tilde{\alpha}^T \mathbf{R}^n$ is analogous to the virtual rotation definition $\delta\mathbf{R} = \delta\tilde{\alpha}^T \mathbf{R}$ of (2.2.9); the components of $\Delta\tilde{\alpha}^T$ represent infinitesimal angles of rotation about the basis vectors of \mathbf{R}^n moving the reference frame from an unperturbed to a perturbed position [4]. The form of the linearized rotation has also been derived using the Frechet derivative concept in [31,34].

2.5.1 Tangent Mass

To obtain the linear portion of the inertia force

$$\delta F^I = \int_{\xi} \{ \delta u^T \quad \delta \alpha^T \} \begin{Bmatrix} M_m \\ M_J \end{Bmatrix} d\xi \quad (2.5.4)$$

$$M_m = \rho A \ddot{u} \quad (2.5.5)$$

$$M_J = J \dot{\omega} + \tilde{\omega} J \omega \quad , \quad (2.5.6)$$

linear perturbations of the translational and rotational acceleration must be derived. The former is given as

$$\ddot{u} \simeq \ddot{u}^n + \Delta u \quad (2.5.7)$$

such that

$$M_m \simeq M_m^n + \rho A \Delta u \quad . \quad (2.5.8)$$

The latter will be obtained from linear expansions of the angular velocity and acceleration in terms of the rotational perturbations about a given orientation. For this purpose, (2.5.3) is employed to give

$$\begin{aligned} \tilde{\omega} &= -\dot{\mathbf{R}} \mathbf{R}^T \\ &\simeq -\frac{d}{dt} [(I + \Delta \tilde{\alpha}^T) \mathbf{R}^n] \mathbf{R}^{n^T} (I + \Delta \tilde{\alpha}) \quad . \end{aligned} \quad (2.5.9)$$

By expanding the above and retaining terms to first order in the rotational perturbation, the consistent approximation of the angular velocity tensor becomes

$$\tilde{\omega} \simeq \tilde{\omega}^n + \Delta \dot{\tilde{\alpha}} + \tilde{\omega}^n \Delta \tilde{\alpha} - \Delta \tilde{\alpha} \tilde{\omega}^n \quad . \quad (2.5.10)$$

The vector dual to the above skew-symmetric tensor is given as

$$\omega \simeq \omega^n + \Delta \dot{\alpha} + \tilde{\omega}^n \Delta \alpha \quad . \quad (2.5.11)$$

Linearization of the angular acceleration is derived in the same manner from the definition

$$\dot{\tilde{\omega}} = -\ddot{\mathbf{R}} \mathbf{R}^T - \dot{\mathbf{R}} \dot{\mathbf{R}}^T \quad ,$$

and the result is given in vector form as

$$\dot{\omega} \simeq \dot{\omega}^n + \ddot{\alpha} + \dot{\tilde{\omega}}^n \Delta \alpha + \tilde{\omega}^n \Delta \dot{\alpha} \quad . \quad (2.5.12)$$

From (2.5.11) and (2.5.12), the linear expansion of the rotational acceleration can then be derived as

$$M_J \simeq M_J^n + J \Delta \ddot{\Theta} + C^G \Delta \dot{\Theta} + K^C \Delta \Theta \quad (2.5.13)$$

where C^G and K^C represent gyroscopic damping and centrifugal stiffening matrices respectively given by

$$C^G = \tilde{\omega}^n J - \widetilde{J\omega^n} + J\tilde{\omega}^n \quad (2.5.14)$$

$$K^C = \tilde{\omega}^n J \tilde{\omega}^n - (\widetilde{J\omega^n}) \tilde{\omega}^n J + J\dot{\tilde{\omega}}^n \quad (2.5.15)$$

2.5.2 Tangent Stiffness

To obtain the linear portion of the internal force

$$\delta \mathbf{F}^S = \int_V T_{mi} \frac{\partial \delta r_i}{\partial \xi_k} \sigma_{mk}^a dV \quad , \quad (2.5.16)$$

linear perturbations of the convected frame transformation matrix, the spatial derivatives, the stress state, and the deformed volume from a given deformed position must be derived. The perturbation of the rotational tensor T_{ij} representing the convected reference frame is given as

$$T_{ij} \simeq (\delta_{ik} - \Delta \tilde{\beta}_{ik}) T_{kj}^n \quad (2.5.17)$$

where $\Delta \tilde{\beta}_{ik}$ are defined as linearized rotation increments of the convected reference frame. To obtain a linear perturbation of the spatial derivative, (2.5.1) is employed to give

$$\frac{\partial x_i}{\partial x_j^n} = (\delta_{ij} + \frac{\partial \Delta x_i}{\partial x_j^n}) \quad (2.5.18)$$

This is then inverted as

$$\frac{\partial x_i^n}{\partial x_j} \simeq (\delta_{ij} - \frac{\partial \Delta x_i}{\partial x_j^n}) \quad (2.5.19)$$

as the displacement increments Δx_i are assumed to be small. The spatial derivative can thus be approximated as

$$\frac{\partial}{\partial x_i} = \frac{\partial x_j^n}{\partial x_i} \frac{\partial}{\partial x_j^n} \simeq (\delta_{ij} - \frac{\partial \Delta x_i}{\partial x_j^n}) \frac{\partial}{\partial x_j^n} \quad (2.5.20)$$

The above can then be transformed to convected coordinates as

$$\begin{aligned} \frac{\partial}{\partial \xi_i} &= T_{ij} \frac{\partial}{\partial x_j} \\ &\simeq (\delta_{ik} - \Delta \tilde{\beta}_{ik}) T_{kj}^n (\delta_{pj} - \frac{\partial \Delta x_p}{\partial x_j^n}) \frac{\partial}{\partial x_p^n} \end{aligned} \quad (2.5.21)$$

by incorporating (2.5.17) and (2.5.20). The final approximation is given as

$$\frac{\partial}{\partial \xi_i} \simeq (\delta_{ik} - \Delta \tilde{\beta}_{ik} - T_{kp}^n \frac{\partial \Delta x_p}{\partial \xi_i^n}) \frac{\partial}{\partial \xi_i^n} \quad (2.5.22)$$

by transforming (2.5.21) back to convected coordinates and retaining all terms to first order. A consistent perturbation of the deformed volume is obtained in a similar manner as

$$\begin{aligned} dV &= \det \left(\frac{\partial x_i}{\partial x_j^n} \right) dV^n \\ &= \det \left(\delta_{ij} + T_{mi}^n \frac{\partial \Delta x_j}{\partial \xi_m^n} \right) dV^n \\ &\simeq \left(1 + T_{ms}^n \frac{\partial \Delta x_s}{\partial \xi_m^n} \right) dV^n \end{aligned} \quad (2.5.23)$$

A consistent perturbation to the Cauchy stress state is defined from the constitutive law (2.4.13) and (2.4.14) as

$$\sigma_{ij}^a \simeq \sigma_{ij}^{a^n} + \Delta \sigma_{ij}^a \quad (2.5.24)$$

The proper stress increment is deduced from the time derivative of the convected Cauchy stress components. This is obtained by rearranging (2.4.14) and conceptualizing ($\dot{} \Rightarrow \Delta$) to give

$$\begin{aligned} \Delta \sigma_{ij}^a &= (C_{ijkl} - \delta_{kl} \sigma_{ij}^a + \delta_{il} \sigma_{jk}^a + \delta_{jl} \sigma_{ik}^a) T_{ks} \frac{\partial \Delta x_s}{\partial \xi_i^n} \\ &\quad + \sigma_{lj}^a \Delta \tilde{\beta}_{li} + \sigma_{il}^a \Delta \tilde{\beta}_{lj} \end{aligned} \quad (2.5.25)$$

The linear perturbation of the internal force can be identified by substituting the approximations (2.5.17, 2.5.22 - 2.5.24) into (2.5.16). After an extensive set of calculations with some convenient algebraic cancellations, the result becomes

$$\delta F^S \simeq \delta F^{S^N} + \int_v T_{ki} \frac{\partial \delta x_i}{\partial \xi_l} c_{klmp} T_{ms} \frac{\partial \Delta x_s}{\partial \xi_p} + T_{ki} \frac{\partial \delta x_i}{\partial \xi_l} \sigma_{pl}^a T_{ks} \frac{\partial \Delta x_s}{\partial \xi_p} dv .$$

This is further simplified as

$$\delta F^S \simeq \delta F^{S^N} + \delta K^M + \delta K^G \quad (2.5.26)$$

$$\delta K^M = \int_v \delta \varepsilon_{kl}^a c_{klmp} \Delta \varepsilon_{mp}^a dv \quad (2.5.27)$$

$$\delta K^G = \int_v \frac{\partial \delta x_i}{\partial \xi_l} \sigma_{pl}^a \frac{\partial \Delta x_i}{\partial \xi_p} dv \quad (2.5.28)$$

in which the material tangent stiffness operator δK^M and the the geometric tangent stiffness operator δK^G have been identified.

Explicit expressions for the material and geometric tangent stiffness operators are given as follows. The material stiffness is simply

$$\delta K^M = \int_{\xi} \{ \delta u^T \quad \delta \alpha^T \} B^T C B \begin{Bmatrix} \Delta u \\ \Delta \alpha \end{Bmatrix} d\xi \quad (2.5.29)$$

where B is the strain-displacement operator defined in (2.3.28) and

$$C = \text{Diag} (EA , GA , GA , GJ , EI_2 , EI_3)$$

is the elastic constitutive matrix incorporating the area integration through the cross-section variables. To obtain the geometric tangent stiffness, (2.5.28) is written in terms of the relevant components as

$$\delta K^G = \int_v \sigma_{\xi\xi} \frac{\partial \delta \mathbf{r}}{\partial \xi} \cdot \frac{\partial \Delta \mathbf{r}}{\partial \xi} + \sigma_{\xi\eta} \left(\frac{\partial \delta \mathbf{r}}{\partial \xi} \cdot \frac{\partial \Delta \mathbf{r}}{\partial \eta} + \frac{\partial \delta \mathbf{r}}{\partial \eta} \cdot \frac{\partial \Delta \mathbf{r}}{\partial \xi} \right) + \sigma_{\xi\zeta} \left(\frac{\partial \delta \mathbf{r}}{\partial \xi} \cdot \frac{\partial \Delta \mathbf{r}}{\partial \zeta} + \frac{\partial \delta \mathbf{r}}{\partial \zeta} \cdot \frac{\partial \Delta \mathbf{r}}{\partial \xi} \right) . \quad (2.5.30)$$

The expressions (2.3.15 - 2.3.17) as well as (2.4.19) are then substituted into above and the integration through the cross-sectional area is performed. The result becomes

$$\begin{aligned}
 \delta K^G = & \int_{\xi} \frac{\partial \delta u^T}{\partial \xi} N_1 \frac{\partial \Delta u}{\partial \xi} + \\
 & \frac{\partial \delta u^T}{\partial \xi} T^T M^* \frac{\partial \Delta \beta}{\partial \xi} + \frac{\partial \delta u^T}{\partial \xi} T^T N^* \Delta \beta + \\
 & \frac{\partial \delta \beta^T}{\partial \xi} M^{*T} T \frac{\partial \Delta u}{\partial \xi} + \delta \beta^T N^{*T} T \frac{\partial \Delta u}{\partial \xi} + \\
 & \frac{\partial \delta \beta^T}{\partial \xi} \sigma_{\xi\xi}^0 J \frac{\partial \Delta \beta}{\partial \xi} + \\
 & \frac{\partial \delta \beta^T}{\partial \xi} O^* \Delta \beta + \delta \beta^T O^{*T} \frac{\partial \Delta \beta}{\partial \xi} d\xi \quad (2.5.31)
 \end{aligned}$$

where the stress dependent matrices introduced in the above are given as

$$\begin{aligned}
 N^* &= \begin{bmatrix} 0 & N_3 & -N_2 \\ -N_3 & 0 & 0 \\ N_2 & 0 & 0 \end{bmatrix}, \quad M^* = \begin{bmatrix} 0 & M_2 & M_3 \\ -M_2 & 0 & 0 \\ -M_3 & 0 & 0 \end{bmatrix} \\
 O^* &= \begin{bmatrix} \sigma_{\xi\eta}^{\ell_2} I_3 + \sigma_{\xi\zeta}^{\ell_3} I_2 & 0 & 0 \\ 0 & \sigma_{\xi\zeta}^{\ell_3} I_2 & -\sigma_{\xi\eta}^{\ell_3} I_2 \\ 0 & -\sigma_{\xi\zeta}^{\ell_2} I_3 & \sigma_{\xi\eta}^{\ell_2} I_3 \end{bmatrix}
 \end{aligned}$$

Finally, the convected frame virtual rotations $\delta\beta$ and their spatial derivatives are transformed back to the cross-section reference frame via (2.3.26) or (2.3.27). The tangent stiffness matrices K^M and K^G can thus be identified from the above derivations such that the linearized internal force is given as

$$\begin{aligned}
 \delta F^S &= \int_{\xi} \{ \delta u^T \quad \delta \alpha^T \} S d\xi \\
 &\simeq \{ \delta u^T \quad \delta \alpha^T \} \left\{ S^n + [K^G + K^M] \begin{Bmatrix} \Delta u \\ \Delta \alpha \end{Bmatrix} \right\} \quad (2.5.32)
 \end{aligned}$$

2.7 Concluding Remarks

A formulation for the dynamics of flexible beams that admits the effects of large rigid-body motions as well as large deformations has been presented. The present formulation adopts an inertial reference frame for describing the translational motions and a body-fixed frame for the rotational motions. As such, the beam inertia operator is identical in form to that of rigid body dynamics and the formulation is easily adapted into the methodologies of general multibody dynamics. To effect the kinematic description, nonlinear strain theories are incorporated from the outset which account for both finite rotations and large deformations. The present nonlinear strain measures are deduced from the form of the virtual work of the internal force of the beam as parameterized by the kinematic definition. A rate-type constitutive law is employed to complete the formulation. A key feature of the formulation is the use of a convected reference for the stress representation. This leads to conceptual simplifications which enable a Cauchy stress representation of the beam deformation as opposed to the classical Piola-Kirchhoff stress representations typically used in finite-deformation analysis. A consistent linearization of the equations are presented for reference in future chapters in which the tangent stiffness matrices are inherently symmetric as a consequence of the Cauchy stress representation.

The next chapter discusses the discretization of the equations of motion and the numerical procedures developed for the computation of the discrete internal force expression.

CHAPTER III

COMPUTATIONAL TREATMENT OF THE DISCRETE INTERNAL FORCE

3.1 Introduction

The previous chapter has presented a formalism for modeling the spatial dynamics of flexible beams. The formalism accounts for both the finite rotations and the finite deformations of a beam component. The dynamics of the beam motion are described using an inertial reference for translational displacements and a body-fixed reference for rotational quantities. To effect this description, finite strain rod theories are defined.

The numerical treatment of the formalism is now considered in detail in the next two chapters. The present chapter is devoted to the numerical treatment of the internal force operator, and the next chapter discusses the dynamic solution procedures. For the effective treatment of the internal force, a computational invariance to rigid body motion must be satisfied within a discrete beam model to achieve realistic static and dynamic simulations. As the degrees of freedom contain information of both rigid motion and strain deformation, the internal force computation depends on a judicious procedure which filters out the rigid motions implicitly embedded within the variables. This internal force computation can then be interfaced with multibody dynamics solution procedures, to be discussed in Chapter IV, with confidence that spurious strains are not computationally generated in the process. For this purpose, a unique procedure for the computation of the internal force has been developed by exploiting characteristics of the

strain formulation as well as finite rotation theory.

The finite element method is employed to give a finite-dimensional representation of the continuum beam model. The variational form of the partial differential equations presented in Section 2.3 provides the basis for a displacement-based finite element methodology [64], resulting in a set of ordinary differential equations to be integrated by procedures discussed in Chapter IV. As such, the beam is represented as an assemblage of elements interconnected at nodal points on the element boundaries, and the degrees of freedom of the beam become the position and orientation coordinates of plane sections at the nodal points.

This procedure is a unique contribution to the computational research in the area of flexible multibody dynamics. Previous inertial reference beam formulations are based on total strain measures which are defined with respect to constant material coordinates of an initial configuration [25-27,31-36]. The invariance of the particular strain computation has not been specifically proven within these works. The present work is based on an incremental formulation, thus providing a more natural interpretation of large deformations by retaining the history of the motion in determining the current stress state. This formulation differs from the previous works in which the stress state is determined by comparing the current shape of the continuum to its original reference configuration. In a manner similar to the previous works, the present formulation employs non-commutative orthogonal matrices for the general representation of finite rotations. A complete freedom is thus allowed in choosing the parametrization of the orthogonal transformation which achieves the most effective computational scheme. The present work exploits this freedom by incorporating various

parameterizations to derive accurate methods for the computation of strain increments within the stress update procedure.

The stress within a beam finite element is computed from the nodal translational and rotational quantities as follows. Previous inertial reference beam formulations are based on total strain measures which are defined with respect to constant material coordinates of an initial configuration [25-27,31-36]. As such, the stress state is determined by comparing the current shape of the continuum to its original reference configuration in these works. The present work is based on an incremental formulation, thus providing a more natural interpretation of large deformations by retaining the history of the motion in determining the current stress state. As discussed in Section 2.4, the present formulation adopts an incremental procedure based on rate-type constitutive laws in which the current stress state is updated from the past stress state via a strain increment and appropriate constitutive matrix. A computational procedure has been designed from this incremental interpretation of the continuum-based formulation such that the computed finite strain increments are invariant to arbitrary rigid body motions implicitly contained within the finite displacements. To achieve this invariance, various rotational parameterizations are incorporated in deriving accurate methods for the computation of strain increments within the stress update procedure. As will be shown, the success of the computation hinges on a proper extraction of the rotation increments from the various rotational matrices embedded in the formulation. Given the strain increments, the elemental internal force is then formed via the multiplication of a discrete strain-displacement operator with the updated stress state.

The computation of the elemental internal force thus involves the

proper treatment of large rotations. A great deal of literature exists on the subject of finite rotations. An extensive derivation of the kinematics of large rotations is presented in [55], and an overview of different methods for parameterizing an arbitrary rotational orientation is given in [56]. A brief overview of the various parameterizations employed in previous works involving large rotations is given as follows. Euler angles or Bryant angles, which are based on successive angular rotations about a predetermined set of axes, were historically used for specialized rigid body systems and attitude dynamics [47-48]. To alleviate problems associated with the non-commutative nature of this type of definition, commutative semitangential rotations were derived and applied to a large displacement-small strain structural theory [54]. The rotational vector, which is based on the Euler-Chasles description of a single rotation about an appropriate axis [55], has been used within fully nonlinear beam and shell theories [31-34,57]. While the angle-based geometrical interpretation of these parameterizations is recognized, the rotational transformation matrix and subsequent angular velocity and acceleration vectors are complicated trigonometric functions of these rotation parameters. To avoid the complications of these nonlinear functions, alternative parameterizations were developed such that the rotational matrix, the angular velocity vector, and the angular acceleration vector become algebraic functions of the rotation parameters. Examples of these alternative parameterizations include the Rodrigues parameters [28,55], the conformal rotation vector [36,58], and the Euler parameters [59-63]. In general, the algebraic nature of these parameterizations is exploited when developing computational strategies for general finite element and articulated system models. The present formulation incorporates both the Rodrigues parame-

ter and the Euler parameter representations in developing an efficient computation of the internal force which remains invariant to arbitrary rigid body motions. The Euler parameter representation is further exploited in Chapter IV for the integration of general spatial kinematic systems.

The computational procedure developed in this chapter is compared to previous works through an analysis of static problems. The nonlinear static equilibrium equations are solved in an iterative manner using the Newton-Rhapson technique. The procedure is included for verification purposes as the present formulation is intended more for use with multibody dynamic applications rather than to compete with existing large rotation and deformation beam finite elements used within static analysis.

The rest of the chapter is organized as follows. Section 3.2 gives an overview of the rotational vector and Euler parameter representations of finite rotations. The constant-strain finite element discretization of the equations of motion is presented in Section 3.3. The algorithmic treatment of the internal force is detailed in Section 3.4, and the static solution verification is given in Section 3.5.

3.2 Finite Rotation Representations

The Euler-Chasles theorem states that any finite rotation can be uniquely represented with a rotation angle θ and a rotation axis \mathbf{n} [47-48]. This representation is shown below in Figure 3.1.

From this picture, we see a new vector \mathbf{r}' is obtained by rotating a given vector \mathbf{r} by an angle θ about an axis \mathbf{n} . The mathematical description of this process is given by [47-48]

$$\mathbf{r}' = \mathbf{R} \cdot \mathbf{r} \quad (3.2.1)$$

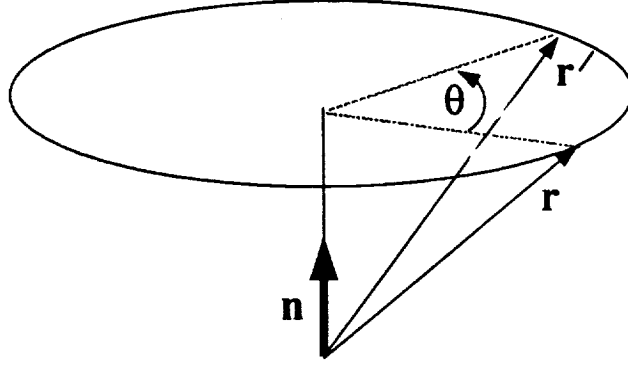


Figure 3.1 Euler-Chasles rotation representation

where \mathbf{R} denotes the dyadic form of the rotational operator given as

$$\mathbf{R}(\mathbf{n}, \theta) = \mathbf{n}\mathbf{n} + \cos \theta (\mathbf{I} - \mathbf{n}\mathbf{n}) + \sin \theta (\mathbf{I} \times \mathbf{n}) \quad (3.2.2)$$

with \mathbf{I} representing the (3×3) identity operator. The above definition is consistent with that of the angular velocity given in (2.2.9). The matrix representation of the above definition is given as

$$\mathbf{R} = \mathbf{I} + \frac{\sin \theta}{\theta} \tilde{\Theta}^T + \frac{1 - \cos \theta}{\theta^2} \tilde{\Theta} \tilde{\Theta} \quad (3.2.3)$$

In this representation, the parameter

$$\Theta \equiv \mathbf{n} \theta = \begin{Bmatrix} \Theta_1 \\ \Theta_2 \\ \Theta_3 \end{Bmatrix}$$

is termed the rotational vector, and $\tilde{\Theta}$ is the skew-symmetric dual matrix

$$\tilde{\Theta} = \begin{bmatrix} 0 & -\Theta_3 & \Theta_2 \\ \Theta_2 & 0 & -\Theta_1 \\ -\Theta_2 & \Theta_1 & 0 \end{bmatrix}$$

defined from the three components of the rotational vector. The matrix (3.2.3) is equivalent to the following series expansion [55]

$$\mathbf{R} = \mathbf{I} + \tilde{\Theta}^T + \frac{1}{2!} \tilde{\Theta}^T{}^2 + \frac{1}{3!} \tilde{\Theta}^T{}^3 + \dots + \frac{1}{n!} \tilde{\Theta}^T{}^n + \dots$$

The above representation is precisely the matrix exponential

$$\mathbf{R} = \exp(\tilde{\Theta}^T) \quad , \quad (3.2.4)$$

and thus the rotation matrix is a nonlinear exponential function of the rotational vector components.

An incremental rotation which relates an existing body-frame basis \mathbf{b}^n to a new basis \mathbf{b}^{n+1} is defined as follows [56]. Given that the existing basis is defined with respect to an inertial basis \mathbf{e} by the rotation matrix \mathbf{R}^n as $\mathbf{b}^n = \mathbf{R}^n \mathbf{e}$, and likewise a new basis is defined as $\mathbf{b}^{n+1} = \mathbf{R}^{n+1} \mathbf{e}$, the rotation matrix \mathbf{R}^{n+1} is obtained from the product of an incremental rotation matrix \mathbf{R} and the existing rotation matrix \mathbf{R}^n . This matrix product can be performed as

$$\mathbf{R}^{n+1} = \mathbf{R}_{(l)} \mathbf{R}^n \quad (3.2.5)$$

in which the incremental rotation operator $\mathbf{R}_{(l)}$, termed a spatial rotation, is applied to the existing body frame \mathbf{b}^n . A material rotation can also be defined in which an incremental operator $\mathbf{R}_{(r)}$ is applied to the inertial reference frame as

$$\mathbf{R}^{n+1} = \mathbf{R}^n \mathbf{R}_{(r)} \quad (3.2.6)$$

The rotational vectors Θ and Φ that correspond to the spatial or material incremental rotations $\mathbf{R}_{(l)}$ and $\mathbf{R}_{(r)}$, respectively, can be introduced as

$$\mathbf{R}_{(l)} = e^{\tilde{\Theta}^T} \quad \mathbf{R}_{(r)} = e^{\tilde{\Phi}^T} \quad (3.2.7)$$

The two rotational vectors are related via $\Theta = \mathbf{R}^n \Phi$.

While the definition of the rotational vector is straightforward, the drawback to this parameterization is the nonlinear expression for the rotational matrix. To avoid the nonlinearity seen in (3.2.3) or (3.2.4), alternative parameterizations have been developed which lead to algebraic expressions of the rotational matrix. For example, the Rodrigues parameters are defined as

$$\Theta_t = \theta_t \mathbf{n} \quad , \quad \theta_t \equiv \tan \frac{\theta}{2} \quad (3.2.8)$$

such that the rotational matrix is given as a function of these parameters as

$$\mathbf{R} = \mathbf{I} + \frac{2}{1 + \theta_t^2} (\tilde{\Theta}_t^T + \tilde{\Theta}_t \tilde{\Theta}_t) \quad . \quad (3.2.9)$$

The drawback to the above parameterization is that it becomes singular whenever the magnitude of the rotation becomes an odd multiple of π . In general, a singularity condition is encountered within any three-parameter representation of orthonormal rotation matrices [65]. An alternative non-minimal parameterization, termed the Euler parameters, remains singularity free throughout all possible orientations. The Euler parameters are defined as

$$q_0 = \cos \frac{\theta}{2} \quad , \quad \mathbf{q} = \sin \frac{\theta}{2} \mathbf{n} \quad , \quad (3.2.10)$$

and the four parameters are subject to the constraint

$$q_0^2 + \mathbf{q}^T \mathbf{q} = 1 \quad . \quad (3.2.11)$$

The rotation matrix is given as a function of the Euler parameters as

$$\mathbf{R} = \mathbf{I} + 2 q_0 \tilde{\mathbf{q}}^T + 2 \tilde{\mathbf{q}} \tilde{\mathbf{q}} \quad . \quad (3.2.12)$$

Given these examples, for computational purposes it is necessary to extract the various rotational parameterizations from given rotational matrices. If an inverse exists, the rotational vector can be obtained from (3.2.4) as

$$\tilde{\Theta}^T = \log_e \mathbf{R} = \frac{1}{\tau} \sin^{-1} \frac{\tau}{2} \tilde{\mathbf{R}}^a \quad (3.2.13)$$

where

$$\tilde{\mathbf{R}}^a \equiv \mathbf{R} - \mathbf{R}^T \quad (3.2.14)$$

is formed from the anti-symmetric part of \mathbf{R} and τ is the norm of the dual vector to $\tilde{\mathbf{R}}^a$ [66]. For the Rodrigues parameters, the inverse of (3.2.8) is the following algebraic expression [28]

$$\tilde{\Theta}_t^T = \frac{\tilde{\mathbf{R}}^a}{1 + \text{tr } \mathbf{R}} \quad (3.2.15)$$

For the Euler parameters, a very robust method involving only algebraic computations has been derived in [67] to extract the Euler parameters from the rotation matrix.

To complete this introduction to finite rotations and their parameterizations, it remains to express the angular variation, angular velocity, and curvature vectors as functions of the given rotational parameterizations. The body-fixed components of the skew-symmetric tensors representing the angular variation, angular velocity, and curvature are defined as

$$\delta \tilde{\alpha}^T = \delta \mathbf{R} \mathbf{R}^T, \quad \tilde{\omega}^T = \dot{\mathbf{R}} \mathbf{R}^T, \quad \tilde{\kappa}^T = \frac{\partial \mathbf{R}}{\partial \xi} \mathbf{R}^T,$$

respectively. These definitions constitute spatial representations; the corresponding material representation is given as

$$\delta \tilde{\alpha}_e^T = \mathbf{R}^T \delta \tilde{\alpha}^T \mathbf{R} = \mathbf{R}^T \delta \mathbf{R}$$

for the angular variation with corresponding definitions for the material angular velocity and curvature tensors. From the above definitions, it is seen that the derivative of the rotation matrix is necessary to obtain explicit expressions for these functions in terms of a desired parameterization.

For the rotational vector parameterization, the derivative of the exponential map is derived in [31,66]. The spatial angular variation is then given as a function of the spatial rotational vector and its derivative as

$$\delta \tilde{\alpha} = \frac{\theta - \sin \theta}{\theta^3} (\Theta \cdot \delta \Theta) \tilde{\Theta} + \frac{\sin \theta}{\theta} \delta \tilde{\Theta} + \frac{1 - \cos \theta}{\theta^2} (\tilde{\Theta} \delta \tilde{\Theta} - \delta \tilde{\Theta} \tilde{\Theta}) . \quad (3.2.16)$$

The equivalent vector expression for the above skew-symmetric tensor is given as

$$\delta \alpha = \mathbf{T}_r (\Theta) \delta \Theta \quad (3.2.17)$$

where

$$\mathbf{T}_r (\Theta) = \frac{\theta - \sin \theta}{\theta^3} \Theta \Theta^T + \frac{\sin \theta}{\theta} \mathbf{I} + \frac{1 - \cos \theta}{\theta^2} \tilde{\Theta}^T .$$

The material components of the angular variation are related to the material-based rotational vector definition in the same manner as $\delta \alpha_e = \mathbf{T}_r (\Phi) \delta \Phi$ [56]. Analogous expressions exist for the angular velocity and curvature tensors.

For the Rodrigues parameters, the functional relation

$$\delta \alpha = \mathbf{T}_t (\Theta_t) \delta \Theta_t \quad (3.2.18)$$

results [56], where

$$\mathbf{T}_t (\Theta_t) = \frac{2}{1 + \theta_t^2} (\mathbf{I} + \tilde{\Theta}_t^T) . \quad (3.2.19)$$

The identical relation holds for the material components of the angular variation using the material components of the Rodrigues parameters.

The corresponding functional relation in terms of the Euler parameters is given as

$$\begin{Bmatrix} 0 \\ \delta\alpha \end{Bmatrix} = 2 \begin{bmatrix} q_0 & \mathbf{q}^T \\ -\mathbf{q} & q_0\mathbf{I} - \tilde{\mathbf{q}} \end{bmatrix} \begin{Bmatrix} \delta q_0 \\ \delta\mathbf{q} \end{Bmatrix} \quad (3.2.20)$$

This expression can be inverted to give the Euler parameter derivatives in terms of the body-frame angular variation components as

$$\begin{Bmatrix} \delta q_0 \\ \dot{\mathbf{q}} \end{Bmatrix} = \frac{1}{2} \begin{bmatrix} 0 & -\delta\alpha^T \\ \delta\alpha & \delta\tilde{\alpha}^T \end{bmatrix} \begin{Bmatrix} q_0 \\ \mathbf{q} \end{Bmatrix} \quad (3.2.21)$$

in which the constraint conditions

$$q_0^2 + \mathbf{q}^T\mathbf{q} = 1, \quad \delta q_0 q_0 + \delta\mathbf{q}^T\mathbf{q} = 0 \quad (3.2.22)$$

are embedded. The corresponding inversions of (3.2.17) and (3.2.18) have been derived in [66].

The Euler parameters do not possess any singularity limitation within their definition, nor within the forward or inverse transformations between the angular and parameter variation. As such, the Euler parameters are the only set that allows the treatment of rotations of arbitrary magnitude without resorting to any special precautions. In contrast, the Rodrigues parameters possess an unavoidable singularity in their definition [28], and the rotational vector parameterization possess a “hole in differentiability” in which the transformation matrix of (3.2.17) becomes singular [34]. Thus, the Euler parameter representation of the angular velocity and curvature has been chosen in the present work in developing the computational procedures to be discussed shortly. For the representation of incremental rotations, both the rotational vector and the Rodrigues parameters

are introduced where appropriate, again with the motivation of achieving effective computations dictating the particular choice of the parameterization. These concepts are referred to and further illuminated in the following sections.

3.3 Finite Element Discretization

A finite element representation of the continuous beam model is obtained from the variational form of the partial differential equations presented in Section 2.3. The present study is based on the use of linear shape functions in approximating the displacement field within a beam finite element [64], viz.,

$$u = \sum_{I=1}^{npe} N_I(x) u_I(t) \quad (3.3.1)$$

where N_I denotes the spatial linear shape functions, u_I represents the degrees of freedom at the element nodes, and npe denotes the number of nodes per element. In the present beam formulation, the rotational variables are treated independently from the translational variables. As such, only C_0 displacement continuity across element boundaries is required for the shape function approximations. Thus, the linear interpolation functions result in a consistent approximation which leads to a constant strain finite element.

As defined above in (3.3.1), the interpolation of the translational quantities is straightforward as the components are expressed with respect to a common reference frame. However, the interpolation of the rotational variations requires special consideration. The virtual rotation components $\delta\alpha$ used within the present formulation are defined with respect to a body-fixed reference frame which is continuously changing along the beam neutral axis. As such, these virtual rotation components cannot be directly inter-

polated, but rather must be transformed to a parameterization defined with respect to a fixed configuration prior to the interpolation. To this end, the virtual rotations can be parameterized in terms of the rotational vector via (3.2.17), where Θ is the rotational vector orienting the moving basis from a common reference as the inertial frame. The components of the rotational vector are defined with respect to a fixed coordinate system as

$$\Theta \equiv \theta \mathbf{n} = \theta_i^e \mathbf{e}_i \quad ,$$

and hence the variations of the rotational vector can be interpolated as

$$\delta\Theta = \sum_{I=1}^{npe} N_I \delta\Theta_I \quad .$$

From the above, the virtual rotations $\delta\alpha$ can then be interpolated as

$$\begin{aligned} \delta\alpha &= \mathbf{T}(\Theta) \delta\Theta \\ &\simeq \sum_{I=1}^{npe} \mathbf{T}(\Theta) N_I \delta\Theta_I \\ &= \sum_{I=1}^{npe} N_I \mathbf{T}(\Theta) \mathbf{T}^{-1}(\Theta_I) \delta\alpha_I \quad . \end{aligned}$$

If $\Theta \Rightarrow \Theta_I$, the product $\mathbf{T}(\Theta) \mathbf{T}^{-1}(\Theta_I) \Rightarrow \mathbf{I}$ [34]. Thus, if the relative change of the cross-section orientation along the finite element remains small, the virtual rotations are approximated in the same manner as the displacements as

$$\delta\alpha \simeq \sum_{I=1}^{npe} N_I \delta\alpha_I \quad . \quad (3.3.2)$$

The angular velocity and angular acceleration are then also interpolated as

$$\omega \simeq \sum_{I=1}^{npe} N_I \omega_I \quad , \quad \dot{\omega} \simeq \sum_{I=1}^{npe} N_I \dot{\omega}_I \quad . \quad (3.3.3)$$

From this introduction to the finite element approximations, a discrete form of the present beam formulation is readily obtained as follows.

3.3.1 Discrete Equations of Motion

A discrete form of the variational equations (2.3.1) is obtained from the finite element approximations

$$\delta u = \sum_{I=1}^{npe} N_I \delta u_I, \quad \delta \alpha = \sum_{I=1}^{npe} N_I \delta \alpha_I \quad (3.3.4)$$

for the virtual displacements and virtual rotations, respectively. As standard linear shape functions are chosen for N_I , u_I and $\delta \alpha_I$ represent the quantities at the two element nodes. From the above interpolations, a discrete form of the inertia, internal, and external force operators presented in Section 2.3 are obtained for a single finite element. Finite element assembly procedures are then applied to the element operators to achieve discrete variational equations in terms of the nodal degrees of freedom of the beam configuration. To this end, the discrete form of the elemental operators are given as follows.

The internal force operator of an individual finite element is obtained in terms of the virtual displacements and rotations at the element nodes from (2.3.25) and (3.3.4) as

$$\delta F^S = \sum_{I=1}^{npe} \{ \delta u_I \quad \delta \alpha_I \} \int_{\xi} [B_I^E]^T \left\{ \begin{matrix} N_\gamma \\ M_\kappa \end{matrix} \right\} d\xi \quad (3.3.5)$$

$$[B_I^E] = \begin{bmatrix} \mathbf{T} \frac{\partial N_I}{\partial \xi} & \tilde{\mathbf{i}}_1 N_I \mathbf{S}_I^T \\ \mathbf{0} & \mathbf{S}_I^T (\tilde{\kappa}_S N_I + \frac{\partial N_I}{\partial \xi}) \end{bmatrix} \quad (3.3.6)$$

By introducing linear shape functions into the above and integrating across the element length, the above equation can be written as

$$\delta F^S = \{ \delta u_1 \quad \delta u_2 \quad \delta \alpha_1 \quad \delta \alpha_2 \} [B^E] \left\{ \begin{matrix} N_\gamma \\ M_\kappa \end{matrix} \right\} \quad (3.3.7)$$

where

$$[B^E] = \begin{bmatrix} -\frac{1}{\ell} \mathbf{T} & \frac{1}{\ell} \mathbf{T} & \frac{1}{2} \tilde{i}_1 \mathbf{S}_1^T & \frac{1}{2} \tilde{i}_1 \mathbf{S}_2^T \\ 0 & 0 & \mathbf{S}_1^T (\frac{1}{2} \tilde{\kappa}_S - \frac{1}{\ell} \mathbf{I}) & \mathbf{S}_2^T (\frac{1}{2} \tilde{\kappa}_S + \frac{1}{\ell} \mathbf{I}) \end{bmatrix} \quad (3.3.8)$$

In deriving the above expression, an underintegration of the rotational variables associated with transverse shear strain has been performed to avoid the locking phenomena associated with the Timoshenko beam formulations. The convected frame \mathbf{T} matrix, body frame curvature tensor $\tilde{\kappa}_S$, element neutral-axis length ℓ , and resultant stresses N_γ and M_κ are constant quantities over the element domain, while the relative cross-section deformation \mathbf{S} matrices are nodal quantities as denoted by their subscripts.

In the same manner, the element external force operator is obtained from (2.3.29) and (3.3.4) as

$$\delta F^E = \sum_{I=1}^{npe} \{ \delta u_I \quad \delta \alpha_I \} \left\{ \begin{matrix} f_I^e \\ f_I^b \end{matrix} \right\}, \quad f_I^{e,b} = \int_{\xi} N_I f^{e,b} d\xi, \quad (3.3.9)$$

and the traction operator is implemented as boundary conditions on the nodes. Likewise, the element inertia operator is obtained from the (2.3.4), (3.3.3), and (3.3.4) as

$$\delta F^I = \sum_{I=1}^{npe} \sum_{K=1}^{npe} \left\{ \delta u_I^T \quad \rho A \quad M_{IK}^E \quad \frac{d^2 u_K}{dt^2} \right\} + \sum_{I=1}^{npe} \sum_{K=1}^{npe} \left\{ \delta \alpha_I^T \quad \rho J_I \quad M_{IK}^E \quad \frac{d^b \omega_K}{dt} \right\} +$$

$$\sum_{I=1}^{npe} \delta \alpha_I^T D_I^E \quad (3.3.10)$$

where

$$M_{IK}^E = \int_{\xi} N_I N_K d\xi, \quad D^E(\omega)_I = \int_{\xi} (\tilde{\omega} J \omega)_I d\xi$$

represent the element mass matrix and nonlinear angular acceleration vector. The former will be evaluated as a standard lumped mass matrix for the computational efficiency of explicit integration techniques to be described in Chapter IV, and the latter will be evaluated in a consistent manner by averaging the element nodal angular velocities.

When standard finite element assembly procedures are applied to the element operators presented above, one obtains the discrete variational equations

$$\begin{aligned} \{ \delta u_d^T \quad \delta \alpha_d^T \} & \left[\begin{array}{c} \left\{ \begin{array}{c} m_d \ddot{u}_d \\ J_d \dot{\omega}_d \end{array} \right\} + \left\{ \begin{array}{c} 0 \\ D_d(\omega) \end{array} \right\} + \left\{ \begin{array}{c} S_d^e \\ S_d^b \end{array} \right\} \end{array} \right] \\ & = \{ \delta u_d^T \quad \delta \alpha_d^T \} \left\{ \begin{array}{c} f_d^e \\ f_d^b \end{array} \right\} \end{aligned} \quad (3.3.11)$$

where δu_d and $\delta \alpha_d$ now represent the nodal virtual displacements and rotations of the assembled finite elements modeling the beam configuration. The following notation has also been introduced in the above equation; m_d and J_d represent the assembled mass and inertia matrices; \ddot{u}_d and $\dot{\omega}_d$ represent the nodal acceleration vectors; $D_d(\omega)$ represents the assembled nonlinear acceleration, and $S_d^{e,b}$ and $f_d^{e,b}$ represent the assembled internal and external force vectors partitioned into translational and rotational parts, respectively. As δu_d and $\delta \alpha_d$ represent arbitrary independent variations, the final discrete equations of motion are given as

$$\begin{bmatrix} m_d & 0 \\ 0 & J_d \end{bmatrix} \begin{Bmatrix} \ddot{u}_d \\ \dot{\omega}_d \end{Bmatrix} + \begin{Bmatrix} 0 \\ D_d(\omega) \end{Bmatrix} + \begin{Bmatrix} S_d^e \\ S_d^b \end{Bmatrix} = \begin{Bmatrix} f_d^e \\ f_d^b \end{Bmatrix} . \quad (3.3.12)$$

These equations can be specialized to the case of static equilibrium as

$$S_d = f_d . \quad (3.3.13)$$

The static equilibrium equations provide the basis for the remainder of the chapter which is devoted to the computation of the internal force. The extension of the computational procedure to include the dynamics of the inertia operator is presented in Chapter IV.

To present the algorithmic treatment of the discrete internal force S_d , the rest of the chapter is organized as follows. The evaluation of (3.3.8) is detailed by presenting the computation of the discrete rotation matrices in Section 3.3.2 and the computation of the element curvature in Section 3.3.3. The computation of the resultant element stresses N_γ and M_κ , necessary to complete (3.3.7), is then presented in Section 3.4. Finally, the numerical solution of the static equations (3.3.13) is presented in Section 3.5.

3.3.2 Discrete Rotation Matrix Computations

The rotational matrices representing the various reference frames introduced in the present formulation are computed as follows. The computational procedure for the solution of the discrete equations of motion will be discussed in Chapter IV. From this solution procedure, the orientation of the cross-section and the displacement of the neutral-axis at the finite element nodes are output as known quantities. The matrices \mathbf{R}_i , representing the cross-sectional orientation at each element node, are computed directly from the rotational parameterization of the given solution method.

The rigid motion of the convected reference frame \mathbf{a} of a given finite element is then deduced as follows. The translational displacements are used to compute the tangent to the neutral axis \mathbf{a}_1 ; for the linear finite element interpolations the tangent is simply the straight line connecting the two element nodes. The remaining two basis \mathbf{a}_2 and \mathbf{a}_3 of the convected reference frame are then constructed from the tangent \mathbf{a}_1 and the cross-sectional orientation \mathbf{R}_1 . The \mathbf{a}_2 vector is defined as the cross product of \mathbf{a}_1 with the \mathbf{b}_3 axis of \mathbf{R}_1 , and the \mathbf{a}_3 axis is then defined to complete the right-hand coordinate system. The computed axes $\{ \mathbf{a}_1, \mathbf{a}_2, \mathbf{a}_3 \}$, as shown below in Figure 3.2, define the rows of the \mathbf{T} matrix.

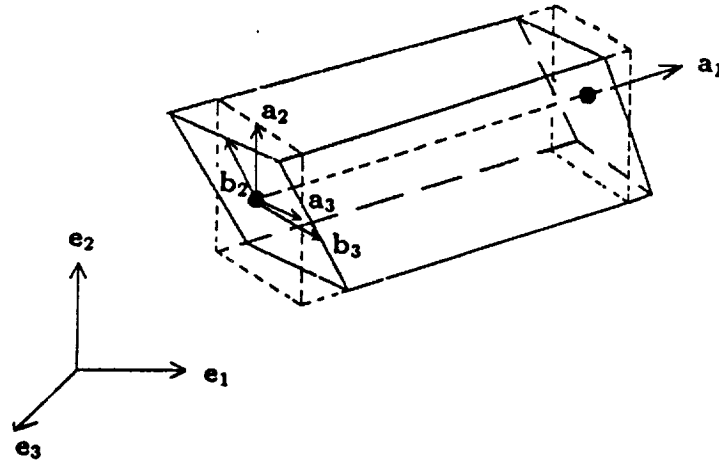


Figure 3.2 Convected Reference Frame

The rotation matrices \mathbf{S}_i , defined at each element node as the relative difference between the element convected frame and the nodal body frames, are thus

$$\mathbf{S}_i = \mathbf{R}_i \mathbf{T}^T, \quad i = 1, 2 \quad . \quad (3.3.14)$$

The computation is an approximation applicable for moderate strains such that the \mathbf{S}_i matrices contain information solely due to transverse shear and torsional deformations [28].

3.3.3 Discrete Curvature Computation

To complete the evaluation of (3.3.8), the discrete computation of the element curvature is presented as follows. The body frame components of the curvature tensor $\tilde{\kappa}_S^T$ can be equivalently defined using the \mathbf{R} or \mathbf{S} matrices as

$$\tilde{\kappa}_S^T = \begin{bmatrix} 0 & \kappa_3 & -\kappa_2 \\ -\kappa_3 & 0 & \kappa_1 \\ \kappa_2 & -\kappa_1 & 0 \end{bmatrix} = \frac{\partial^a \mathbf{S}}{\partial \xi} \mathbf{S}^T = \frac{\partial^e \mathbf{R}}{\partial \xi} \mathbf{R}^T \quad (3.3.15)$$

since by construction the convected frame \mathbf{T} matrix is constant along the element domain where the differentiation is performed. Thus the curvature, which was originally defined from the shear matrix in (2.3.27), can be directly computed from the nodal rotational variables of \mathbf{R} denoting the total cross-section orientation. This is advantageous as the Euler parameters of \mathbf{R} are directly available from the generalized coordinate integrator discussed in Chapter IV, whereas additional computations are required to obtain the Euler parameters corresponding to the \mathbf{S} matrix.

The Euler parameter representation of finite rotations can be exploited to achieve a simple and robust computation of the element curvature. The Euler parameter - curvature relation, introduced in (3.2.20), is given as

$$\begin{Bmatrix} 0 \\ \kappa \end{Bmatrix} = \mathbf{E}(q) \frac{\partial q}{\partial \xi}, \quad \kappa = \begin{Bmatrix} \kappa_1 \\ \kappa_2 \\ \kappa_3 \end{Bmatrix} \quad (3.3.16)$$

where

$$\mathbf{E}(\mathbf{q}) = 2 \begin{bmatrix} q_0 & \mathbf{q}^T \\ -\mathbf{q} & q_0 \mathbf{I} - \tilde{\mathbf{q}} \end{bmatrix}, \quad \frac{\partial \mathbf{q}}{\partial \xi} = \left\{ \begin{array}{c} \frac{\partial q_0}{\partial \xi} \\ \frac{\partial \mathbf{q}}{\partial \xi} \end{array} \right\}.$$

The above is evaluated from the Euler parameters of the element nodes by using the normalized average

$$q_a = \frac{\frac{1}{2} (q_1 + q_2)}{\left\| \frac{1}{2} (q_1 + q_2) \right\|} \quad (3.3.17)$$

for the matrix \mathbf{E} and the approximation

$$\frac{\partial \mathbf{q}}{\partial \xi} = \frac{1}{\ell} (q_2 - q_1) \quad (3.3.18)$$

for the derivative. Within the geometric context of rotations, the Euler parameters q_a of (3.3.17) correspond to an orientation averaged from the two nodes. The computation of (3.3.16) from (3.3.17) and (3.3.18) is consistent in that the constraint conditions

$$q_0^2 + \mathbf{q}^T \mathbf{q} = 1, \quad \frac{\partial q_0}{\partial \xi} q_0 + \frac{\partial \mathbf{q}}{\partial \xi}^T \mathbf{q} = 0$$

are identically satisfied in the discrete sense. Due to the singularity free nature of Euler parameters, the computation is valid for any size nodal rotation. The use of an alternative rotational parameterization for the computation of the element curvature requires special treatment to avoid the inherent singularities within the representation [34].

To show the robustness of the averaging scheme adopted herein, we offer the following analysis. By examining the rigid rotation of a finite element in a state of constant curvature, it can be shown the computational strategy effectively filters out the large rigid-body motions implicitly contained within the nodal Euler parameters. For this purpose, the total

orientation of the nodal cross-sections are described by separating from the outset the effects due to rigid motion and that due to deformation. The orientation of the convected element frame is characterized by a rotation of an angle ϕ about an axis \mathbf{n}_a from the inertial reference frame, and the relative nodal cross-section orientations are characterized by a rotation from the convected frame of angles $-\tau$ and τ about axis \mathbf{n}_b for nodes 1 and 2, respectively, as shown below in Figure 3.3.

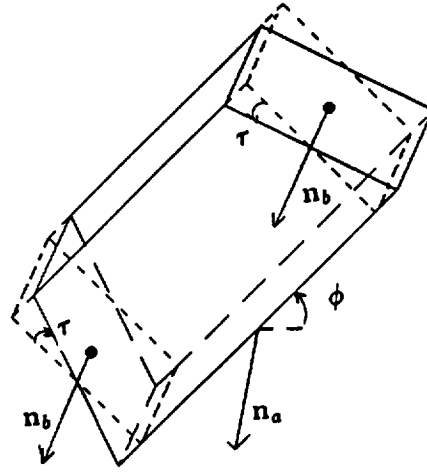


Figure 3.3 Pure Bending of Beam Element

From these definitions, the Euler parameters q_{r_1} and q_{r_2} representing the relative nodal orientations and q_a representing the convected orientation are given as

$$q_{r_1} = \begin{Bmatrix} \cos \frac{\tau}{2} \\ -\sin \frac{\tau}{2} \mathbf{n}_b \end{Bmatrix}, \quad q_{r_2} = \begin{Bmatrix} \cos \frac{\tau}{2} \\ \sin \frac{\tau}{2} \mathbf{n}_b \end{Bmatrix}, \quad q_a = \begin{Bmatrix} \cos \frac{\phi}{2} \\ \sin \frac{\phi}{2} \mathbf{n}_a \end{Bmatrix}$$

The Euler parameters q_1 and q_2 designating the total cross section orientation of the two nodes due to these combined effects can be obtained by

applying the quaternion product rule [68] to the above definitions to yield

$$q_1 = \left\{ \begin{array}{l} \cos \frac{\phi}{2} \cos \frac{\tau}{2} + \mathbf{n}_a \cdot \mathbf{n}_b \sin \frac{\phi}{2} \sin \frac{\tau}{2} \\ -\cos \frac{\phi}{2} \sin \frac{\tau}{2} \mathbf{n}_b + \cos \frac{\tau}{2} \sin \frac{\phi}{2} \mathbf{n}_a - \sin \frac{\tau}{2} \sin \frac{\phi}{2} \mathbf{n}_a \times \mathbf{n}_b \end{array} \right\}$$

$$q_2 = \left\{ \begin{array}{l} \cos \frac{\phi}{2} \cos \frac{\tau}{2} - \mathbf{n}_a \cdot \mathbf{n}_b \sin \frac{\phi}{2} \sin \frac{\tau}{2} \\ \cos \frac{\phi}{2} \sin \frac{\tau}{2} \mathbf{n}_b + \cos \frac{\tau}{2} \sin \frac{\phi}{2} \mathbf{n}_a + \sin \frac{\tau}{2} \sin \frac{\phi}{2} \mathbf{n}_a \times \mathbf{n}_b \end{array} \right\}$$

The average of the above nodal parameters is simply

$$\frac{1}{2} (q_1 + q_2) = \left\{ \begin{array}{l} \cos \frac{\phi}{2} \cos \frac{\tau}{2} \\ \cos \frac{\tau}{2} \sin \frac{\phi}{2} \mathbf{n}_a \end{array} \right\},$$

the norm of which is $\cos \frac{\tau}{2}$. It is seen the normalized average precisely represents the orientation of the cross-section at mid-element which contains no relative deformation as equal but opposite relative rotations were applied to the ends of the element. The normalized average of the nodal Euler parameters thus corresponds to an orientation geometrically midway between that of the two nodes. It is then easily shown from the constructed parameters that the computed curvature for the pure bending of the finite element becomes

$$\kappa = \frac{4}{\ell} \sin \frac{\tau}{2} \mathbf{n}_b$$

as opposed to the true curvature of $\frac{2}{\ell} \tau \mathbf{n}_b$. It is noted that the above computation retains only the rotation parameters τ originally defined relative to the rigid body orientation, and is thus invariant to any rigid body motions. The approximation is valid for small relative rotations of the cross-sections. For instances when the validity of the approximation is challenged, an incremental curvature computation can be made as discussed in the next section, from which the total curvature is obtained from an appropriate update procedure.

3.4 Incremental Strain Computations

To complete the algorithmic treatment of the nonlinear stiffness operator, it remains to discuss the computation of the element stresses. The stress update procedure, discussed in Section 2.4, requires an effective computation of the increment of strain between a past converged solution and a current solution. A specific computational strategy has been developed for use with this incremental interpretation of the continuum-based formulation. The fundamental property motivating this development is the condition that the finite strain increments be computed from the nodal degrees of freedom in a manner that is invariant to any arbitrary rigid body motions contained within these variables. Given an accurate computation of the incremental strains, the stress update procedure directly follows as discussed in Section 2.4.

The incremental strains are defined to approximate the time integration of the strain rate tensor over a given time interval. To effect this approximation within the present virtual work formulation, the kinematically admissible virtual displacements and rotations within the virtual strain displacement relations are defined to coincide with the actual displacements and rotations occurring within a finite increment of time. The strain increments are thus defined in the same manner as (2.3.20) and (2.3.21) as

$$\begin{aligned}\hat{\Delta}\gamma &= \mathbf{T} \frac{\partial \hat{\Delta}u}{\partial \xi} + \begin{Bmatrix} 0 \\ -\hat{\Delta}\beta_3 \\ \hat{\Delta}\beta_2 \end{Bmatrix} \\ \hat{\Delta}\kappa &= \frac{\partial \hat{\Delta}\beta}{\partial \xi}\end{aligned}$$

where $\hat{\Delta}u$ and $\hat{\Delta}\beta$ are finite displacement and rotation increments, respectively. For computational purposes, it becomes necessary to separate the

rotation due to rigid body motion from that due to deformation within the convected frame components of the incremental rotations $\hat{\Delta}\beta$. The convected frame virtual rotations $\delta\beta$ can be decomposed as

$$\delta\beta = \delta\tau_a + \delta\varphi \quad (3.4.1)$$

where $\delta\varphi$ and $\delta\tau_a$ are the convected frame components of the rigid body and deformation virtual rotations, respectively. These virtual rotations are defined as

$$\delta\tilde{\varphi}^T = \delta\mathbf{T} \mathbf{T}^T, \quad \delta\tilde{\tau}_a^T = \mathbf{S}^T \delta\mathbf{S}. \quad (3.4.2)$$

The definitions (3.4.1) and (3.4.2) have been derived from the identity

$$\mathbf{R} = \mathbf{S} \mathbf{T}, \quad \delta\mathbf{R} = \delta\mathbf{S} \mathbf{T} + \mathbf{S} \delta\mathbf{T}$$

and the following definitions

$$\delta\tilde{\alpha}^T = \delta\mathbf{R}\mathbf{R}^T, \quad \delta\tilde{\beta}^T = \mathbf{S}^T \delta\tilde{\alpha}^T \mathbf{S}$$

$$\delta\tilde{\tau}^T = \delta\mathbf{S} \mathbf{S}^T, \quad \delta\tilde{\tau}_a^T = \mathbf{S}^T \delta\tilde{\tau}^T \mathbf{S}.$$

With the decomposition (3.4.1) interpreted incrementally, the membrane and transverse shear strain increments are then given by

$$\hat{\Delta}\gamma = \mathbf{T} \frac{\partial \hat{\Delta}u}{\partial \xi} + \begin{Bmatrix} 0 \\ -\hat{\Delta}\varphi_3 \\ \hat{\Delta}\varphi_2 \end{Bmatrix} + \begin{Bmatrix} 0 \\ -\hat{\Delta}\tau_{a_3} \\ \hat{\Delta}\tau_{a_2} \end{Bmatrix} \quad (3.4.3)$$

Likewise, the incremental curvature representing the torsion and bending strains is given by

$$\hat{\Delta}\kappa = \frac{\partial \hat{\Delta}\tau_a}{\partial \xi} \quad (3.4.4)$$

as the incremental rotations $\Delta\varphi$ defined from the \mathbf{T} matrix are constant over the element length.

A proper definition and subsequent computation of the finite displacement and finite rotation increments introduced in these incremental strain definitions is essential. The incremental translations are defined as the difference between a current and past displacement configuration as

$$\hat{\Delta}u \equiv u^{n+1} - u^n . \quad (3.4.5)$$

The incremental rotations are interpreted from properly defined rotation matrices which represent the difference between current and past orientations. It is important to note that the angular variation definitions (3.4.2) are consistent with the following spatial and material rotation updates

$$\mathbf{T}^{n+1} = \Delta\mathbf{T} \mathbf{T}^n , \quad \mathbf{S}^{n+1} = \mathbf{S}^n \Delta\mathbf{S} , \quad (3.4.6)$$

respectively. In the above relations, the matrix $\Delta\mathbf{T}$ represents the relative orientation between the current and past convected reference frames, and $\Delta\mathbf{S}$ represents the relative orientation between the current deformation matrix \mathbf{S}^{n+1} and the past deformation matrix \mathbf{S}^n rigidly rotated to the current convected reference frame. The incremental rotations of the rigid body motion, $\hat{\Delta}\varphi$, are then defined as the rotational vector representation of the rotation matrix $\Delta\mathbf{T}$, while the incremental rotations of the deformational motion, $\hat{\Delta}\tau_a$, are defined as the Rodrigues parameter representation of the matrix $\Delta\mathbf{S}$. The latter choice is possible as it is highly improbable that a singularity is encountered due to large rotational deformations. The different parameterizations are chosen such that objective computations of the incremental strains (3.4.3) and (3.4.4) are achieved.

3.4.1 Membrane Strain Increments

To achieve an objective computation, the first two terms of (3.4.3), given as

$$\hat{\Delta}\gamma_1 = \mathbf{T} \frac{\partial \hat{\Delta}u}{\partial \xi} + \begin{Bmatrix} 0 \\ -\hat{\Delta}\varphi_3 \\ \hat{\Delta}\varphi_2 \end{Bmatrix}, \quad (3.4.7)$$

must be computed such that rotation increment $\hat{\Delta}\varphi$ compensates for the rigid motion contained within the displacement increment $\hat{\Delta}u$. This is accomplished by defining the skew-symmetric matrix containing the convected frame rotation increments as

$$\hat{\Delta}\tilde{\varphi}^T = (\mathbf{T}^{n+1} - \mathbf{T}^n) \mathbf{T}^{n+\frac{1}{2}T}. \quad (3.4.8)$$

This definition is a varied form of the approximation

$$\mathbf{T}^{n+1} \simeq (I + \Delta\tilde{\varphi}^T) \mathbf{T}^n$$

for the rotational vector $\Delta\varphi$ which parameterizes $\Delta\mathbf{T}$ as

$$\mathbf{T}^{n+1} = e^{\Delta\tilde{\varphi}^T} \mathbf{T}^n. \quad (3.4.9)$$

The reference frame $\mathbf{T}^{n+\frac{1}{2}}$ introduced in (3.4.8) is defined to be geometrically midway between the current and past convected reference frames as

$$\begin{aligned} \mathbf{T}^{n+\frac{1}{2}} &= \Delta\mathbf{T}^{n+\frac{1}{2}} \mathbf{T}^n \\ \Delta\mathbf{T}^{n+\frac{1}{2}} &\equiv \exp \left(\frac{1}{2} \Delta\tilde{\varphi} \right). \end{aligned} \quad (3.4.10)$$

This mid-configuration matrix is necessary in (3.4.8) such that a skew symmetric matrix results for $\hat{\Delta}\tilde{\varphi}^T$; this follows from (3.4.8) and (3.4.10) as

$$\begin{aligned} \hat{\Delta}\tilde{\varphi}^T &= \mathbf{T}^{n+1} \mathbf{T}^{n+\frac{1}{2}T} - \mathbf{T}^n \mathbf{T}^{n+\frac{1}{2}T} \\ &= \Delta\mathbf{T}^{n+\frac{1}{2}} - \Delta\mathbf{T}^{n+\frac{1}{2}T}. \end{aligned}$$

To incorporate the computation (3.4.8) within (3.4.7), the matrix $\mathbf{T}^{n+\frac{1}{2}}$ must be used within the first term of (3.4.7) to rotate the translational derivatives. The reasoning for this is given as follows as well as examples exhibiting the invariance of the computation.

To illustrate that the preceding computation preserves rigid motions, let us consider a beam element which is rigidly rotated such that $\Delta\gamma_1 \equiv 0$. The nodal incremental translations for the rigid rotation of a beam element pinned at the first node becomes

$$\begin{aligned}\hat{\Delta}u_1 &= 0 \\ \hat{\Delta}u_2 &= \ell (t_\xi^{n+1} - t_\xi^n) \quad , \quad t_\xi = \begin{Bmatrix} T_{11} \\ T_{12} \\ T_{13} \end{Bmatrix}\end{aligned}$$

where t_ξ corresponds to the first row of the \mathbf{T} matrix containing the direction cosines of the rotation and ℓ is the length of the beam element. The translational derivative within (3.4.7) is then evaluated as

$$\frac{\partial \hat{\Delta}u}{\partial \xi} = t_\xi^{n+1} - t_\xi^n \quad , \quad (3.4.11)$$

and the rotation increments are obtained from (3.4.8) as

$$\begin{Bmatrix} 0 \\ -\Delta\varphi_3 \\ \Delta\varphi_2 \end{Bmatrix} = -\mathbf{T}^{n+\frac{1}{2}} (t_\xi^{n+1} - t_\xi^n) \quad . \quad (3.4.12)$$

With this information, equation (3.4.7) is evaluated as

$$\hat{\Delta}\gamma_1 = \mathbf{T}^{n+\frac{1}{2}} \left(\frac{\partial \hat{\Delta}u}{\partial \xi} - t_\xi^{n+1} + t_\xi^n \right) \quad (3.4.13)$$

by combining (3.4.12) with the translational derivative term rotated by $\mathbf{T}^{n+\frac{1}{2}}$. It is then easily seen from (3.4.11) that this particular computation leads to

$$\begin{aligned}\Delta\gamma_1 &= \mathbf{T}^{n+\frac{1}{2}} (t_\xi^{n+1} - t_\xi^n - t_\xi^{n+1} + t_\xi^n) \\ &\equiv 0\end{aligned}$$

as desired.

As in the preceding example exhibiting the rigid rotation of a beam element, an accurate computation of the neutral-axis stretch which is invariant to arbitrary rigid rotations can also be accomplished. For this case, the incremental displacements for an arbitrary rotation and stretch are given by

$$\begin{aligned}\hat{\Delta}u_1 &= 0 \\ \hat{\Delta}u_2 &= ((\ell + d) t_\xi^{n+1} - \ell t_\xi^n)\end{aligned}$$

where d represents a stretch relative to the element length ℓ at a past configuration. The rotational expression (3.4.12) remains valid, and the translational derivative is now evaluated as

$$\frac{\partial \hat{\Delta}u}{\partial \xi} = \frac{1}{\ell^*} \{ (\ell + d) t_\xi^{n+1} - \ell t_\xi^n \}$$

where ℓ^* corresponds to the deformed element length at a given configuration. The above is substituted into (3.4.13) to give

$$\hat{\Delta}\gamma_1 = \mathbf{T}^{n+\frac{1}{2}} \left(\frac{\ell + d}{\ell^*} t_\xi^{n+1} - \frac{\ell}{\ell^*} t_\xi^n - t_\xi^{n+1} + t_\xi^n \right) \quad (3.4.14)$$

for this particular example. From the above, it is immediately seen that if the length derivative is evaluated at the current configuration as $\ell^* \equiv \ell_e + d$, then

$$\Delta\gamma_1 = \frac{d}{\ell + d} \mathbf{T}^{n+\frac{1}{2}} t_\xi^n$$

By incorporating (3.4.10), this is equivalent to

$$\begin{aligned}\Delta\gamma_1 &= \frac{d}{\ell + d} \Delta\mathbf{T}^{n+\frac{1}{2}} \mathbf{T}^n t_\xi^n \\ &= \frac{d}{\ell + d} \Delta\mathbf{T}^{n+\frac{1}{2}} \begin{Bmatrix} 1 \\ 0 \\ 0 \end{Bmatrix}\end{aligned}$$

To achieve a computation representative of a pure stretch in which the two transverse shear components are identically equal to zero, the above computation can be premultiplied by $\Delta \mathbf{T}^{n+\frac{1}{2}T}$ to give

$$\Delta \gamma_1 = \frac{d}{\ell + d} \begin{Bmatrix} 1 \\ 0 \\ 0 \end{Bmatrix}.$$

Thus the general strain computation, obtained by premultiplying (3.4.13) by $\Delta \mathbf{T}^{n+\frac{1}{2}T}$ and using the relation

$$\Delta \mathbf{T} = \mathbf{T}^{n+1} \mathbf{T}^{nT},$$

becomes

$$\Delta \gamma_1 = \mathbf{T}^n \frac{\partial \hat{\Delta} u}{\partial \xi^{n+1}} + \begin{Bmatrix} 1 - \Delta T_{11} \\ \Delta T_{12} \\ \Delta T_{13} \end{Bmatrix}. \quad (3.4.15)$$

It is noted that this computation does not require an explicit evaluation of $\mathbf{T}^{n+\frac{1}{2}}$. In effect, the convected frame strain components were evaluated at the configuration $\mathbf{T}^{n+\frac{1}{2}}$ as at this location the computation is invariant to rigid motion. The mid-configuration computation is then transformed to the current configuration \mathbf{T}^{n+1} to achieve the proper stretch evaluation.

The same type of result can be achieved in a slightly varied manner as follows. The length derivative ℓ^* in (3.4.14) can also be evaluated at the past configuration as $\ell^* \equiv \ell$. Equation (3.4.14) then yields

$$\Delta \gamma_1 = \frac{d}{\ell} \mathbf{T}^{n+\frac{1}{2}} t_{\xi}^{n+1}.$$

This expression must be premultiplied by $\Delta \mathbf{T}^{n+\frac{1}{2}}$ to yield a computation representative of a pure stretch as

$$\Delta \gamma_1 = \frac{d}{\ell} \begin{Bmatrix} 1 \\ 0 \\ 0 \end{Bmatrix}.$$

Premultiplication of (3.4.13) by $\Delta \mathbf{T}^{n+\frac{1}{2}}$ gives the alternative generic computation

$$\Delta \gamma_1 = \mathbf{T}^{n+1} \frac{\partial \hat{\Delta} u}{\partial \xi^n} + \begin{Bmatrix} \Delta T_{11} - 1 \\ \Delta T_{21} \\ \Delta T_{31} \end{Bmatrix} \quad (3.4.16)$$

Either evaluation, (3.4.15) or (3.4.16), yields a membrane strain computation which is invariant to arbitrary rigid body motions. The convected frame strain components were evaluated at configuration $\mathbf{T}^{n+\frac{1}{2}}$ in (3.4.13) to filter out the rigid motion; this mid-configuration computation was then transformed to an appropriate configuration, \mathbf{T}^n or \mathbf{T}^{n+1} , such that the membrane strain component is non-zero and the transverse shear strain components are identically equal to zero. To effect a strain evaluation at the mid-configuration as dictated by the stress-update procedure, the computations (3.4.15) or (3.4.16) need only be multiplied by the factor

$$\frac{\ell^*}{\frac{1}{2} (\ell^n + \ell^{n+1})}.$$

3.4.2 Transverse Shear and Curvature Strain Increments

Given the computation of the incremental membrane strain involving the displacement and rigid rotation increments, it remains to compute the incremental transverse shear and curvature strain increments involving deformational rotation increments. To this end, the strain terms

$$\hat{\Delta} \gamma_2 = \begin{Bmatrix} 0 \\ -\hat{\Delta} \tau_{a_3} \\ \hat{\Delta} \tau_{a_2} \end{Bmatrix} \quad (3.4.17)$$

representing the transverse shear strain and

$$\hat{\Delta} \kappa = \frac{\partial \hat{\Delta} \tau_a}{\partial \xi} \quad (3.4.18)$$

representing the curvature strain are computed independently from the membrane strain $\hat{\Delta}\gamma_1$ as follows.

The deformational rotation increments $\hat{\Delta}\tau_a$ correspond to the rotational vector parameterization of $\Delta\mathbf{S}$. The computation of (3.4.17) would thus require the nonlinear exponential inverse (3.2.13), and the computation of (3.4.18) would require an even more complicated derivative of (3.2.13). A simpler and more efficient computation can be achieved by incorporating Rodrigues parameters to represent $\hat{\Delta}\tau_a$ and its derivative. The Rodrigues parameter representation of the angular variation (3.2.18) is interpreted incrementally as

$$\Delta\tau_a = \frac{2}{1 + \Theta_t^2} [I + \tilde{\Theta}^T] \Delta\Theta_t \quad . \quad (3.4.19)$$

The parameters Θ_t and $\Delta\Theta_t$, which represent the \mathbf{S}^{n+1} and $\Delta\mathbf{S}$ matrices, respectively, can be easily computed from (3.2.15). In addition, as the \mathbf{S} matrices are nodal orientations relative to a common elemental reference frame \mathbf{T} , the corresponding nodal Rodrigues parameters are defined with respect to a common basis and thus can be properly interpolated to achieve a discrete evaluation of the elemental strains (3.4.17) and (3.4.18). With this introduction, the incremental transverse shear and curvature strains are computed as follows.

The elemental shear strain can be computed in two ways. A set of Rodrigues parameters can be computed at each of the element nodes as the matrices \mathbf{S}^{n+1} and $\Delta\mathbf{S}$ are nodal quantities themselves. The algebraic average of these nodal parameters, consistent with the standard underintegration of transverse shear to prevent locking, can then be used to evaluate

(3.4.19). A more accurate method interprets the underintegration in a geometric sense by defining one set of Rodrigues parameters from the relative orientation of the mid-element cross-section. This mid-element shear matrix \mathbf{S}_a is defined as

$$\mathbf{S}_a = \mathbf{R}_a \mathbf{T}^T$$

where the matrix \mathbf{R}_a corresponds to the geometric average of the total cross-section orientation matrices at the element nodes and \mathbf{T} is the element convected frame. The mid-element total orientation matrix \mathbf{R}_a can be immediately found using the normalized average of the nodal Euler parameters as defined in (3.3.17). The Rodrigues parameters Θ_i and $\Delta\Theta_i$ used to evaluate (3.4.19) are then obtained from the matrices

$$\mathbf{S}_a^{n+1} = \mathbf{R}_a^{n+1} \mathbf{T}^{n+1^T} \quad (3.4.20)$$

$$\Delta\mathbf{S}_a = \mathbf{S}_a^{n^T} \mathbf{S}_a^{n+1}, \quad (3.4.21)$$

respectively.

The elemental curvature (3.4.18) is computed by differentiating (3.4.19) as

$$\begin{aligned} \frac{\partial \hat{\Delta}\tau_a}{\partial \xi} &= \frac{2}{1 + \Theta_t^2} [I + \tilde{\Theta}^T] \frac{\partial \Delta\Theta_t}{\partial \xi} + \frac{2}{1 + \Theta_t^2} \frac{\partial \tilde{\Theta}_t}{\partial \xi} \Delta\Theta_t \\ &\quad - \frac{4\Theta_t}{(1 + \Theta_t^2)^2} [I + \tilde{\Theta}^T] \Delta\Theta_t \end{aligned} \quad (3.4.22)$$

The derivative terms are approximated over an element of length ℓ as

$$\begin{aligned} \frac{\partial \Theta_t}{\partial \xi} &= \frac{1}{\ell} (\Theta_{t_2} - \Theta_{t_1}) \\ \frac{\partial \Delta\Theta_t}{\partial \xi} &= \frac{1}{\ell} (\Delta\Theta_{t_2} - \Delta\Theta_{t_1}) \end{aligned}$$

using the nodal Rodrigues parameters Θ_{t_i} and $\Delta\Theta_{t_i}$, $i = 1, 2$. The non-derivative terms are evaluated using the mid-element shear matrices defined

in (3.4.20) and (3.4.21). This choice is obtained using the same concepts introduced in (3.3.17) and (3.3.18) to evaluate a total curvature from the Euler parameters of the nodal orientations.

Thus completes the computational details of the incremental strain evaluations. The strain computations are given by (3.4.15) or (3.4.16) for the incremental membrane strain, (3.4.17) and (3.4.19) for the incremental transverse shear strain, and (3.4.18) and (3.4.22) for the incremental curvature. These accurate incremental strain computations are a vital ingredient of the stress update procedure detailed in Section 2.4.

3.5 Static Solutions

The ability of the computational procedure to effectively model large deformations is demonstrated as follows. Static equilibrium configurations corresponding to given external forces are compared to results in the existing literature. A solution to the nonlinear static equations

$$S (u^{n+1} , \mathbf{R}^{n+1}) = f_{ext}^{n+1} \quad (3.5.1)$$

for the configuration which maintains equilibrium between the internal stresses and externally applied forces can be obtained from a Newton-Rhapson iteration procedure. The Newton-Rhapson technique requires the consistent linearization of the internal force as derived in Section 2.5. Given the geometric and material tangent stiffness matrices K^G and K^M representing the linearized internal force, the equations

$$[K^G + K^M]_{(k+1)} \begin{Bmatrix} \Delta u \\ \Delta \alpha \end{Bmatrix}_{(k+1)} = -\mathbf{r}_{(k+1)}^{n+1} \quad (3.5.2)$$

$$\mathbf{r}^{n+1} = S (u^{n+1} , \mathbf{R}^{n+1}) - f_{ext}^{n+1} \quad (3.5.3)$$

are solved at the $k + 1^{th}$ iteration for the incremental translations Δu and rotations $\Delta \alpha$. From this incremental solution, the nodal translations are updated via

$$u_{(k+1)}^{n+1} = u_{(k)}^{n+1} + \Delta u, \quad (3.5.4)$$

and the nodal orientations are updated via

$$\mathbf{R}_{(k+1)}^{n+1} = \exp(\Delta \tilde{\alpha}^T) \mathbf{R}_{(k)}^{n+1}. \quad (3.5.5)$$

The procedure is initiated with a prediction for $(u_0^{n+1}, \mathbf{R}_0^{n+1})$. The residual is then reevaluated with the updated solution, and the procedure continues until the norm of the residual converges within a given range of zero. A discussion of the tangent stiffness matrices within (3.5.2) and static results obtained from the Newton procedure are given as follows.

3.5.1 Discrete Tangent Stiffness Matrices

The finite element method is used to obtain discrete representations of the material and geometric tangent stiffness operators presented in (2.5.29) and (2.5.31) in the same manner as discussed in Section 3.3 for the finite element discretization of the internal force operator. The discrete elemental matrices are given as

$$\delta K^M = \{\delta u_1 \quad \delta u_2 \quad \delta \alpha_1 \quad \delta \alpha_2\}^T \begin{bmatrix} K_{11}^M & K_{12}^M \\ K_{12}^{M^T} & K_{22}^M \end{bmatrix} \begin{Bmatrix} \Delta u_1 \\ \Delta u_2 \\ \Delta \alpha_1 \\ \Delta \alpha_2 \end{Bmatrix}$$

for the material tangent stiffness where the partitions K_{ij}^M are given as

$$K_{11}^M = \frac{1}{\ell} \begin{bmatrix} T^T C_1 T & -T^T C_1 T \\ -T^T C_1 T & T^T C_1 T \end{bmatrix}$$

$$K_{12}^M = \frac{1}{2} \begin{bmatrix} -T^T C_1 \tilde{i}_1 S_1^T & -T^T C_1 \tilde{i}_1 S_2^T \\ T^T C_1 \tilde{i}_1 S_1^T & T^T C_1 \tilde{i}_1 S_2^T \end{bmatrix}$$

$$K_{22}^M = \begin{bmatrix} \frac{\ell}{4} S_1 \tilde{i}_1^T C_1 \tilde{i}_1 S_1^T & \frac{\ell}{4} S_1 \tilde{i}_1^T C_1 \tilde{i}_1 S_2^T \\ -\frac{1}{\ell} S_1 C_2 S_1^T & +\frac{1}{\ell} S_1 C_2 S_2^T \\ sym & \frac{\ell}{4} S_2 \tilde{i}_1^T C_1 \tilde{i}_1 S_2^T \\ & +\frac{1}{\ell} S_2 C_2 S_2^T \end{bmatrix}$$

where

$$C_1 = \text{Diag} (EA, GA, GA)$$

$$C_2 = \text{Diag} (GJ, EI_2, EI_3) .$$

It can be seen that this material tangent stiffness matrix is simply a transformation of the standard linear Timoshenko beam stiffness matrix as

$$K^M = T_K^T K_{TM} T_K$$

where

$$T_K = \text{Diag} (T, T, S_1, S_2)$$

and

$$K_{TM} = \begin{bmatrix} \frac{1}{\ell} C_1 & -\frac{1}{\ell} C_1 & -\frac{1}{2} C_1 \tilde{i}_1 & -\frac{1}{2} C_1 \tilde{i}_1 \\ -\frac{1}{\ell} C_1 & \frac{1}{\ell} C_1 & \frac{1}{2} C_1 \tilde{i}_1 & \frac{1}{2} C_1 \tilde{i}_1 \\ -\frac{1}{2} \tilde{i}_1^T C_1 & -\frac{1}{2} \tilde{i}_1^T C_1 & \frac{\ell}{4} \tilde{i}_1^T C_1 \tilde{i}_1 & \frac{\ell}{4} \tilde{i}_1^T C_1 \tilde{i}_1 \\ \frac{1}{2} \tilde{i}_1^T C_1 & \frac{1}{2} \tilde{i}_1^T C_1 & \frac{\ell}{4} \tilde{i}_1^T C_1 \tilde{i}_1 & \frac{\ell}{4} \tilde{i}_1^T C_1 \tilde{i}_1 \end{bmatrix}$$

$$+ \begin{bmatrix} 0 & 0 & 0 & 0 \\ 0 & 0 & 0 & 0 \\ 0 & 0 & \frac{1}{\ell}C_2 & -\frac{1}{\ell}C_2 \\ 0 & 0 & \frac{1}{\ell}C_2 & -\frac{1}{\ell}C_2 \end{bmatrix} .$$

As seen from the above decomposition, K_{TM} possesses the correct number of singularities to correspond to the six rigid body modes. Thus, the material stiffness matrix K^M is not rank deficient when reduced integration methods are introduced for the rotational degrees of freedom associated with the transverse shear strain.

Likewise, the geometric element stiffness kernel is given as

$$\delta K^G = \{ \delta u_1 \quad \delta u_2 \quad \delta \alpha_1 \quad \delta \alpha_2 \}^T \begin{bmatrix} K_{11}^G & K_{12}^G \\ K_{12}^{G^T} & K_{22}^G \end{bmatrix} \begin{Bmatrix} \Delta u_1 \\ \Delta u_2 \\ \Delta \alpha_1 \\ \Delta \alpha_2 \end{Bmatrix}$$

where the partitions K_{ij}^G become

$$K_{11}^G = \frac{N_1}{\ell} \begin{bmatrix} I & -I \\ -I & I \end{bmatrix}$$

$$K_{12}^G = \begin{bmatrix} T^T (\frac{1}{\ell}M^* - \frac{1}{2}N^*) S_1^T & T^T (-\frac{1}{\ell}M^* - \frac{1}{2}N^*) S_2^T \\ T^T (-\frac{1}{\ell}M^* + \frac{1}{2}N^*) S_1^T & T^T (\frac{1}{\ell}M^* + \frac{1}{2}N^*) S_2^T \end{bmatrix}$$

$$K_{22}^G = \frac{\sigma_{\xi\xi}^0}{\ell} \begin{bmatrix} S_1 J S_1^T & -S_1 J S_2^T \\ -S_2 J S_1^T & S_2 J S_2^T \end{bmatrix} +$$

$$\frac{1}{2} \begin{bmatrix} S_1 (-O^* - O^{*T}) S_1^T & S_1 (-O^* + O^{*T}) S_2^T \\ S_2 (O^* - O^{*T}) S_1^T & S_2 (O^* + O^{*T}) S_2^T \end{bmatrix} .$$

The geometric stiffness is simply

$$K^G = T_K^T K_{TG} T_K$$

where

$$K_{TG} = \begin{bmatrix} \frac{N_1}{\ell} I & -\frac{N_1}{\ell} I & \frac{1}{\ell} M^* & -\frac{1}{\ell} M^* \\ -\frac{N_1}{\ell} I & \frac{N_1}{\ell} I & -\frac{1}{\ell} M^* & \frac{1}{\ell} M^* \\ \frac{1}{\ell} M^{*T} & -\frac{1}{\ell} M^{*T} & \frac{\sigma_{\xi\xi}^0}{\ell} J & -\frac{\sigma_{\xi\xi}^0}{\ell} J \\ -\frac{1}{\ell} M^{*T} & \frac{1}{\ell} M^{*T} & -\frac{\sigma_{\xi\xi}^0}{\ell} J & \frac{\sigma_{\xi\xi}^0}{\ell} J \end{bmatrix}$$

$$+ \begin{bmatrix} 0 & 0 & -\frac{1}{2} N^* & -\frac{1}{2} N^* \\ 0 & 0 & \frac{1}{2} N^* & \frac{1}{2} N^* \\ -\frac{1}{2} N^{*T} & \frac{1}{2} N^{*T} & -\frac{1}{2} O^* & \frac{1}{2} O^* \\ -\frac{1}{2} N^{*T} & \frac{1}{2} N^{*T} & -\frac{1}{2} O^* & \frac{1}{2} O^* \end{bmatrix}$$

$$+ \begin{bmatrix} 0 & 0 & 0 & 0 \\ 0 & 0 & 0 & 0 \\ 0 & 0 & -\frac{1}{2} O^{*T} & \frac{1}{2} O^{*T} \\ 0 & 0 & -\frac{1}{2} O^{*T} & \frac{1}{2} O^{*T} \end{bmatrix}$$

Again, it is seen from the above decomposition that the geometric stiffness also contains the correct number of singularities to correspond to the six rigid body modes. The geometric stiffness matrix is not rank deficient when the reduced integration techniques are employed.

Two remarks are made in regard to the above derivations. First, it is noticed that the elemental curvature κ has been neglected. The transformation from convected coordinates to body frame coordinates of the virtual rotation spatial derivative is effected via (2.3.26) as opposed to (2.3.27). In this manner, the spatial derivative employed is as witnessed by the convected reference frame rather than the cross-section reference frame. For static analysis, better convergence results from this interpretation. For dynamic analysis however, the transformation (2.3.27) is retained to coincide with the analogous angular velocity representation. As such, the interaction between the curvature and angular velocity is accurately represented. Second, the tangent stiffness matrices are symmetric. Previous works achieve symmetric tangent operators by incorporating specific rotational parameterizations within the formulation [34-35]. The additional complexity regarding the potential symmetry in these works arises due to the use of the unsymmetric first Piola-Kirchoff stress representation, whereas the present formulation directly achieves symmetric tangent matrices due to the use of the Cauchy stress representation.

3.5.2 Example Problems

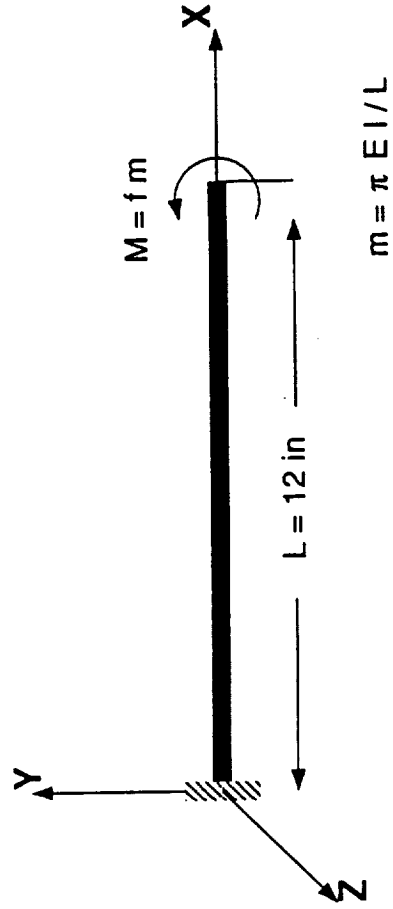
In this section, two numerical examples are given to demonstrate the effectiveness of the formulation in modeling large deformations. The results are compared to those reported in the literature.

In the first example, a cantilever beam is subjected to a concentrated end moment M about the b_3 axis as shown in Figure 3.3a. The beam is modeled with twelve linear elements. The total load of $M = 2\ m$ is applied in ten equal load increments, and an average of 8 iterations is required at each increment to reach a converged configuration. The deformed shapes of the beam at each load increment are shown in Figure 3.3b. The tip position coordinates at each load increment are compared to results reported in [27] in Table 3.1 and also the true arc segments of a circle of the appropriate radius of curvature.

In the second example, a cantilever 45-degree bend located in a horizontal plane is subjected to a concentrated vertical static end load as shown in Figure 3.4a. The bend, of radius 100, is modeled with 8 linear beam elements. A total load of 600 is applied in twelve equal load increments, and an average of 10 iterations is required at each increment to reach a converged configuration. The deformed shapes of the beam at each load increment are shown in Figure 3.4b. The tip position coordinates at each load increment are compared to results reported in [24,32] in Table 3.2.

The results are given as follows.

Problem Definition



Material Properties

$$\begin{aligned} E &= 30 \times 10^6 \text{ lb/in}^2 \\ G &= 15 \times 10^6 \text{ lb/in}^2 \\ A &= 1 \text{ in}^2 \\ I &= 1/12 \text{ in}^4 \end{aligned}$$

Mesh

12 Linear Elements

Figure 3.4a Cantilever beam subjected to end moment: problem data.

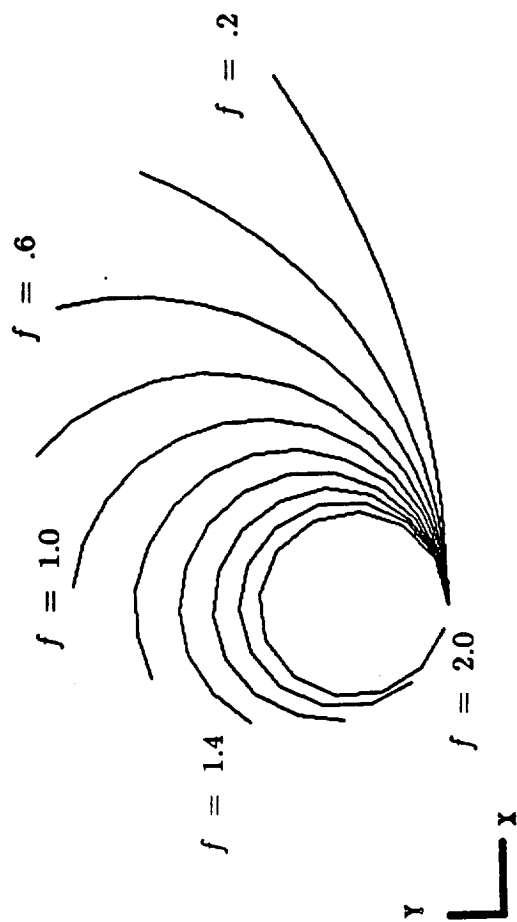
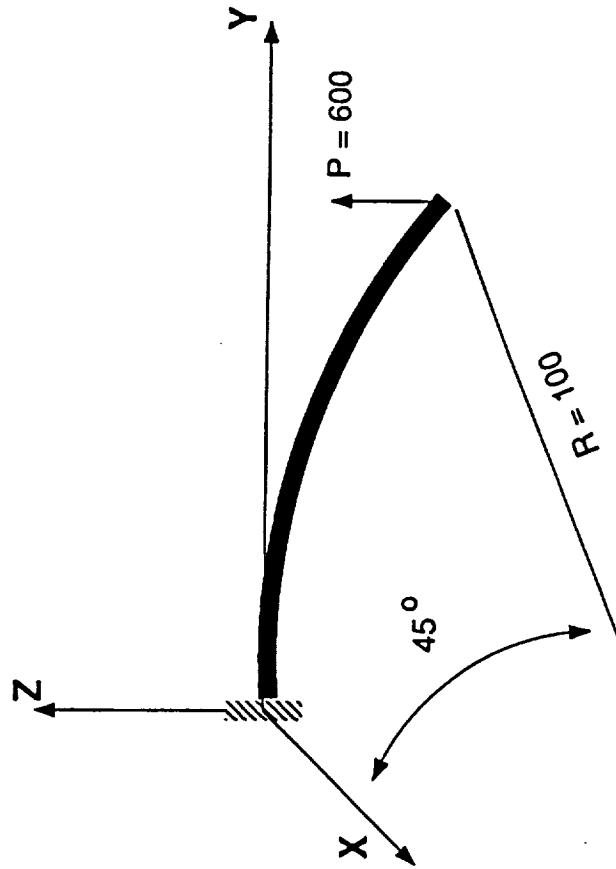


Figure 3.4b Cantilever beam subjected to end moment: deformed shapes.

Problem Definition



Material Properties

$$\begin{aligned} E &= 1 \times 10^7 \text{ lb/in}^2 \\ G &= .5 \times 10^7 \text{ lb/in}^2 \\ A &= 1 \text{ in}^2 \\ I &= 1/12 \text{ in}^4 \end{aligned}$$

Mesh

8 Linear Elements

Figure 3.5a Cantilever 45-degree bend subjected to end load: problem data.

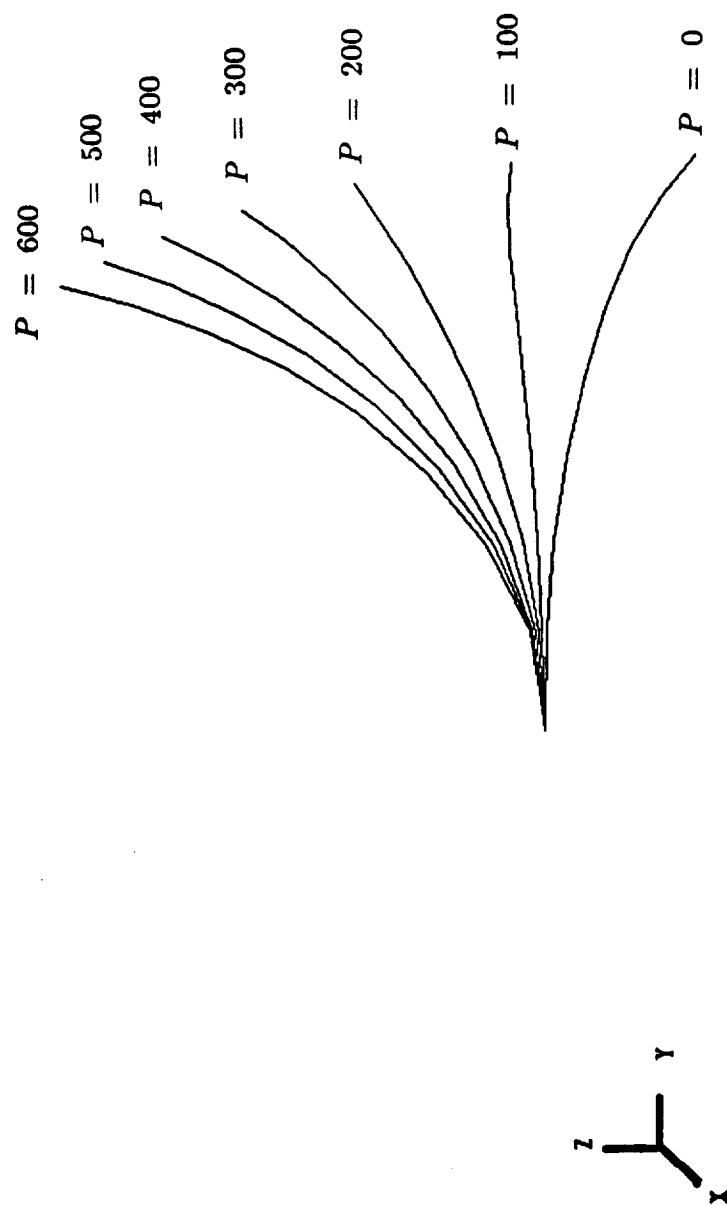


Figure 3.5b Cantilever 45-degree bend subjected to end load: deformed shapes.

Table 3.1 Comparison of results for the cantilever subjected to an end moment

f	Ref. [27] (u,v)	Present (u,v)	True (u,v)
.2	(-.7652,3.623)	(-.7728,3.648)	(-.7741,3.648)
.4	(-2.899,6.574)	(-2.914,6.601)	(-2.918,6.598)
.6	(-5.955,8.328)	(-5.939,8.342)	(-5.945,8.333)
.8	(-9.293,8.620)	(-9.188,8.653)	(-9.194,8.637)
1.0	(-12.215,7.507)	(-12.0,7.662)	(-12.0,7.639)
1.2	(-14.12,5.376)	(-13.88,5.783)	(-13.87,5.758)
1.4	(-14.66,2.877)	(-14.61,3.592)	(-14.59,3.571)
1.6	(-13.85,.797)	(-14.29,1.662)	(-14.27,1.650)
1.8	(-12.18,-.123)	(-13.26,.4095)	(-13.25,.4053)
2.0	-	(-12.00,1.2 $\times 10^{-5}$)	(-12.00,0.00)

Table 3.2 Comparison of results for the cantilever 45-degree bend

f	Ref. [24] (x,y,z)	Ref. [32] (x,y,z)	Present (x,y,z)
300	(22.33,58.84,40.08)	(22.5,59.2,39.5)	(19.75,61.06,39.24)
450	(18.62,52.32,48.39)	—	(15.17,54.94,47.86)
600	(15.79,47.23,53.37)	(15.9,47.2,53.4)	(12.00,49.85,53.08)

3.6 Concluding Remarks

The finite element representation of the equations of motion derived in Chapter II has been presented. Much attention was focused on the discrete form of the internal force, an accurate computation of which remains key to any static and/or dynamic simulations. The numerical procedure for the computation of the nonlinear internal force, as developed from the continuum formulation, was proven to be invariant to arbitrary rigid motions of the beam while effectively modeling the strains due to stretching, transverse shear, torsion, and bending deformations. Particular developments include the discrete computation of rotational matrices embedded within the formulation, a discrete computation of the element curvature based on the Euler parameter functional relation, and incremental strain computations to effect the stress update procedure. The fundamental property motivating these developments is the condition that quantities be computed from the nodal degrees of freedom in a manner that is invariant to any arbitrary rigid body motions implicitly contained within these variables. The success of the incremental strain computational procedure hinges on a proper extraction of the rotation increments from the various rotational matrices embedded in the formulation.

The developments of multibody dynamic solution procedures is presented in the following chapter. The present internal force computation is interfaced with these developments to achieve effective dynamic simulations.

CHAPTER IV

MULTIBODY DYNAMICS SOLUTION PROCEDURES

4.1 Introduction

The formulation modeling the large rotation dynamics of a flexible beam has been developed in Chapter II. The algorithmic treatment of the beam internal force such that the strain computations are preserved under the large rotations was detailed in Chapter III. The purpose of the present chapter to extend these developments to the framework of flexible multibody systems. To achieve an effective simulation methodology, an automatic formulation of the equations of motion for multibody systems is necessary. In addition, efficient numerical solution procedures need to be developed for the solution of these equations. The numerical procedures for multibody systems must include a proper treatment of the spatial rotations and the constraint conditions. The analytical and computational formalisms presented in Chapters II and III are highly conducive to these goals. The present chapter develops an effective numerical solution strategy for flexible multibody dynamic systems.

To formulate the equations of motion for multibody systems, two basic approaches have been discussed in the literature. One approach analytically eliminates the constraint conditions a priori to achieve a minimal set of second order differential equations [69-76]. In these recursive type formulations, relative coordinates between bodies are used to define the kinematic relations, and modal coordinates are used to define the local deformations. However, when the kinematic constraint equations are intro-

duced in the early stages of analysis, the development of the equations of motion becomes unnecessarily complicated. Equations with a high degree of nonlinearity and low degree of sparsity result when the relative coordinates are employed. In contrast, a second approach introduces absolute or Cartesian coordinates to model the kinematic relations of each individual body in the system. The Lagrange multiplier technique is then employed to couple the algebraic constraint equations with the differential equations of motion; the result is a maximum set of differential and algebraic equations. This approach has been applied to the floating frame formulations of beam dynamics where the displacements of elastic bodies are modeled by superposing local elastic deformation coordinates onto rigid-body reference coordinates [8-11,16,77]. To employ the approach within multibody applications, the assumed elastic displacement field must be consistent with the nonlinear constraint equations. As simple free-body modes are not suitable to describe the deformation shape of many constrained components, consistent displacement fields are defined via a proper choice of the body reference frame [8]. To better account for reactions due to joint connections, static correction modes are introduced to model the elastic displacements of flexible components [10-11]. The important issue thus becomes the proper choice of modal coordinates to represent constrained components.

The present beam formulation alleviates this issue and is extended into the field of multibody dynamics as follows. As discussed in Chapter II, the beam components are modeled using inertially-based degrees of freedom which embody both the rigid and deformation motions. As these degrees of freedom are kinematically of the same sense as the physical coordinates of rigid body components, the equations of motion for an arbitrary

configuration of flexible beams and rigid bodies can automatically be generated in terms of an identical set of physical coordinates. Incorporation of multibody system constraints via the Lagrange multiplier technique becomes straightforward. A salient feature of this type of formulation is that numerical solution procedures for treatment of multibody systems can be directly applied to the generalized coordinates of both the rigid and flexible components. In comparison to the floating frame types of formulations, concerns of correct modal representation of the deformation are eliminated as well as the separate numerical treatment of the contrasting characters of the reference and elastic coordinates.

Given the flexible multibody system model, specialized numerical procedures must be developed for the solution of the equations of motion. As the equations of these articulated systems inherently involve large rotations and constraint conditions, numerical procedures must include treatment of these effects as well as the integration of the generalized coordinates. In the context of present type flexible beam dynamics formulations, the extension of the implicit Newmark algorithm to include proper treatment of the nonlinear rotation fields was proposed in [32], and consequently used in the works of [34,36]. To treat the spatial rotations, the equations of motion are written in terms of a particular rotational parameterization and then discretized by an implicit algorithm. The configuration orientation and angular velocity are updated from the solution for the rotational parameters by implementing discrete counterparts to the functional relations overviewed in Section 3.2. In contrast to these implicit integration techniques, the present work develops explicit integration techniques for use within the rotational dynamics context [44]. For this purpose, a two-stage modification of the

central difference algorithm is presented to integrate the translational coordinates and the angular velocity vector. Once the angular velocities are obtained, the angular orientations are updated by incorporating an implicit trapezoidal algorithm to solve the kinematical relation in terms of the Euler parameters.

In addition to the integration of the generalized coordinates and the update of the angular orientation, solution techniques must be developed to enforce the algebraic constraint conditions for multibody equations of motions formulated by incorporating Lagrange multipliers. For this purpose, techniques have been developed which eliminate excess or dependent variables numerically by incorporating the singular value decomposition [78-80], the coordinate partitioning technique [81], the zero eigenvalue theorem [82], and other matrix procedures [83-85]. Another approach applies an implicit integration algorithm to the generalized coordinates of the constraint-augmented equations, and then solves for both the generalized coordinates and the Lagrange multipliers simultaneously [86-88]. However, in some instances, numerical difficulties were encountered from this discretization as ill-conditioned matrices and artificially stiff problems resulted. Another simultaneous solution procedure attempted to alleviate this problem by constructing a modified differential equation to model the constraint equations [89-90]. Drawbacks to the procedure included a somewhat ad-hoc selection of certain factors that influence the accuracy of solutions and a lack of a positive error control on the constraint violations. To address these drawbacks, a technique which implicitly integrates an alternative stabilized companion differential equation for the constraint forces was proposed in [91-92]. A principal feature of this method is that the errors committed in

each constraint condition decay with a characteristic time scale associated with the constraint force. In addition, the method is conducive to an attractive modular software implementation as the solution of the constraint forces can be performed separate from the integrations of the generalized coordinates. This stabilized constraint solution procedure is employed in the present work.

The multibody dynamics solution procedure adopted for the flexible multibody system equations of motion is presented in detail in this chapter. Section 4.2 will briefly describe the extension of the beam formulation into the equations of motion for multibody systems. Section 4.3 will discuss the application of integration procedures, both implicit and explicit, in the context of finite rotation dynamics. To complete the multibody dynamic solution, Section 4.4 will present a unique procedure to update the configuration orientation from the angular velocity solution and Section 4.5 will discuss a separate computational procedure for the Lagrange multipliers. Finally, example problems demonstrating the software capabilities are presented in Section 4.6, and conclusions are given in Section 4.7.

4.2 Multibody System Equations

The present formulation of spatial beam dynamics can readily be incorporated into a general multibody dynamics methodology. The discrete equations of motion of an unconstrained flexible beam as derived in (3.3.12) are rewritten below as

$$\begin{bmatrix} m & 0 \\ 0 & J \end{bmatrix} \begin{Bmatrix} \ddot{u} \\ \dot{\omega} \end{Bmatrix} + \begin{Bmatrix} 0 \\ \tilde{\omega} J \omega \end{Bmatrix} + \begin{Bmatrix} S^e \\ S^b \end{Bmatrix} = \begin{Bmatrix} f^e \\ f^b \end{Bmatrix} \quad (3.3.12)$$

where the subscript d representing nodal discretizations has been dropped.

It is recalled the beam nodal degrees of freedom (u, ω) corresponding to

the inertial coordinates of the beam neutral axis position and the body-fixed coordinates of the cross-sectional angular velocity. These degrees of freedom are of the same sense as those of a rigid body, namely the inertially-based translational position of the center of mass and the angular velocity of a moving reference frame orienting the body. Thus the equations of motion (3.3.12) can equally well represent a rigid body system by setting the internal force S equal to zero. The unconstrained equations of an arbitrary configuration of flexible beams and rigid bodies can be written in terms of one set of kinematical coordinates denoting both the nodal coordinates of the flexible members and the physical coordinates of the rigid bodies.

It remains to augment the nonlinear algebraic equations which model the contact conditions of the various bodies of the multibody system. The Lagrange multiplier technique augments these constraint equations to the unconstrained differential equations of motion. Two types of constraint conditions exist, holonomic or configuration constraints and nonholonomic or motion constraints. A holonomic constraint condition can be expressed as a definite relation between the displacement coordinates, whereas a nonholonomic constraint condition can only be expressed as a relation between the differentials of the coordinates and not as a finite relation between the coordinates themselves [98]. A set of algebraic equations representing holonomic constraint conditions between the displacement coordinates u are written as

$$\Phi^H (u, t) = 0 \quad (4.2.1)$$

and the differential of these constraints is given as

$$\delta \Phi^H = \frac{\partial \Phi^H}{\partial u} \delta u = \mathbf{B}^H \delta u = 0 \quad . \quad (4.2.2)$$

A set of non-integrable equations concerning nonholonomic constraint conditions between the virtual displacements and rotations $\delta u, \delta \alpha$ are written as

$$\delta \Phi_N (u, \delta u, R, \delta \alpha) = \mathbf{B}_N \begin{Bmatrix} \delta u \\ \delta \alpha \end{Bmatrix} = 0 \quad . \quad (4.2.3)$$

Given these constraint conditions, the virtual work expression (2.3.2) for the unconstrained system is modified by the inclusion of the virtual work which enforces the constraints through the Lagrange multiplier technique as [98]

$$\delta F^I + \delta F^S + \lambda_H \cdot \delta \Phi_H + \lambda_N \cdot \delta \Phi_N = \delta F^E + \delta F^T \quad .$$

By incorporating the Lagrange multipliers λ , the virtual displacements and rotations of the generalized coordinates can be treated as independent variations. The equations of motion for constrained flexible multibody systems are thus obtained as

$$\begin{bmatrix} m & 0 \\ 0 & J \end{bmatrix} \begin{Bmatrix} \ddot{u} \\ \dot{\omega} \end{Bmatrix} + \mathbf{B}^T \lambda = \begin{Bmatrix} Q_u \\ Q_\omega \end{Bmatrix} \quad . \quad (4.2.4)$$

In the above equation, the notation contains both the holonomic and non-holonomic constraints in the constraint force vector $\mathbf{B}^T \lambda$ as

$$\mathbf{B} = \begin{bmatrix} B_H \\ B_N \end{bmatrix} \quad , \quad \lambda = \begin{Bmatrix} \lambda_H \\ \lambda_N \end{Bmatrix} \quad (4.2.5)$$

and the right-hand side vector contains the remaining force-type terms as

$$\begin{Bmatrix} Q_u \\ Q_\omega \end{Bmatrix} = \begin{Bmatrix} f^e - S^e \\ f^b - S^b - \tilde{\omega} J \omega \end{Bmatrix} \quad . \quad (4.2.6)$$

To achieve a determined system of equations, the equations (4.2.4) must be solved in conjunction with the constraint equations.

The \mathbf{B} matrix in (4.2.4), termed the constraint Jacobian matrix, is deduced from the kinematic relationship between the bodies of the system.

To model these kinematic relations, conditions can be directly imposed on the nodal degrees of freedom of two separate flexible beams, or between a beam nodal degree of freedom and a rigid body modeling a portion of a more complex joint. Typical Jacobian matrices modeling standard joints used in multibody systems, such as universal, spherical, revolute, and translational joints, have been derived in [99]. Given the Jacobian matrices for the joints and the beam connections, the models representing an arbitrary assemblage of articulated flexible and rigid components can be constructed in a systematic manner.

4.3 Integration of Generalized Coordinates

The solution of the generalized coordinates via the application of numerical integration techniques to the multibody equations of motion are discussed next. To present the application of integration methods to problems concerning nonlinear rotational dynamics, the equations of motion at time t^{n+1} are written in terms of a generalized coordinate d which represents both the displacement coordinates u and a suitable rotational parameterization as

$$M (\ddot{d}^{n+1}, \dot{d}^{n+1}, d^{n+1}) + S (d^{n+1}) = f(t^{n+1}) \quad (4.3.1)$$

where $d^{n+1} \equiv d(t^{n+1})$. In the above equation, M represents both the translational and rotational terms of the inertia operator as

$$M \equiv \begin{Bmatrix} M_m \\ M_J \end{Bmatrix} = \begin{Bmatrix} m\ddot{u} \\ J\dot{\omega} + \tilde{\omega}J\omega \end{Bmatrix}, \quad (4.3.2)$$

S represents the nonlinear internal force, and f represents the external force including any constraint forces $f = f^{ext} - \mathbf{B}^T \lambda$. For the present analysis,

the constraint forces are assumed to be given; a separate solution technique in which the constraint forces may be obtained in conjunction with the solution of the generalized coordinates is discussed in Section 4.5. Numerical algorithms are implemented to advance the generalized coordinate solution to a discrete point in time $t^{n+1} = t^n + h$ given that the solution at the past step in time t^n has been found.

To solve equations of motion involving nonlinear rotational dynamics, implicit integration techniques were first considered [32,34,36]. The advantage of the implicit algorithms is the exceptional stability properties, while the disadvantages include the implementation complexities inherently associated with nonlinear problems. Most of the implicit methods that are commonly used, i.e. the trapezoidal rule, Newmark, Houbolt, Wilson, and others, are unconditionally stable for linear problems. However, to achieve this unconditional stability, the solution of a simultaneous system of equations is required at each discrete time step where the dynamic solution is sought. To apply implicit techniques to nonlinear problems, a linearization of the equations with respect to the generalized displacement coordinates is necessary. For the linearization within the context of finite rotations, the rotational degrees of freedom are parameterized by the rotational vector defined in Section 3.2 [32]. Implicit integration methods are then used to obtain the rotational vector and its time derivative at the discrete time stations, after which the angular orientation and the angular velocity are updated accordingly.

The alternative to the implicit formulas is the explicit formulas. Explicit formulas are attractive from an implementation standpoint as the solution can be achieved from simple vector operations. However, explicit

algorithms retain stability only within a restricted step size between discrete time stations. To use explicit methods within the context of finite rotations, the angular velocity vector is first deduced via an integration of the angular acceleration [44]. A suitable discretization of the Euler parameter representation of angular velocity is then used to update the rotational orientation.

To demonstrate the above concepts, the application of the implicit midpoint rule is discussed next in Section 4.3.1, while the explicit techniques are discussed in Section 4.3.2.

4.3.1 Implicit Integration Techniques

A traditional algorithm to solve (4.3.1), termed the Newmark algorithm, is given as

$$\begin{aligned} d^{n+1} &= d^n + h \dot{d}^n + \left(\frac{1}{2} - \beta \right) h^2 \ddot{d}^n + \beta h^2 \ddot{d}^{n+1} \\ \dot{d}^{n+1} &= \dot{d}^n + (1 - \gamma) h \ddot{d}^{n+1} \end{aligned}$$

where β and γ are free parameters whose choice results from a compromise between computational simplicity, stability, and accuracy requirements. The choice $\gamma = \frac{1}{2}$, $\beta = \frac{1}{4}$ yields the most accurate integration scheme with unconditional stability. The resulting algorithm, termed the average constant acceleration scheme or trapezoidal rule, can be rewritten as

$$\begin{aligned} d^{n+1} &= d^n + \frac{h}{2} (\dot{d}^n + \dot{d}^{n+1}) \\ \dot{d}^{n+1} &= \dot{d}^n + \frac{h}{2} (\ddot{d}^n + \ddot{d}^{n+1}) \end{aligned}$$

A variation of this scheme, termed the midpoint rule, is given as

$$d^{n+1} = d^n + h \dot{d}^{n+\frac{1}{2}} \quad (4.3.3a)$$

$$\dot{d}^{n+1} = \dot{d}^n + h \ddot{d}^{n+\frac{1}{2}} \quad (4.3.3b)$$

where a computation of the velocities and accelerations at a half time station are evaluated from the application of

$$d^{n+\frac{1}{2}} = d^n + \frac{h}{2} \dot{d}^{n+\frac{1}{2}} \quad (4.3.4a)$$

$$\dot{d}^{n+\frac{1}{2}} = \dot{d}^n + \frac{h}{2} \ddot{d}^{n+\frac{1}{2}} \quad (4.3.4b)$$

to the equations of motion. By evaluating the velocities and accelerations at the half time station for use in the full station displacement and velocity computation as opposed to using a numerical average as seen in the trapezoidal rule, the midpoint algorithm yields a more accurate computational scheme.

The midpoint solution is obtained by using the Newton-Rhapson iteration procedure to solve the nonlinear residual equations

$$\begin{aligned} r^{n+\frac{1}{2}} &\equiv M(\ddot{d}^{n+\frac{1}{2}}, \dot{d}^{n+\frac{1}{2}}, d^{n+\frac{1}{2}}) + S(d^{n+\frac{1}{2}}) - f^{n+\frac{1}{2}} \\ &= 0 \end{aligned} \quad (4.3.5)$$

To this end, a linearized set of equations

$$E_{(k+1)} \Delta d_{(k+1)} = -r_{(k+1)}^{n+\frac{1}{2}}, \quad E \equiv \frac{\partial r^{n+\frac{1}{2}}}{\partial d^{n+\frac{1}{2}}} \quad (4.3.6)$$

are solved at the $k+1^{th}$ iteration for the incremental displacements Δd which are then used to update the solutions obtained at the k^{th} iteration via a discrete evaluation of

$$d_{(k+1)}^{n+\frac{1}{2}} = d_{(k)}^{n+\frac{1}{2}} + \Delta d \quad (4.3.7)$$

until a convergence criterion is reached. The iterative procedure is started with a prediction for $d_{(0)}^{n+1}$, usually taken to be d^n . The configuration update (4.3.7) symbolically designates the vector update

$$u_{(k+1)}^{n+1} = u_{(k)}^{n+1} + \Delta u \quad (4.3.8)$$

for the translational displacements u and the rotational orientation update

$$\mathbf{R}_{(k+1)}^{n+1} = \exp (\Delta \tilde{\Theta}^T) \mathbf{R}_{(k)}^{n+1} \quad (4.3.9)$$

for the rotational vector parameterization Θ . The system angular velocity must be updated from the rotational vector and its derivative in an appropriate manner via

$$\omega^{n+1} = \mathbf{T} (\Theta^{(n+1)}) \dot{\Theta}^{n+1}$$

where the operator $\mathbf{T} (\Theta)$ has been defined in 3.2.17.

To obtain the linear equations, the incremental solution matrix E is derived from (4.3.5) and (4.3.6) as

$$E = \frac{\partial M^{n+\frac{1}{2}}}{\partial \ddot{d}^{n+\frac{1}{2}}} \frac{\partial \ddot{d}^{n+\frac{1}{2}}}{\partial d^{n+\frac{1}{2}}} + \frac{\partial M^{n+\frac{1}{2}}}{\partial \dot{d}^{n+\frac{1}{2}}} \frac{\partial \dot{d}^{n+\frac{1}{2}}}{\partial d^{n+\frac{1}{2}}} + \frac{\partial M^{n+\frac{1}{2}}}{\partial d^{n+\frac{1}{2}}} + \frac{\partial S^{n+\frac{1}{2}}}{\partial d^{n+\frac{1}{2}}} \quad (4.3.10)$$

where the terms

$$\frac{\partial \ddot{d}^{n+\frac{1}{2}}}{\partial d^{n+\frac{1}{2}}} = \frac{1}{\delta^2} \quad , \quad \frac{\partial \dot{d}^{n+\frac{1}{2}}}{\partial d^{n+\frac{1}{2}}} = \frac{1}{\delta} \quad , \quad \delta \equiv \frac{h}{2} \quad (4.3.11)$$

are identified from the integration algorithm (4.3.3). The partial derivatives of M and S represent coefficients of the first-order Taylor-series expansion of the respective operators about a past equilibrium configuration at time t^n as

$$M \simeq M^n + \frac{\partial M}{\partial \ddot{d}} \Delta \ddot{d} + \frac{\partial M}{\partial \dot{d}} \Delta \dot{d} + \frac{\partial M}{\partial d} \Delta d \quad (4.3.12)$$

$$S \simeq S^n + \frac{\partial S}{\partial d} \Delta d \quad (4.3.13)$$

where $\Delta d \equiv d - d^n$. Derivation of the linear expansions in the context where $d \equiv (u, \Theta)$ requires techniques consistent with the particular

translational and rotational update procedures of (4.3.8) and (4.3.9); the derivations for the present beam formulation were presented in Section 2.5. The consistent linearization of the internal force as derived in Section 2.5 and Section 3.5.1 is given as

$$S \simeq S^n + [K^G + K^M] \begin{Bmatrix} \Delta u \\ \Delta \Theta \end{Bmatrix} \quad (4.3.14)$$

where the geometric and material tangent stiffness matrices K^G and K^M are deduced from a finite element discretization of (2.5.28) and (2.5.30). Likewise, the consistent linearization of the translational and rotational inertia as derived in Section 2.5 is given as

$$M_m \simeq M_m^n + m \Delta u \quad , \quad (4.3.15)$$

$$M_J \simeq M_J^n + J \Delta \ddot{\Theta} + C^G \Delta \dot{\Theta} + K^C \Delta \Theta \quad (4.3.16)$$

where C^G and K^C represent discrete versions of the gyroscopic damping and centrifugal stiffening matrices given by (2.5.14) and (2.5.15). From the above linearizations, the incremental solution matrix is seen to be

$$E = \frac{1}{\delta^2} \begin{bmatrix} m & 0 \\ 0 & J \end{bmatrix} + \frac{1}{\delta} \begin{bmatrix} 0 & 0 \\ 0 & C^G \end{bmatrix} + \begin{bmatrix} 0 & 0 \\ 0 & K^C \end{bmatrix} + K^G + K^M$$

This solution matrix E is configuration dependent and thus must be reformulated at least at the beginning of each time step for a modified Newton technique, and at each iteration if a full Newton technique is to be used. In addition, the updates of the configuration orientation and angular velocity from the rotational vector parameterization require additional cumbersome computations. It is seen that the price to pay for the unconditional stability of the implicit algorithm is the complexity of the computational

scheme. For these reasons, explicit integration procedures have been chosen for the present study.

4.3.2 Explicit Integration Techniques

The central difference explicit integration algorithm is written as

$$\dot{d}^{n+\frac{1}{2}} = \dot{d}^{n-\frac{1}{2}} + h \ddot{d}^n \quad (4.3.17a)$$

$$d^{n+1} = d^n + h \dot{d}^{n+\frac{1}{2}} \quad (4.3.17b)$$

$$\ddot{d}^{n+1} = M^{-1} Q (d^{n+1}, \dot{d}^{n+1}) \quad (4.3.17c)$$

where

$$Q \equiv \begin{Bmatrix} f^e \\ f^b \end{Bmatrix} - \begin{Bmatrix} S^e \\ S^b \end{Bmatrix} - \begin{Bmatrix} 0 \\ \tilde{\omega} J \omega \end{Bmatrix} \quad (4.3.18)$$

In this algorithm, the displacements (d) are obtained at the full time steps, ($\dots, n, n+1, n+2, \dots$), while the velocities (\dot{d}) are obtained at the half time steps, ($\dots, n-\frac{1}{2}, n+\frac{1}{2}, n+\frac{3}{2}, \dots$). Given the integrated displacements and velocities, the accelerations are obtained at the full time steps from the equations of motion. The solutions are thus advanced to the next time step using an extrapolation involving only the previous solution vectors, and the implementation of explicit integration techniques to the nonlinear equations of motion is straightforward.

To effect the explicit formulas within the context of finite rotations, the algorithm (4.3.17a) is used to obtain a solution for the angular velocity. The rotational orientation can then be deduced from the angular velocity via a separate numerical procedure discussed in Section 4.4. However, computational difficulties arise when (4.3.17a) with ($\dot{d} \Rightarrow \omega$) is employed to solve the rotational equations

$$J \dot{\omega} + \tilde{\omega} J \omega = f_{\omega} \quad (4.3.19)$$

typical of multibody dynamics. From these equations, it is seen that in order to compute $\dot{\omega}^n$, it is necessary to have ω^n . However, due to the inherent nature of the algorithm, only $\omega^{n-\frac{1}{2}}$ is available. To alleviate this problem, the following approximations may be introduced:

$$\omega^n \simeq \omega^{n-\frac{1}{2}} \quad (4.3.20)$$

$$\omega^n \simeq \frac{1}{2} (\omega^{n+\frac{1}{2}} + \omega^{n-\frac{1}{2}}) \quad (4.3.21)$$

It will be shown that the first approximation results in a computationally unstable algorithm, while the second approximation remains stable but does not retain an explicit nature of computations. These difficulties motivated the development of a modified central difference algorithm termed the two-stage staggered procedure [44]. This algorithm is based on an interlaced application of the central difference algorithm such that the displacements and velocities are advanced one-half time step at a time. As standard of explicit integration methods, the new algorithm remains stable under a restricted step size and is based on vector operations. The stability analysis of the algorithms follows.

4.3.2.1 Standard Central Difference Implementation

For a linearized stability analysis of the central difference algorithm (4.3.17) with approximations (4.3.20) and (4.3.21) as applied to rotational equations typical of multibody dynamics, the linearized equations of dynamics

$$J \ddot{\Delta\theta} + C^G \dot{\Delta\theta} + (K^M + K^G + K^C) \Delta\theta = f_\omega - M_J^n + M_J$$

as derived in Section 2.5.1 will be examined. the torque-free motion of a single spherical rigid body in which the principal inertia terms are equal,

the above linearized equations reduce to

$$I \ddot{\Theta} + \tilde{\omega} \dot{\Theta} = 0 \quad . \quad (4.3.22)$$

This simple case is used to demonstrate important stability characteristics as follows. The effects of the geometric, material, and centrifugal stiffnesses K^G , K^M , and K^C are deduced from numerical experiments to assess the numerical stability of flexible systems.

To first examine the effects of the combination (4.3.17) with (4.3.20) on the linearized equations (4.3.22), we apply (4.3.17) with $(d \Rightarrow \Theta)$ to (4.3.22) to yield

$$\dot{\Theta}^{n+\frac{1}{2}} = \dot{\Theta}^{n-\frac{1}{2}} - h \tilde{\omega} \dot{\Theta}^n \quad (4.3.23)$$

$$\Theta^{n+1} = \Theta^n + h \dot{\Theta}^{n+\frac{1}{2}} \quad . \quad (4.3.24)$$

The approximation (4.3.20) with $(\omega \Rightarrow \dot{\Theta})$ is then introduced to give

$$\dot{\Theta}^{n+\frac{1}{2}} = [I - h \tilde{\omega}] \dot{\Theta}^{n-\frac{1}{2}} \quad (4.3.25)$$

$$\Theta^{n+1} = \Theta^n + h \dot{\Theta}^{n+\frac{1}{2}} \quad . \quad (4.3.26)$$

To assess the stability characteristics, these equations are rewritten in the form of a difference equation in terms of Θ as

$$(\Theta^{n+1} - 2\Theta^n + \Theta^{n-1}) + h \tilde{\omega} (\Theta^n - \Theta^{n-1}) = 0 \quad . \quad (4.3.27)$$

Computational stability is determined by seeking a nontrivial solution of the form

$$\Theta^{n+1} = s \Theta^n = s^2 \Theta^{n-1} \quad . \quad (4.3.28)$$

For a stable algorithm, it is necessary that

$$|s| \leq 1 \quad . \quad (4.3.29)$$

From (4.3.28), the characteristic equation of (4.3.27) becomes

$$\det | (s - 1)^2 + h\omega(s - 1) | = 0 . \quad (4.3.30)$$

In order to test the stability requirement (4.3.29) on the above equation, the unit circle (4.3.29) is transformed into the entire left-half plane of the z -domain via

$$s = \frac{1 + z}{1 - z} \quad (4.3.31)$$

such that (4.3.29) is equivalent to

$$\operatorname{Re}(z) \leq 0 . \quad (4.3.32)$$

The characteristic equation (4.3.30) is evaluated by introducing (4.3.31), and the z -polynomial equation

$$\begin{aligned} h^2 (\omega_1^2 + \omega_2^2 + \omega_3^2) z^2 - 2h^2 (\omega_1^2 + \omega_2^2 + \omega_3^2) z \\ + [4 + h^2 (\omega_1^2 + \omega_2^2 + \omega_3^2)] = 0 \end{aligned} \quad (4.3.33)$$

results. This equation must be examined for possible unstable roots. For this purpose, the Routh-Hurwitz stability criterion. [95] is employed. In order for all of the roots of a second-order polynomial to lie in the stable left-hand plane, each of the coefficients of the polynomial must be non-negative. It is immediately seen that the coefficient of the z -term in the above is always negative. Thus, for the present rigid body example, the central difference algorithm becomes an unstable integration method when the conventional velocity approximation is incorporated. This property is witnessed in numerical simulations of flexible multibody systems when the given procedure is used to integrate the equations of motion. For this reason, this procedure is not suitable for multibody dynamics applications of the form (4.3.19).

The alternative velocity approximation (4.3.21) as implemented into the central difference algorithm (4.3.17) corrects this instability problem. In analyzing this procedure, the substitution of (4.3.21) with $(\omega \Rightarrow \dot{\Theta})$ into (4.3.23) gives the counterparts to (4.3.25-4.3.26) as

$$\begin{aligned} \left(I + \frac{h}{2} \tilde{\omega} \right) \dot{\Theta}^{n+\frac{1}{2}} &= \left(I - \frac{h}{2} \tilde{\omega} \right) \dot{\Theta}^{n-\frac{1}{2}} \\ \Theta^{n+1} &= \Theta^n + h \dot{\Theta}^{n+\frac{1}{2}} \end{aligned}$$

The equivalent difference equation for the above algorithm is

$$\left(\Theta^{n+1} - 2\Theta^n + \Theta^{n-1} \right) + \frac{h}{2} \tilde{\omega} \left(\Theta^{n+1} - \Theta^{n-1} \right) = 0. \quad (4.3.34)$$

The characteristic equation of the above

$$\det \left| \begin{pmatrix} s - 1 \end{pmatrix}^2 + \frac{h}{2} \tilde{\omega} (s^2 - 1) \right| = 0 \quad (4.3.35)$$

is again transformed to the z -domain via (4.3.31). In this case, the z -polynomial equation becomes

$$z^4 \left[16z^2 + h^2 (\omega_1^2 + \omega_2^2 + \omega_3^2) \right] = 0. \quad (4.3.36)$$

It is easily seen that for this case roots are either zero or purely imaginary. As such, the central difference algorithm combined with the alternative velocity approximation is unconditionally stable for the simple rigid body example. For systems of flexible bodies, the stability limit of the above algorithm is governed by the maximum elastic frequency of the beam component which can be determined from the eigenvalues of the tangent stiffness matrices K^G and K^M or by the centrifugal stiffness of the tangent mass K^C . From computational experiments, it has been seen that the stability limit closely corresponds to that as predicted from the elastic frequencies of linear Timoshenko beam stiffness matrices.

The one drawback to the use of this last algorithm is that implicit computations are required to determine the velocity when the equations of motion contain velocity dependent force terms other than diagonal damping. To show this, the algorithm (4.3.17a) with $(\dot{d} \Rightarrow \omega)$ and the approximation (4.3.21) are applied to the nonlinear equations of motion (4.3.19). The following nonlinear residual equation

$$\begin{aligned} r^{n+\frac{1}{2}} &= J \omega^{n+\frac{1}{2}} + \frac{h}{4} (\bar{\omega}^{n+\frac{1}{2}} + \bar{\omega}^{n-\frac{1}{2}}) J (\omega^{n+\frac{1}{2}} + \omega^{n-\frac{1}{2}}) \\ &\quad - J \omega^{n-\frac{1}{2}} - h f_{\omega} = 0 \end{aligned} \quad (4.3.37)$$

results. The Newton-Rhapson technique must be employed to solve the above equation for $\omega^{n+\frac{1}{2}}$. For this case, the following iterative sequence

$$E^k \Delta\omega = -r^{n+1}_k \quad (4.3.38a)$$

$$\omega^{n+1}_{k+1} = \omega^n_k + \Delta\omega \quad (4.3.38b)$$

results, and the solution matrix E is easily derived as

$$E = \begin{bmatrix} J_1 & \frac{h}{4} (J_3 - J_2) \bar{\omega}_3 & \frac{h}{4} (J_3 - J_2) \bar{\omega}_2 \\ \frac{h}{4} (J_1 - J_3) \bar{\omega}_3 & J_2 & \frac{h}{4} (J_1 - J_3) \bar{\omega}_1 \\ \frac{h}{4} (J_2 - J_1) \bar{\omega}_2 & \frac{h}{4} (J_2 - J_1) \bar{\omega}_1 & J_3 \end{bmatrix}$$

$$\bar{\omega} \equiv (\omega^{n+\frac{1}{2}} + \omega^{n-\frac{1}{2}}) \quad .$$

The implicit computation is only necessary to obtain the angular velocities of multibody system equations. The translational displacements and velocities are found from the standard application of the central difference algorithm, and the rotational orientation is found from the angular velocities with a procedure to be discussed in Section 4.4. The necessity for the Newton-Rhapson solution of the angular velocity can be eliminated by the following algorithm.

4.3.2.2 Modified Central Difference Implementation

An alternative algorithm has been derived to alleviate the problems or complications resulting from the velocity approximations which must be introduced when the central difference algorithm is used to integrate the equations of motion for multibody systems. The troublesome velocity approximations can be eliminated by staggering the standard central difference update such that the displacements and velocities are advanced one-half time step at a time. The algorithm advances the solution to the time station $t^{n+\frac{1}{2}}$ given the solutions of the two preceding time stations $t^{n-\frac{1}{2}}$ and t^n as

$$\dot{d}^{n+\frac{1}{2}} = \dot{d}^{n-\frac{1}{2}} + h \ddot{d}^n \quad (4.3.39a)$$

$$d^{n+\frac{1}{2}} = d^{n-\frac{1}{2}} + h \dot{d}^n \quad (4.3.39b)$$

The algorithm is initiated for time $t^{\frac{1}{2}}$ given initial conditions for time t^0 as follows:

$$\dot{d}^{\frac{1}{2}} = \dot{d}^0 + \frac{h}{2} \ddot{d}^0$$

$$d^1 = d^0 + h \dot{d}^{\frac{1}{2}}$$

$$d^{\frac{1}{2}} = \frac{1}{2} (d^0 + d^1) \quad .$$

The result is an explicit computation which remains stable under a restricted stepsize.

The stabilizing effect of this algorithm is demonstrated with the same procedure used in assessing the other algorithms. Application of (4.3.39) to the linearized equations (4.3.22) yields the difference equation

$$(\Theta^{n+1} - 2\Theta^{n-1} + \Theta^{n-3}) + \bar{h} \tilde{\omega} (\Theta^n - \Theta^{n-2}) = 0$$

where $\bar{h} = 2h$. The associated characteristic equation is seen to be

$$\det | (s^2 - 1)^2 + \bar{h} \omega s (s^2 - 1) | = 0$$

from which the z -domain stability polynomial is derived as

$$\bar{h}^2 (\omega_1^2 + \omega_2^2 + \omega_3^2) z^4 + [16 - 2 \bar{h}^2 (\omega_1^2 + \omega_2^2 + \omega_3^2)] z^2 + \bar{h}^2 (\omega_1^2 + \omega_2^2 + \omega_3^2) = 0 .$$

For a fourth-order polynomial of the form

$$a z^4 + b z^2 + c = 0$$

to guarantee stable roots, the conditions

$$a \geq 0 , \quad b \geq 0 , \quad c \geq 0 , \quad b^2 - 4ac \geq 0$$

must all be satisfied. This is accomplished by restricting the stepsize to be

$$h \leq \frac{1}{\sqrt{\omega_1^2 + \omega_2^2 + \omega_3^2}}$$

for the specialized example problem. This linearized stability analysis confirms that the present two-stage explicit procedure in fact remains stable in the presence of gyroscopic damping. The stable stepsize for flexible multi-body applications is dictated by the above and the standard central difference limit

$$h \leq \frac{2\pi}{\omega_b}$$

where ω_b is the highest elastic frequency of the beam component. As verified by computational experiments, the flexible stability limit can be approximated from the linear Timoshenko beam stiffness matrices.

This algorithm, termed the two-stage explicit procedure, can be applied to the nonlinear equations of motion in a straightforward manner; (4.3.39a) with $(\dot{d} \Rightarrow \dot{u}, \omega)$ is used to integrate the translational and angular velocities and (4.3.39b) with $(d \Rightarrow u)$ is used to integrate the

translational displacements. The algorithm advances the solution a half time station at a time, and requires the evaluation of the right-hand side terms Q twice each time step. Included in this evaluation is the computation of the internal force as discussed in Chapter III. The trade-off between this algorithm and the standard central difference algorithm accompanied with the velocity averaging, aside from the step-size restriction, is then a consideration between the extra force evaluation per time step required of the former versus the simultaneous equation solver required of the latter for the iterative angular velocity solution procedure.

Thus concludes the discussion of the integration of the equations of motion for multibody dynamics applications by the central difference algorithm. The two stable algorithms which have been discussed, namely the standard central difference algorithm including the velocity averaging and the two-stage staggered explicit algorithm, were introduced for integration of the translational displacements and velocities and the angular velocities of multibody systems. As the rotational orientation parameters are not directly integrable from the angular velocity vector, a procedure must be developed to update the configuration orientation given the angular velocity. This is discussed next.

4.4 Rotational Orientation Update Procedure

The effective treatment of rotational quantities inherently involved in the multibody system equations requires special consideration. As addressed in Section 4.3.1, implicit algorithms are based on an integration of the displacements and a particular rotational parameterization as the primary variables. Given the rotational parameterization, usually taken to

be the rotational vector, the configuration orientation is directly updated via (4.3.9) or a suitable counterpart. Computationally, this can be accomplished using an exact functional expression for the matrix exponential [32], using the Euler parameter representation of rotation matrices after converting the incremental rotational vector to Euler parameters [32], or using a second-order approximation to the matrix exponential [50]. For the explicit techniques, the rotational orientation must be deduced from the angular velocity solution.

A classical rotational update procedure is based on a discrete approximation

$$\mathbf{R}^{n+1} \simeq \exp(\boldsymbol{\omega}^* h) \mathbf{R}^n \quad (4.4.1)$$

$$\boldsymbol{\omega}^* = \tilde{\boldsymbol{\omega}}(t^n + \beta h) \quad (4.4.2)$$

to the true solution

$$\mathbf{R}^{n+1} = \exp\left(\int_{t^n}^{t^{n+1}} \tilde{\boldsymbol{\omega}}(\tau) d\tau\right) \mathbf{R}^n$$

of the generating differential equation

$$\dot{\mathbf{R}} = \tilde{\boldsymbol{\omega}}^T \mathbf{R} \quad (4.4.3)$$

The evaluation of the angular velocity at time $t^{n+\frac{1}{2}}$ with $\beta = \frac{1}{2}$ in (4.4.2) was determined to provide the highest accuracy [96]. A related result applied the generalized midpoint rule to the generating kinematic differential equation to yield [97]

$$\mathbf{R}^{n+1} \simeq \Delta \mathbf{R} \mathbf{R}^n$$

$$\Delta \mathbf{R} = [I - \beta \boldsymbol{\omega}^* h]^{-1} [I + (1 - \beta) \boldsymbol{\omega}^* h] \quad .$$

In order for $\Delta \mathbf{R}$ to remain an orthogonal rotation matrix, it was shown that for the above expression the value $\beta = \frac{1}{2}$ is needed. The rotational matrix approximation can be inverted as

$$\left(I - \frac{\tilde{\Theta}}{2} \right)^{-1} \left(I + \frac{\tilde{\Theta}}{2} \right) = I + \frac{1}{1 + (\|\Theta\|^2/4)} \left[\tilde{\Theta} + \frac{1}{2} \tilde{\Theta}^2 \right],$$

which is equivalent to the second-order Pade approximation of the matrix exponential $\exp(\tilde{\Theta})$. Therefore, a rotational update is obtained from a true or approximate matrix exponentiation of $\tilde{\Theta} = \tilde{\omega}^{n+\frac{1}{2}} h$.

An alternative procedure introduced here is based on the numerical integration of the following Euler parameter representation of the generating equation

$$\dot{q} = \mathbf{A}(\omega) q, \quad q = \begin{Bmatrix} q_0 \\ \mathbf{q} \end{Bmatrix} \quad (4.4.4)$$

in which \mathbf{A} is given by

$$\mathbf{A}(\omega) = \frac{1}{2} \begin{bmatrix} 0 & -\omega^T \\ \omega & \tilde{\omega}^T \end{bmatrix}$$

for the body-fixed angular velocity coordinate definitions. The configuration orientation is obtained from a numerical time discretization of (4.4.4). Among several possibilities, the approximation that satisfies the inherent constraint condition

$$\dot{q}_0 q_0 + \dot{\mathbf{q}}^T \mathbf{q} = 0 \quad (4.4.5)$$

in the discrete sense is the following trapezoidal formula

$$\frac{q^{n+1} - q^n}{h} = \mathbf{A}(\omega^{n+\frac{1}{2}}) \frac{1}{2} (q^{n+1} + q^n).$$

Due to the structure of \mathbf{A} , the solution matrix can be analytically inverted such that the discrete orientation update is accomplished according to

$$q^{n+1} = \frac{1}{D} \left[I + \frac{h}{2} \mathbf{A}(\omega^{n+\frac{1}{2}}) \right] \left[I + \frac{h}{2} \mathbf{A}(\omega^{n+\frac{1}{2}}) \right] q^n \quad (4.4.6)$$

where

$$D = 1 + \frac{h^2}{4} (w_1^2 + w_2^2 + w_3^2) \quad .$$

The final result is normalized to satisfy the Euler parameter constraint condition.

The resulting update (4.4.6) involves only explicit computations and is readily incorporated into the two-stage explicit integration procedure. This Euler parameter-based solution procedure also interfaces with the internal force computational procedure presented in Chapter III. The concept of an Euler parameter-based orientation update procedure was introduced in [44] for rigid multibody dynamic systems. For the rigid cases, many implicit integration algorithms as applied to (4.4.4) resulted in accurate numerical simulations. For the extension to flexible systems, it was determined that the particular algorithm (4.4.6) must be implemented to achieve a stable simulation. This particular algorithm implicitly satisfies the constraint condition (4.4.5), whereas alternative algorithms do not possess this property. Thus, successful simulations of flexible systems are not necessarily immediately obtained from existing rigid-body dynamic solution procedures. The present formulation, involving the internal force computation of Chapter III, the generalized coordinate integrator of Section 4.3.2.2, and the orientation update procedure of the present section, leads to effective simulations as demonstrated in Section 4.6. The next section discusses the solution of the Lagrange multipliers which have been incorporated to augment the constraint conditions to the differential equations of motion.

4.5 Constraint Force Solution Procedure

A partitioned solution procedure has been employed to solve the the Lagrange multipliers and the corresponding constraint forces separately from the solution for the generalized coordinates. A stabilized constraint force solution procedure originally developed for rigid multibody systems in [91,92] was successfully extended to models incorporating the present beam formulation. Again, the success of various existing constraint force solution procedures developed from analyzing multirigid body systems is not necessarily guaranteed for flexible multibody systems. For this reason, a particular implementation of the basic formalism of [91,92] was determined to yield effective simulations of flexible multibody systems.

To effect a partitioned solution of the constraints, a stabilized companion differential equation for the constraint forces is formed by adopting the penalty procedure. The penalty procedure uses the equations

$$\lambda_H = \frac{1}{\epsilon} \Phi_H \quad , \quad \dot{\lambda}_N = \frac{1}{\epsilon} \dot{\Phi}_N \quad , \quad \epsilon \rightarrow 0 \quad (4.5.1)$$

as the basic constraint conditions instead of (4.2.1) and (4.2.3), respectively. From (4.2.2) and (4.2.3), both penalty equations can be written in the general form,

$$\dot{\lambda} = \frac{1}{\epsilon} B \dot{d} \quad , \quad \dot{d} = \begin{Bmatrix} \dot{u} \\ \omega \end{Bmatrix} \quad (4.5.2)$$

where the notation includes both holonomic and nonholonomic constraints with (4.2.5).

The numerical solution to the companion differential equation (4.5.2) is obtained as follows. The constrained equations of motion (4.2.4) are integrated once using a general implicit integration algorithm given as

$$\dot{d}^{n+1} = \delta \ddot{d}^{n+1} + g^n$$

Two specific algorithms have been shown to work within the context of flexible multibody systems; they are the trapezoidal rule ($g^n \equiv \dot{d}^n + \delta \ddot{d}^n$, $\delta \equiv \frac{h}{2}$) and the forward Euler formula ($g^n \equiv \dot{d}^n$, $\delta \equiv h$) . The result of the integration

$$\dot{d}^{n+1} = \delta M^{-1} (Q^{n+1} - B^T \lambda^{n+1}) + g^n \quad (4.5.3)$$

is substituted into (4.5.2), and a stabilized differential equation

$$\epsilon \dot{\lambda}^{n+1} + \delta B M^{-1} B^T \lambda^{n+1} = \delta B M^{-1} Q^{n+1} + B g^n \quad (4.5.4)$$

is obtained for the Lagrange multipliers. To obtain a discrete update of λ , the same integration rule is applied to this equation as was used for the generalized velocity. The trapezoidal rule

$$\lambda^{n+1} = \lambda^n + \delta (\dot{\lambda}^n + \dot{\lambda}^{n+1})$$

results in a constraint force update of the form

$$\begin{aligned} (\epsilon I + \delta^2 B M^{-1} B^T) \lambda^{n+1} &= (\epsilon I - \delta^2 B M^{-1} B^T) \lambda^n \\ &+ r_{\lambda}^{n+1} + r_{\lambda}^n \end{aligned} \quad (4.5.5)$$

where

$$r_{\lambda}^{n+1} = \delta^2 B M^{-1} Q^{n+1} + \delta B g_d^n, \quad (4.5.6)$$

while the forward Euler formula

$$\lambda^{n+1} = \lambda^n + \delta \dot{\lambda}^{n+1}$$

gives

$$(\epsilon I + \delta^2 B M^{-1} B^T) \lambda^{n+\frac{1}{2}} = \epsilon \lambda^n + r_{\lambda}^{n+1} \quad (4.5.7)$$

These update formulas are easily adopted into the generalized coordinate solvers discussed in the previous section. For each time step, integration of the generalized coordinates is first performed. The solutions are used to update the right-hand side vector Q , which is then input into the Lagrange multiplier update module. The solution of the Lagrange multipliers is then used to correct the right-hand side vector Q with the current constraint forces $\mathbf{B}^T \lambda$. The procedure can then be advanced to the next time step.

4.6 Numerical Examples

The computational techniques, namely the staggered multibody dynamics solution procedure combining the generalized coordinate integrator presented in Section 4.3.2, the orientation update procedure presented in Section 4.4, and the constraint force solver presented in Section 4.5 with the computational procedure for the beam internal force presented in Chapter III, have been implemented into a Fortran 77 software package. The result is a robust method which solves the present formulation of the equations of motion of an arbitrary assemblage of flexible beams and rigid bodies. A distinct feature of the present work is the computational preservation of total energy for undamped systems; this is obtained via the combined developments of the objective strain increment/stress update procedure presented in Chapter III with the dynamic solution procedures of the present chapter. In order to demonstrate the current software capabilities, the following examples highlighting the flexible motion of the beam component are presented.

Example 4.1 Spin-up maneuver. The first example is included to

verify the geometric stiffening phenomena exhibited by a rotating beam [15,23,30,33]. In this case, a pinned beam is subjected to the prescribed angular rotation

$$\theta(t) = \begin{cases} \frac{6}{15} \left[\frac{t^2}{2} + \frac{15^2}{2\pi} \left(\cos \frac{2\pi t}{15} - 1 \right) \right] \text{ rad} & 0 \leq t \leq 15 \text{ sec} \\ (6t - 45) \text{ rad} & t > 15 \text{ sec} \end{cases}$$

about the Z axis at the pinned end as shown in Figure 4.1a. The time history of the tip deflection relative to a reference frame coinciding with the prescribed angular position and the time history of several configurations of the beam are given in Figure 4.1b. An overall steady rotation of the beam gives rise to a centrifugal force which is responsible for a change in the bending stiffness that cannot be predicted using linear deformation theories. After initial increasing tip deflections, the beam begins to stiffen as the angular velocity increases due to the centrifugal inertia force. As the angular velocity reaches a constant state, the beam then reaches a steady state phase of small vibrations. The frequency of these vibrations is higher than those of a nonrotating beam due to the geometric stiffening effect. This example shows the capability of the nonlinear strain formulation to automatically account for this geometric stiffening, and the results are comparable to those presented in [33,100]. To reproduce these results with alternative methods as the substructuring technique [30], a convergence analysis based on the selection of mode shapes must be performed.

Example 4.2 Planar motion of pinned beam. This next example demonstrates the combined large deformation and large rotation capabilities of the present formulation. Two different simulations are presented in which a pinned beam is subjected to the given initial velocity impulses shown

in Figures 4.2a and 4.2c. The resulting time histories of several deformed configurations due to the particular initial velocity impulse are shown in Figures 4.2b and 4.2d. It is noted the versatility of the formulation in its ability to capture the response to a variety of situations in which different fundamental modes of the beam are excited. The approach avoids the difficulty of tailoring the selection of modes shapes of the flexible components to the given problem at hand. The repeatability of the deformation shapes through time is due to the invariance of the internal force computations to the overall rigid motion. This property of computational objectivity is further illustrated in Figures 4.2b and 4.2d in which the time history of the strain, kinetic, and total energy is given over four revolutions of the motion. The nature of the time integration and internal force algorithms are such that the conservation of energy is retained computationally, as seen by the fact that the total energy remains constant for a number of revolutions.

Example 4.3 Closed-loop chain in free flight. This example, also analyzed in [100], demonstrates the capability of the present approach to model the dynamics of flexible multibody systems. A closed-loop chain consisting of four flexible links interconnected by hinges is subjected to a force and a torque at one of the hinges to induce an overall tumbling motion of the chain. The problem data is detailed in Figure 4.3a, and the sequence of the motion is given in Figure 4.3b. The results coincide with those presented in [100]. It is noted that the joint connection can easily be accounted for from a finite element assemblage which leaves the rotational degrees of freedom free at the hinge location. The method was used to verify the results obtained using the Lagrange multiplier solver of Section 4.5.

Example 4.4 Spatial motion of pinned beam. This example presents

the capability of the formulation to model the combined effect of spatial rotations with large deformations. As in Example 4.2, two different simulations are presented in which the pinned beam is subjected to an initial velocity impulse in the horizontal X-Y plane as shown in Figures 4.4a and 4.4e. The beam is also subjected to a gravitational force acting along the $-Z$ axis. The history of the spatial rotation and deformation throughout several revolutions are shown in Figures 4.4b - 4.4c and 4.4e - 4.4f. The energy time histories for both simulations, as given in Figure 4.4g, again verify the computational objectivity of the algorithm for spatial motions.

Example 4.5. Spatial motion of double pendulum. This example presents the motion of a spatial double pendulum. The double pendulum is modeled with two beams; a spherical joint connects the last node of the first beam to the first node of the second beam and also pins the first node of the first beam. As shown in Figure 4.5a, the pendulum is subjected to a gravity field in the vertical Z-direction and an initial velocity impulse in the horizontal X-Y plane such that solely rigid motion is excited. The problem is run for four cases of increasing beam flexibility as given in Figure 4.5a. The spatial trajectories of the mass center of the second beam as projected on the X-Y and X-Z planes for each of the beam flexibilities are given in Figure 4.5b. The trajectory of the first case coincides exactly with a rigid body solution to the problem, and the slight deviation of the trajectories due to the increasing flexibility can be seen. The energy time histories for each case given in Figures 4.5c - 4.5f verify the computational conservation of energy. Again, the invariance of the internal force calculations in the three dimensional environment is witnessed by the negligible strain energy contribution within all of the flexible cases. The time integration of the

spatial kinematics preserves the balance between the kinetic and potential energies of the problem.

It is noted that as the beam becomes more flexible, increasing amounts of strain energy slightly come into effect. Cases in which the beam was made even more flexible were run, and in these cases the conservation of energy was not maintained. After closer examination, it was determined the straining of the beam had reached unrealistic proportions beyond the elastic limit and the parameters were also unrealistic. An examination of the energy history provides an immediate detection of potentially invalid simulations.

Example 4.6. Spatial motion of double pendulum. As a final example, the flexible double pendulum is given an initial velocity impulse to excite deformation motion as well as the rigid motion as shown in Figure 4.6a. The first beam is given an impulse in the X-Y plane, while the second beam is given an impulse in the X-Z plane. Note the material parameters have been changed from the above example, and the gravity force has been removed. The resulting time histories of several deformed configurations are given in Figure 4.6b, and the energy time histories are given in Figure 4.6c. The above example is included to show that the energy is still conserved for computations involving spatial deformations of the double pendulum.

The inclusion of the energy history plots in some of the above examples is a significant detail. This tool provides an effective method for analyzing the accuracy of the computational procedure. Numerous conceptual and computational ‘bugs’ were detected from examination of the energy history. As such, it is believed this detail provides somewhat of an accuracy measure of the given simulation. The figures referred to in the above

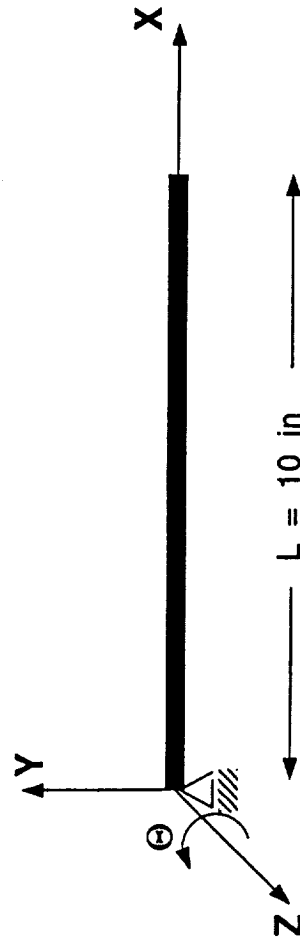
examples follow.

4.7 Concluding Remarks

A computational procedure suitable for the solution of equations of motion for flexible multibody systems has been presented. The equations of motion for an arbitrary assemblage of flexible beam and rigid body components can be constructed in a systematic manner as a result of the beam formulation presented in Chapter II. The dynamics are effectively treated by the following developments in multibody dynamic solution procedures. A two-stage modification of the central difference algorithm is presented to integrate the translational coordinates and the angular velocity vector. This staggered form of the central difference method was adopted for multibody applications due to complications arising from the unavailability of the generalized velocity vector at the time step at which the acceleration vector is evaluated. Given the solution to the angular velocity from the two-stage algorithm, the angular orientation is then obtained from the application of an implicit integration algorithm to the Euler parameter/angular velocity kinematical relation. The constraint conditions, which are augmented to the formulation via Lagrange multipliers, are enforced via a technique which implicitly integrates an alternative stabilized companion differential equation for the Lagrange multipliers. The present multibody dynamics solution procedures are effectively combined with the present internal force computational procedure to achieve a computational preservation of total energy for undamped systems as demonstrated via several numerical examples.

The next chapter presents the extension of the present methodology to model the dynamics of deployment/retrieval of the flexible members.

Problem Definition



Material Properties

$EA = 2.8 \times 10^7 \text{ lb}$
 $GA = 1.0 \times 10^7 \text{ lb}$
 $EI = 1.4 \times 10^4 \text{ lb in}^2$
 $\rho A = 1.2 \text{ lbm / in}$
 $\rho I = 6.0 \times 10^{-4} \text{ lbm in}$

Mesh

5 Linear Elements

Figure 4.1a Spin-up maneuver: problem data.

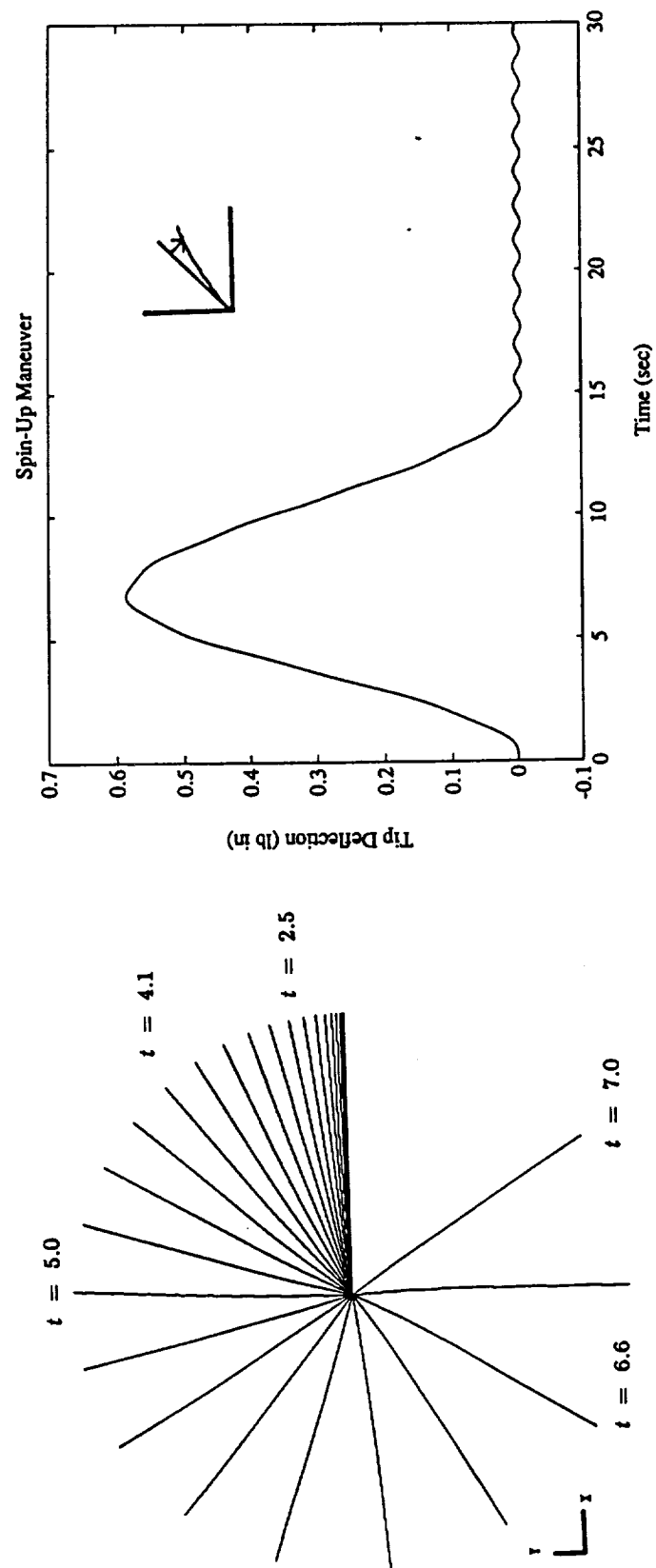
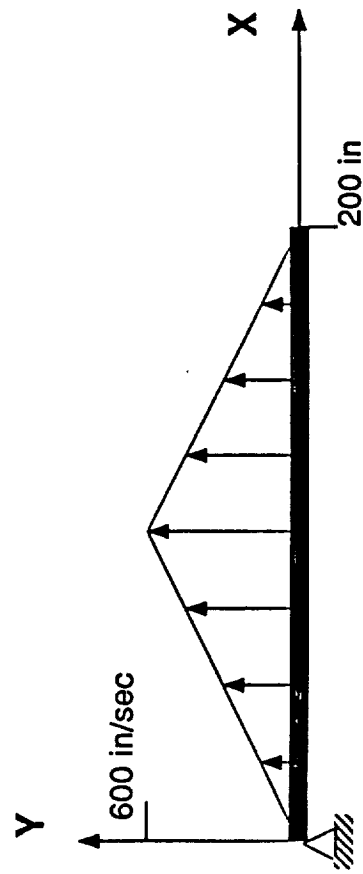


Figure 4.1b Spin-up maneuver: motion history, tip deflection history relative to floating reference.

Initial Beam Position vs. Initial Velocity Profile



Material Properties

$EA = 4.0 \times 10^7 \text{ lb}$
 $GA = 2.0 \times 10^7 \text{ lb}$
 $EI = 1.3 \times 10^7 \text{ lb in}^2$
 $\rho A = .98 \text{ lbm / in}$
 $\rho I = .033 \text{ lbm in}$

Mesh

8 Linear Elements

Figure 4.2a Planar motion of pinned beam (1): problem data.

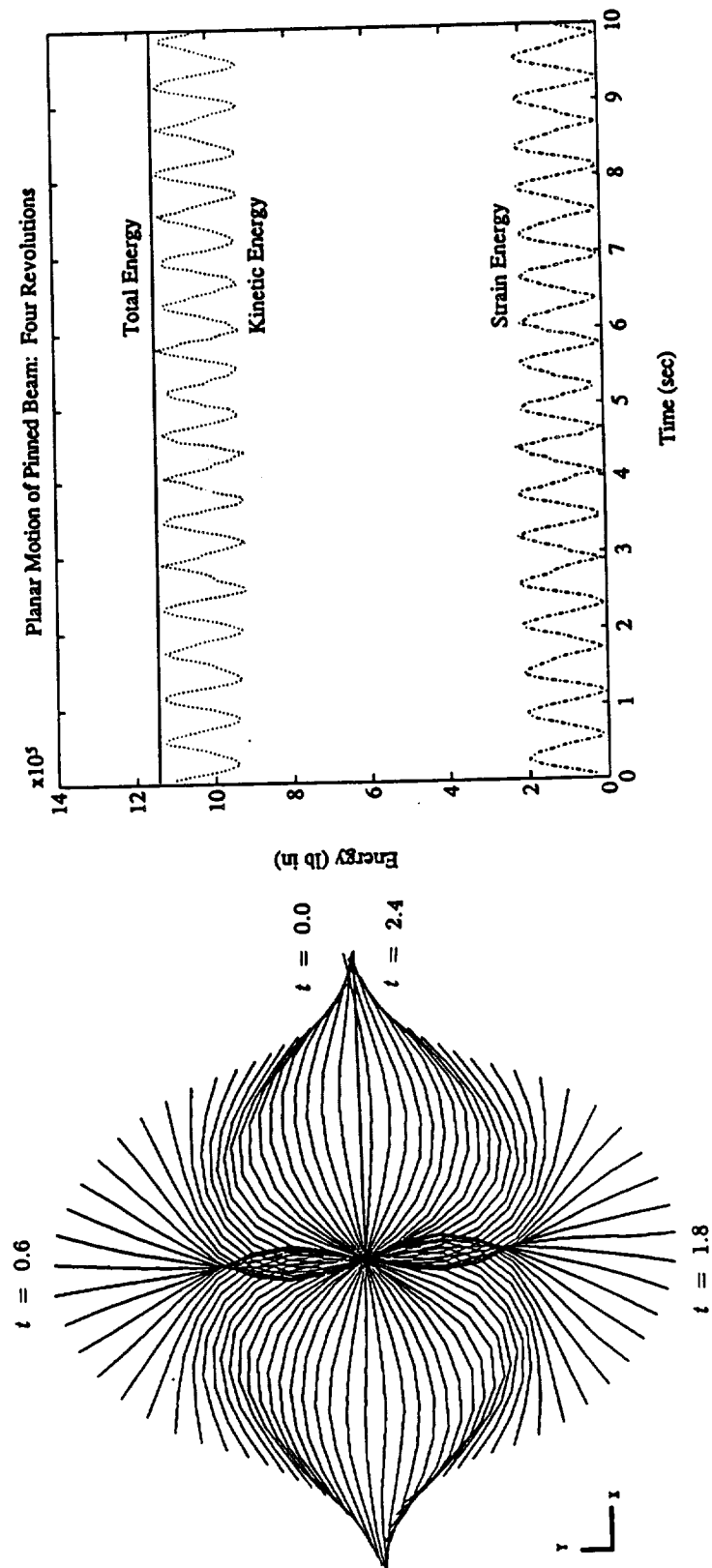
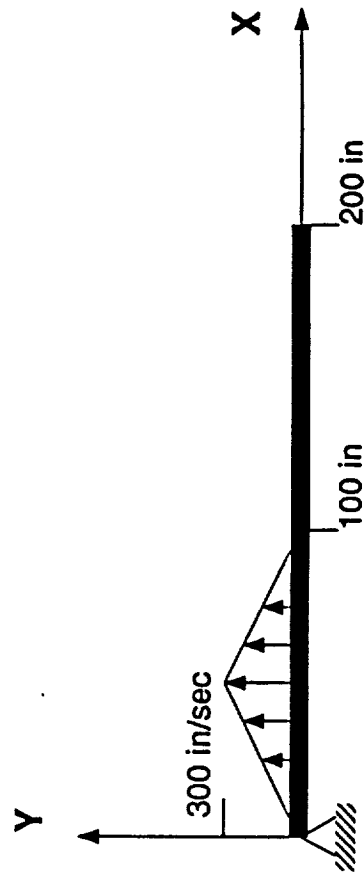


Figure 4.2b Planar motion of pinned beam (1): motion history, energy history.

Initial Beam Position vs. Initial Velocity Profile



Material Properties

$EA = 4.0 \times 10^7 \text{ lb}$
 $GA = 2.0 \times 10^7 \text{ lb}$
 $EI = 1.3 \times 10^7 \text{ lb in}^2$
 $\rho A = .98 \text{ lbm / in}$
 $\rho I = .033 \text{ lbm in}$

Mesh

12 Linear Elements

Figure 4.2c Planar motion of pinned beam (2): problem data.

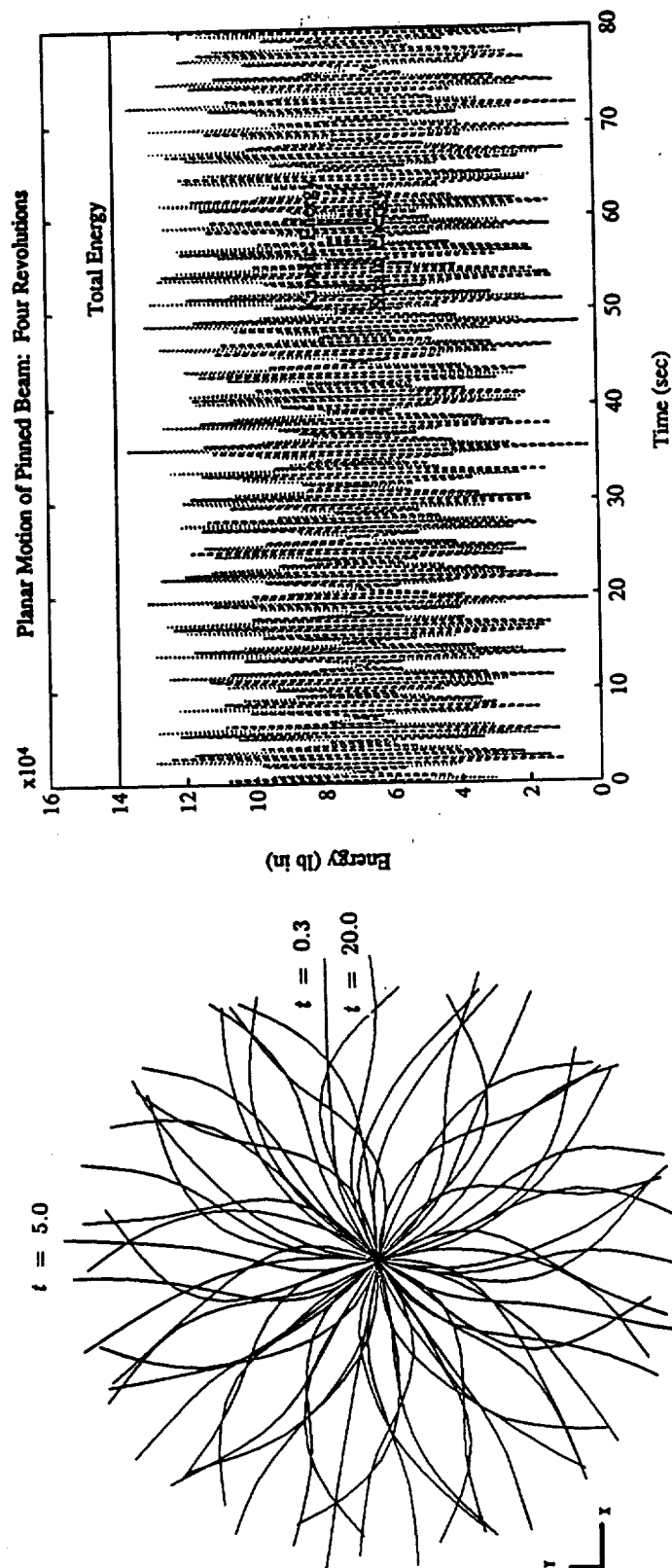
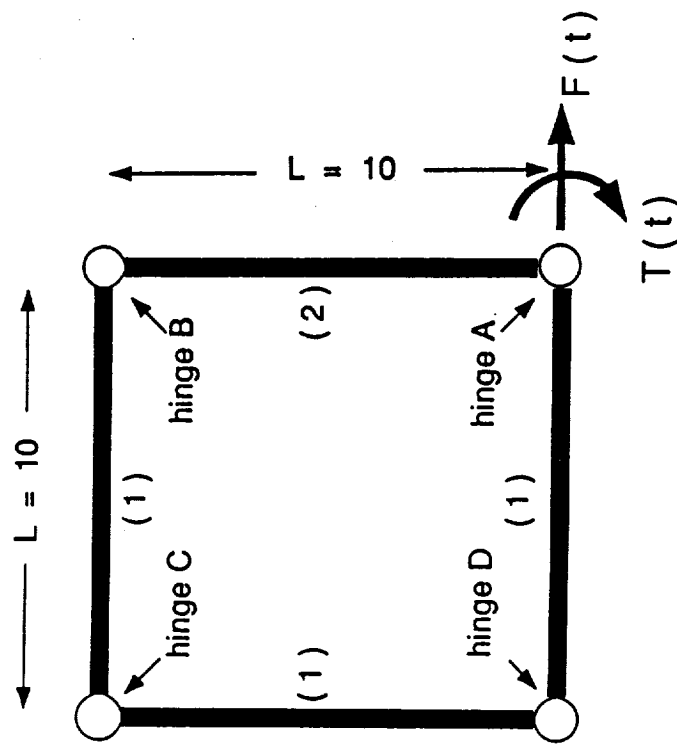


Figure 4.2d Planar motion of pinned beam (2): motion history, energy history.



Material Properties

$$EA = 1 \times 10^6$$

$$GA = 1 \times 10^6$$

$$\rho A = 1$$

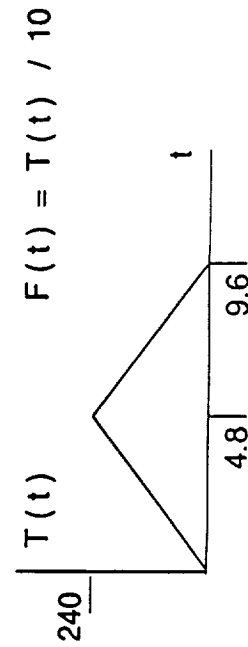
$$\rho I = 10$$

$$(1) EI = 2 \times 10^2$$

$$(2) EI = 1 \times 10^5$$

Mesh

10 Linear Elements / Link



$$F(t) = T(t) / 10$$

Figure 4.3a Closed-loop chain in free flight: problem data.

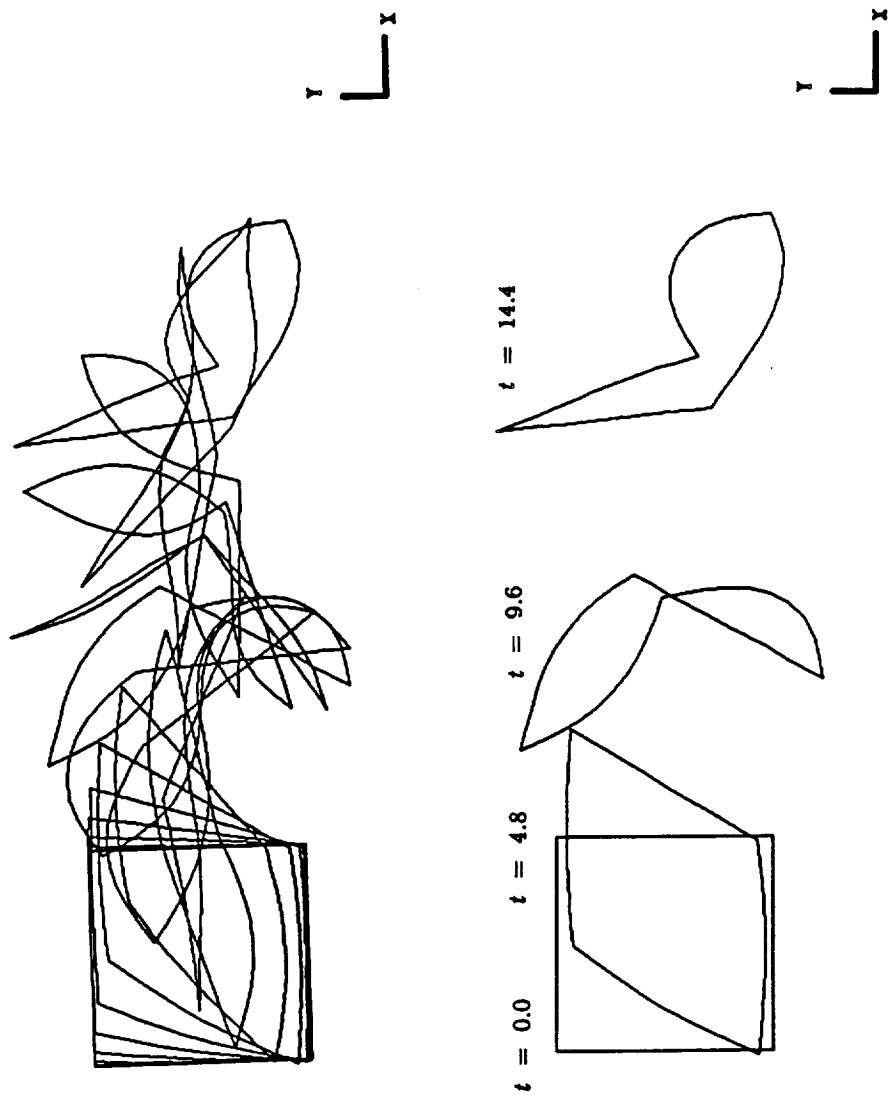
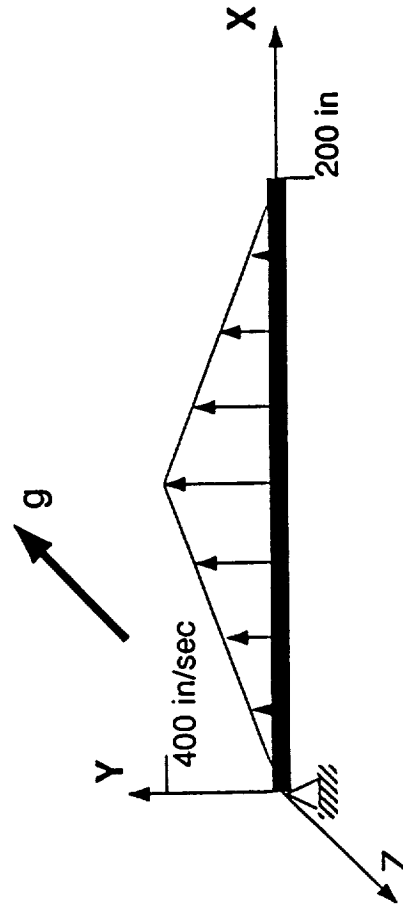


Figure 4.3b Closed-loop chain in free flight: motion history, close-up deformations.

Initial Beam Position vs. Initial Velocity Profile



Material Properties

$EA = 4.0 \times 10^7 \text{ lb}$
 $GA = 2.0 \times 10^7 \text{ lb}$
 $EI = 1.3 \times 10^7 \text{ lb in}^2$
 $\rho A = .98 \text{ lbm / in}$
 $\rho I = .033 \text{ lbm in}$

Mesh

8 Linear Elements

Figure 4.4a Spatial motion of pinned beam (1): problem data.

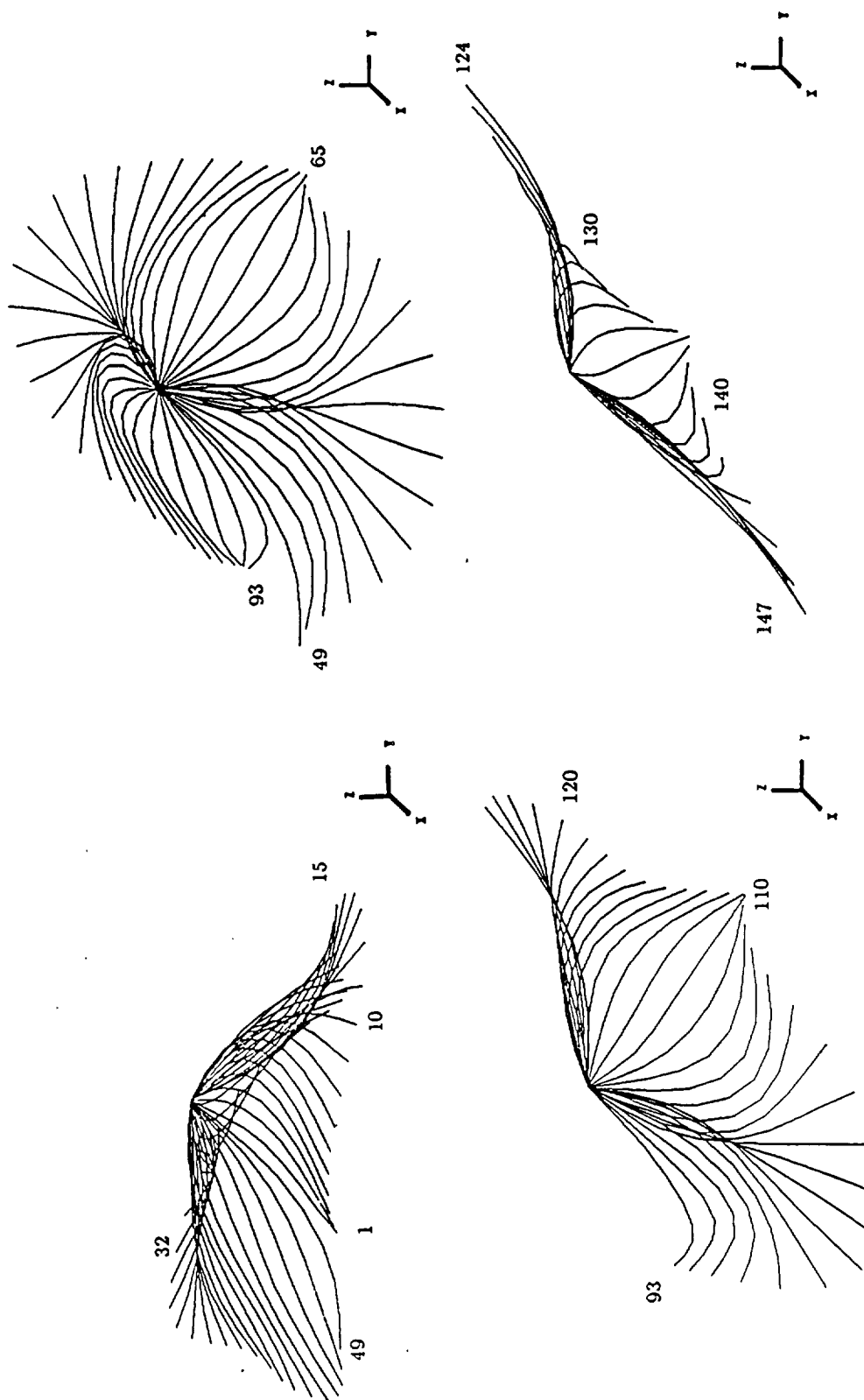


Figure 4.4b Spatial motion of pinned beam (1): motion history.

$$t = .05 n, \quad n = 1, \dots, 147$$

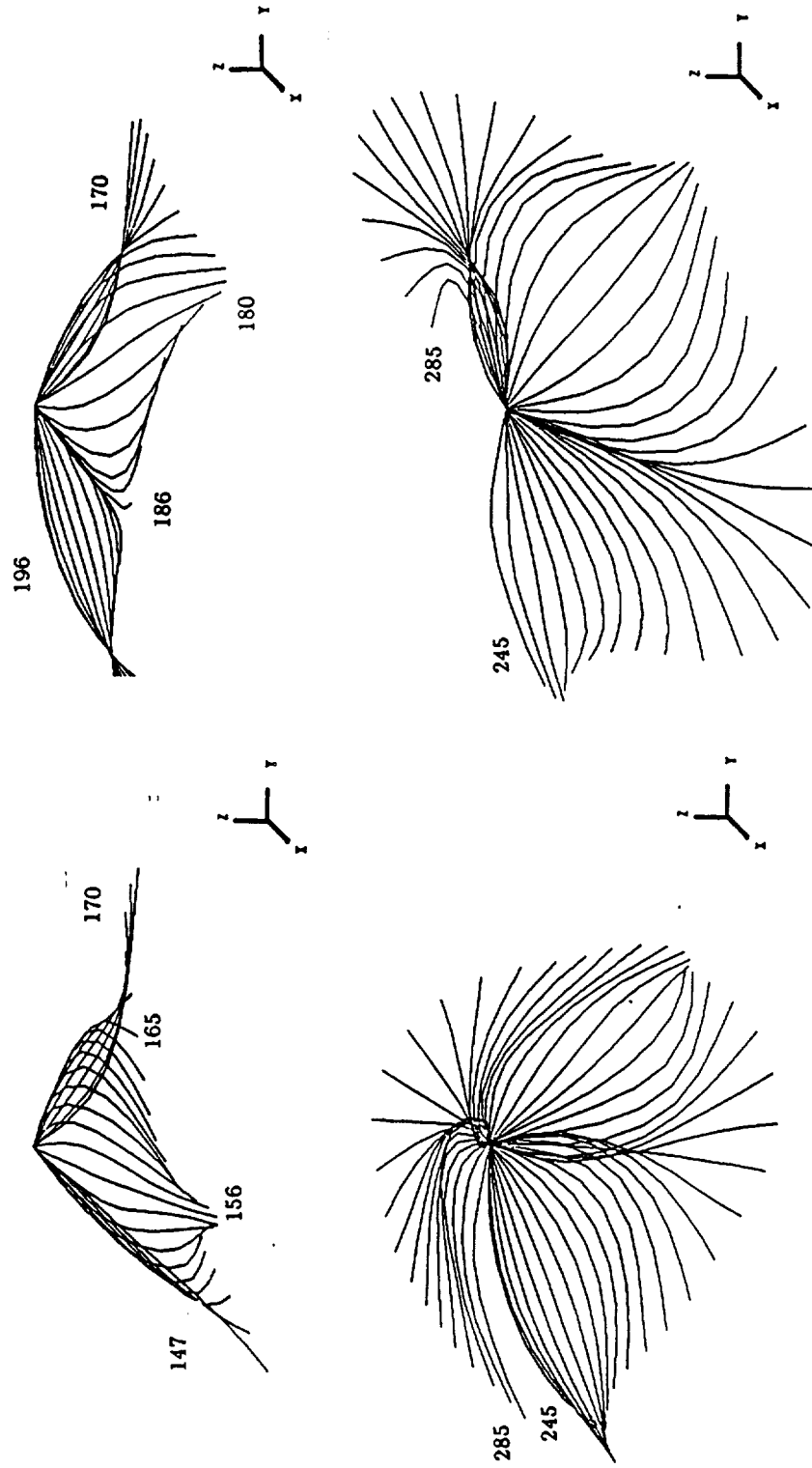


Figure 4.4c Spatial motion of pinned beam (1): motion history.

$t = .05 n, \quad n = 147, \dots, 285$

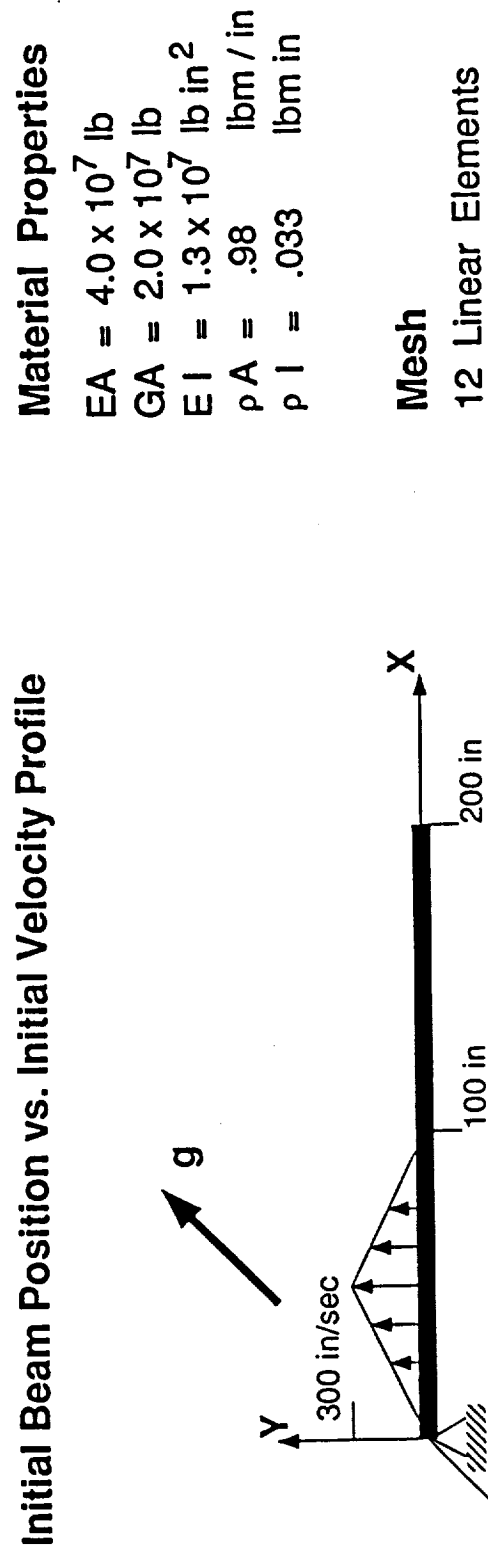


Figure 4.4d Spatial motion of pinned beam (2): problem data.

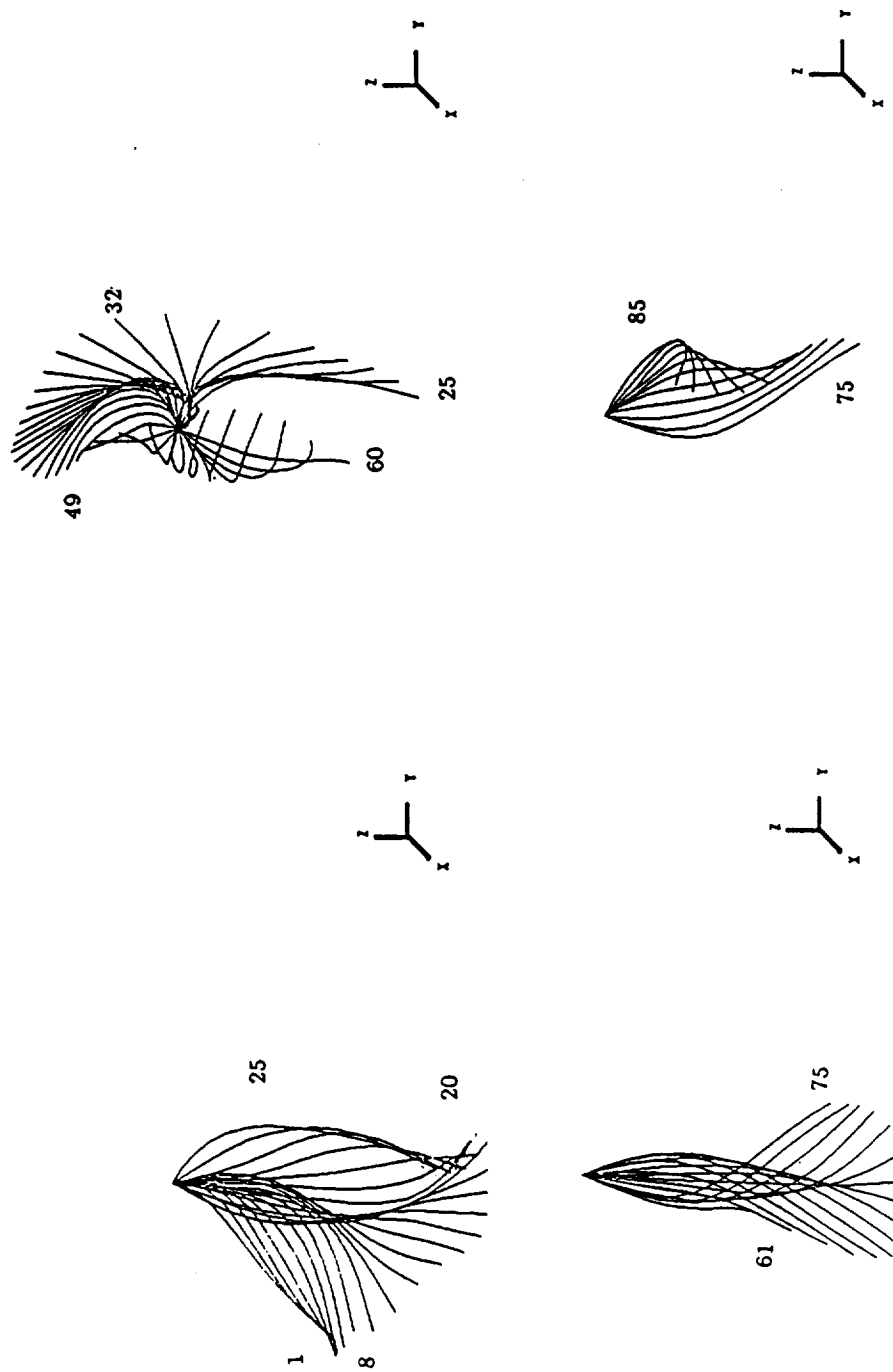


Figure 4.4e Spatial motion of pinned beam (2): motion history.

$$t = .05 n, \quad n = 1, \dots, 85$$

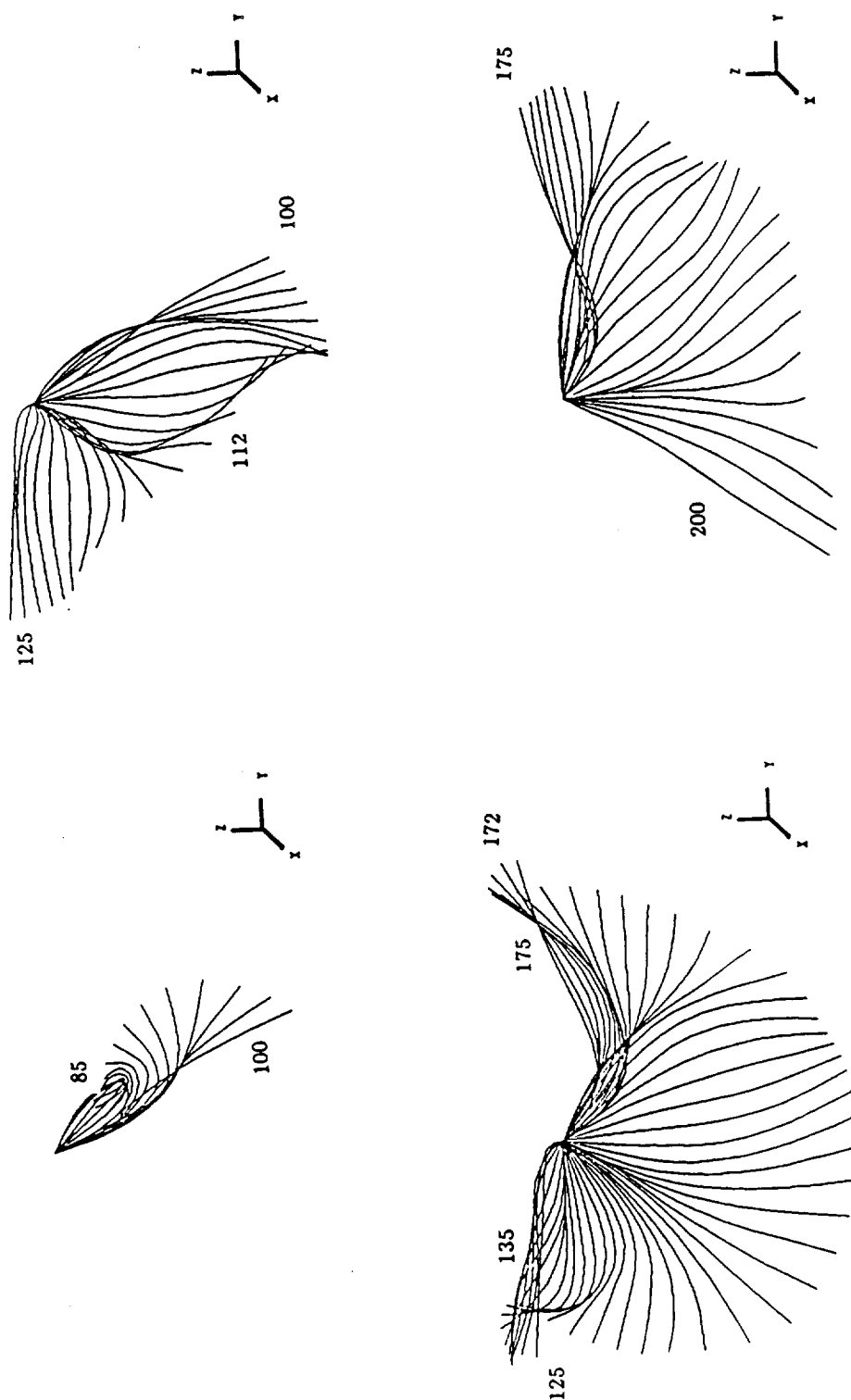


Figure 4.4f Spatial motion of pinned beam (2): motion history.

$$t = .05 n, \quad n = 85, \dots, 200$$

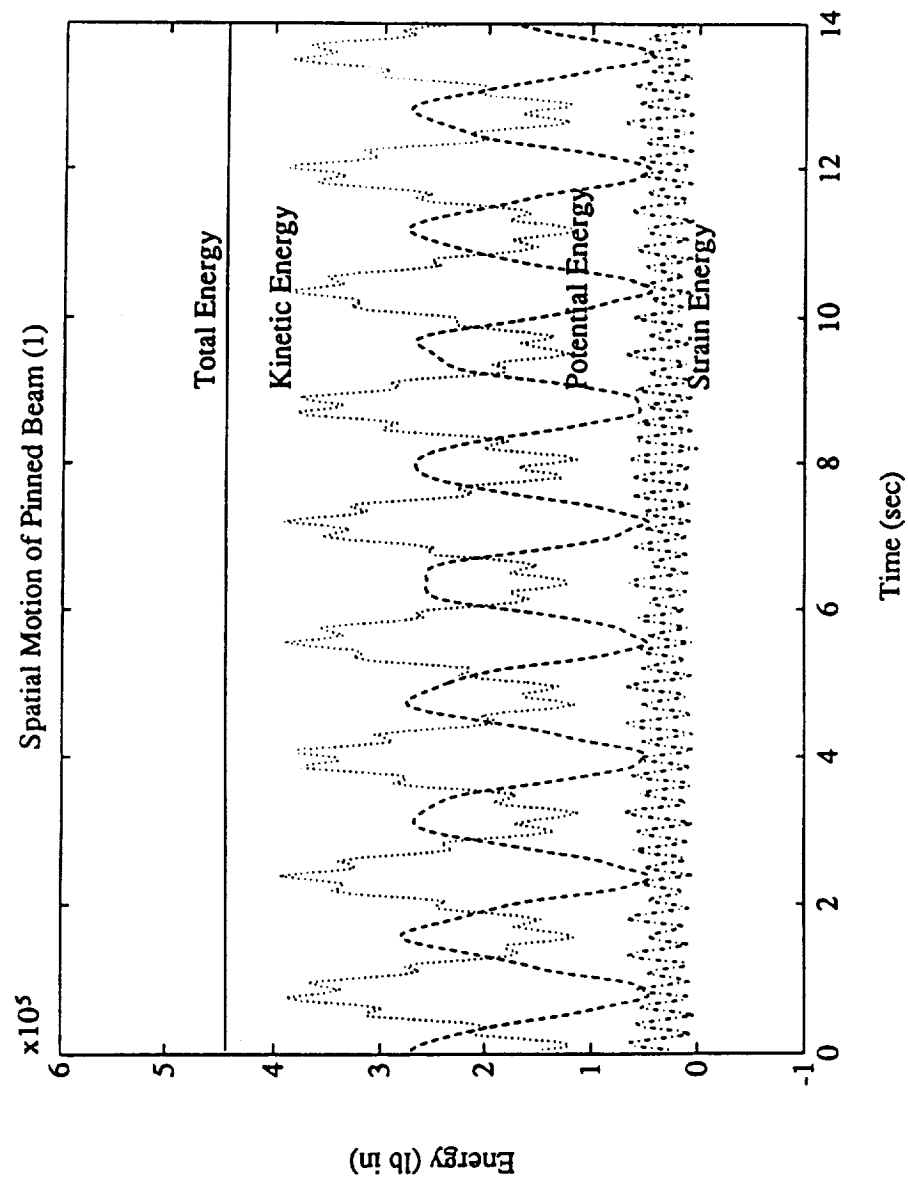


Figure 4.4g Spatial motion of pinned beam: energy history (1).

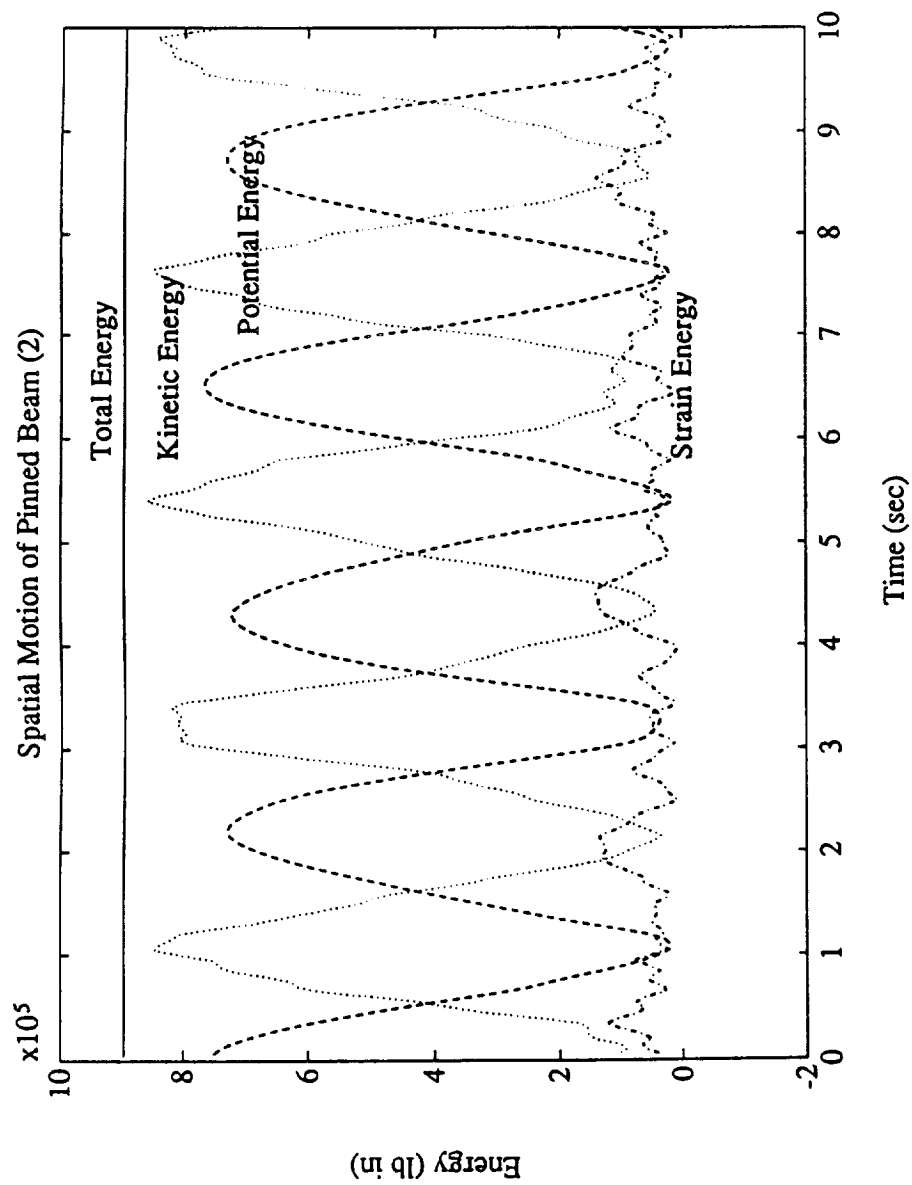
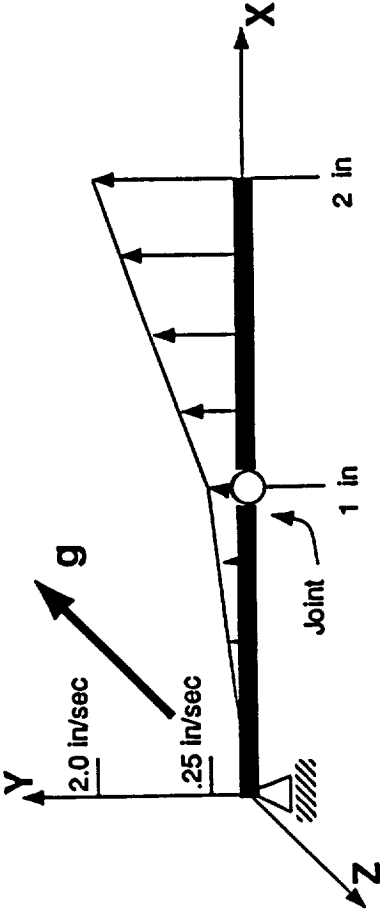


Figure 4.4h Spatial motion of pinned beam: energy history (2).

Initial Beam Position vs. Initial Velocity Profile



Material Properties

	$A = .01$	in^2
	$I = .008333333$	in^4
	$\rho = .259$	lbm / in^3
(1)	$E = 1.0 \times 10^6$	lb / in^2
	$G = .5 \times 10^6$	lb / in^2
(2)	$E = 1.0 \times 10^5$	lb / in^2
	$G = .5 \times 10^5$	lb / in^2
(3)	$E = 2.0 \times 10^4$	lb / in^2
	$G = 1.0 \times 10^4$	lb / in^2
(4)	$E = 1.0 \times 10^4$	lb / in^2
	$G = .5 \times 10^4$	lb / in^2

Mesh

8 Linear Elements / Beam

Figure 4.5a Spatial motion of double pendulum: problem data.

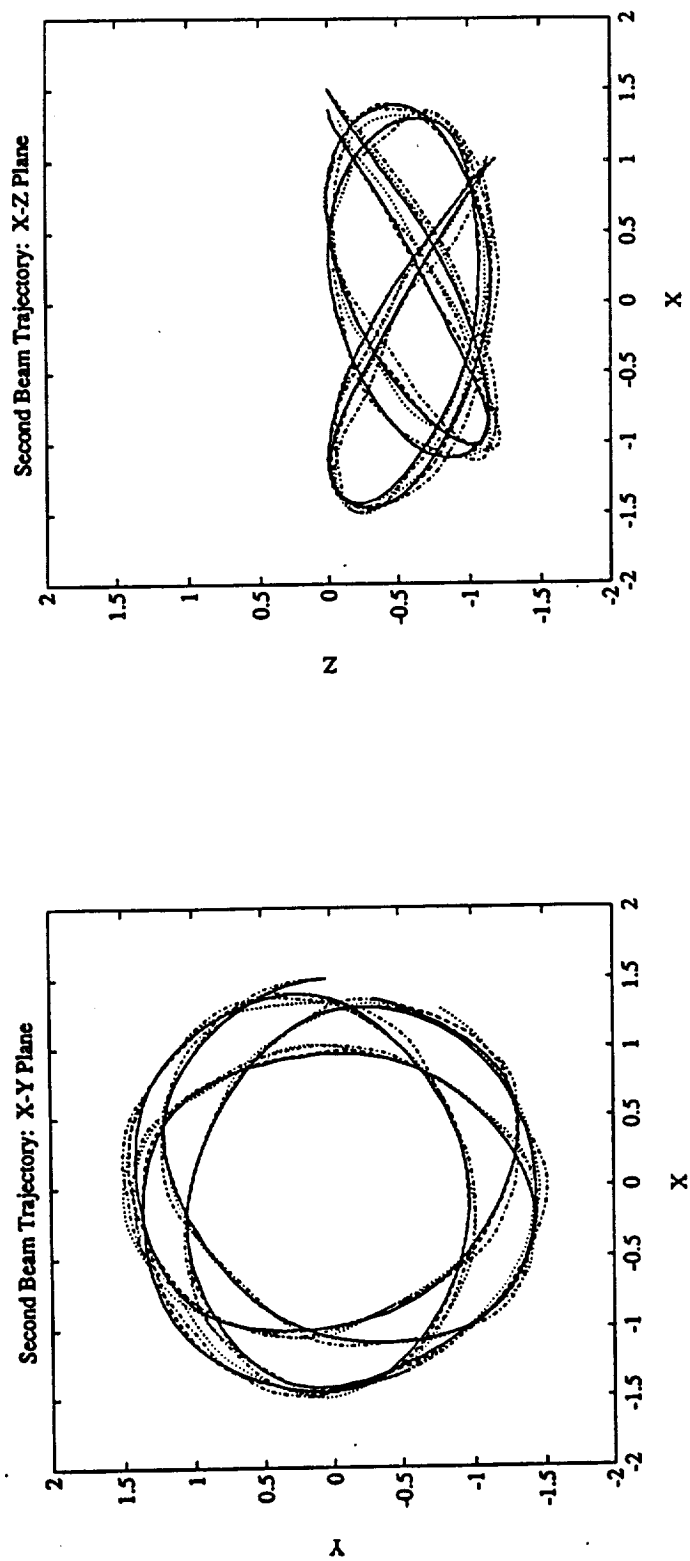


Figure 4.5b Spatial motion of double pendulum: projected trajectories.

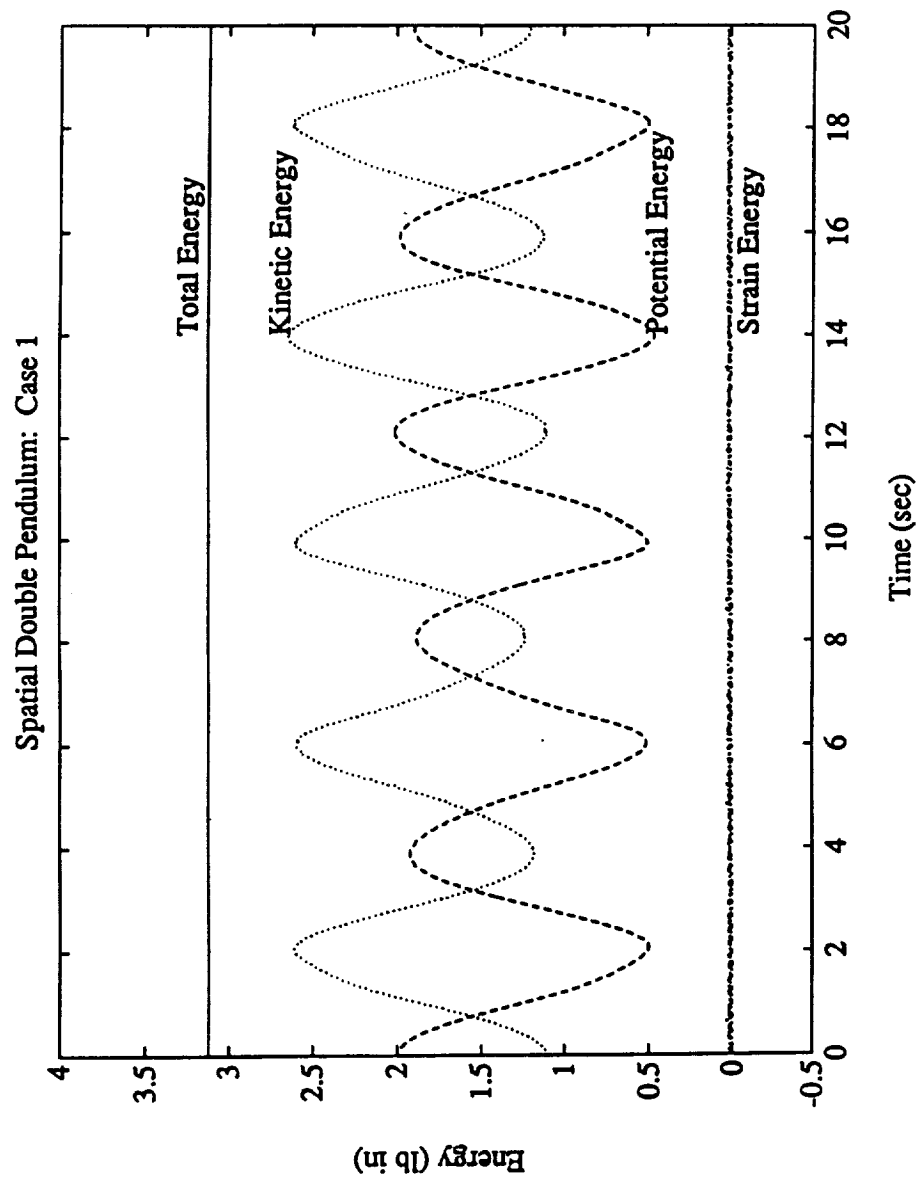


Figure 4.5c Spatial motion of pinned beam: energy history (1).

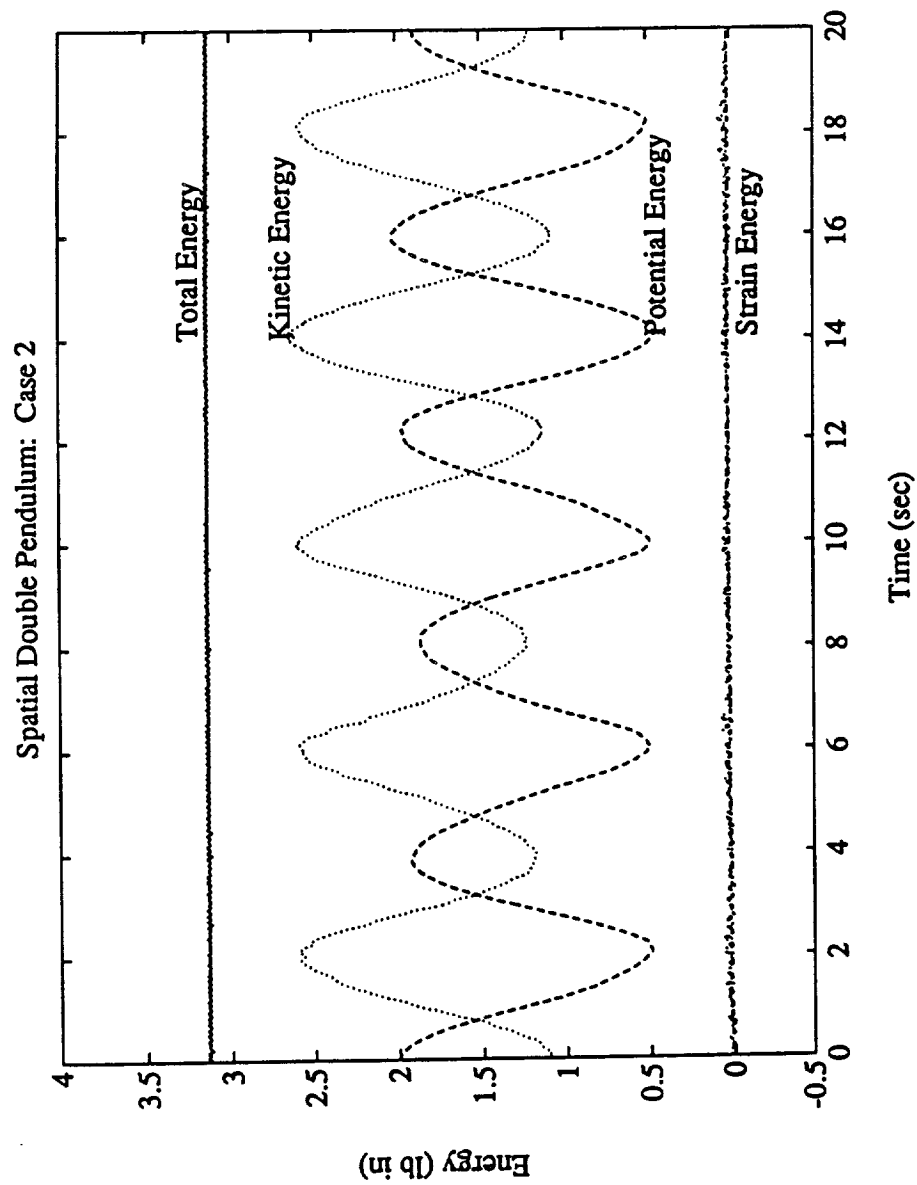


Figure 4.5d Spatial motion of pinned beam: energy history (2).

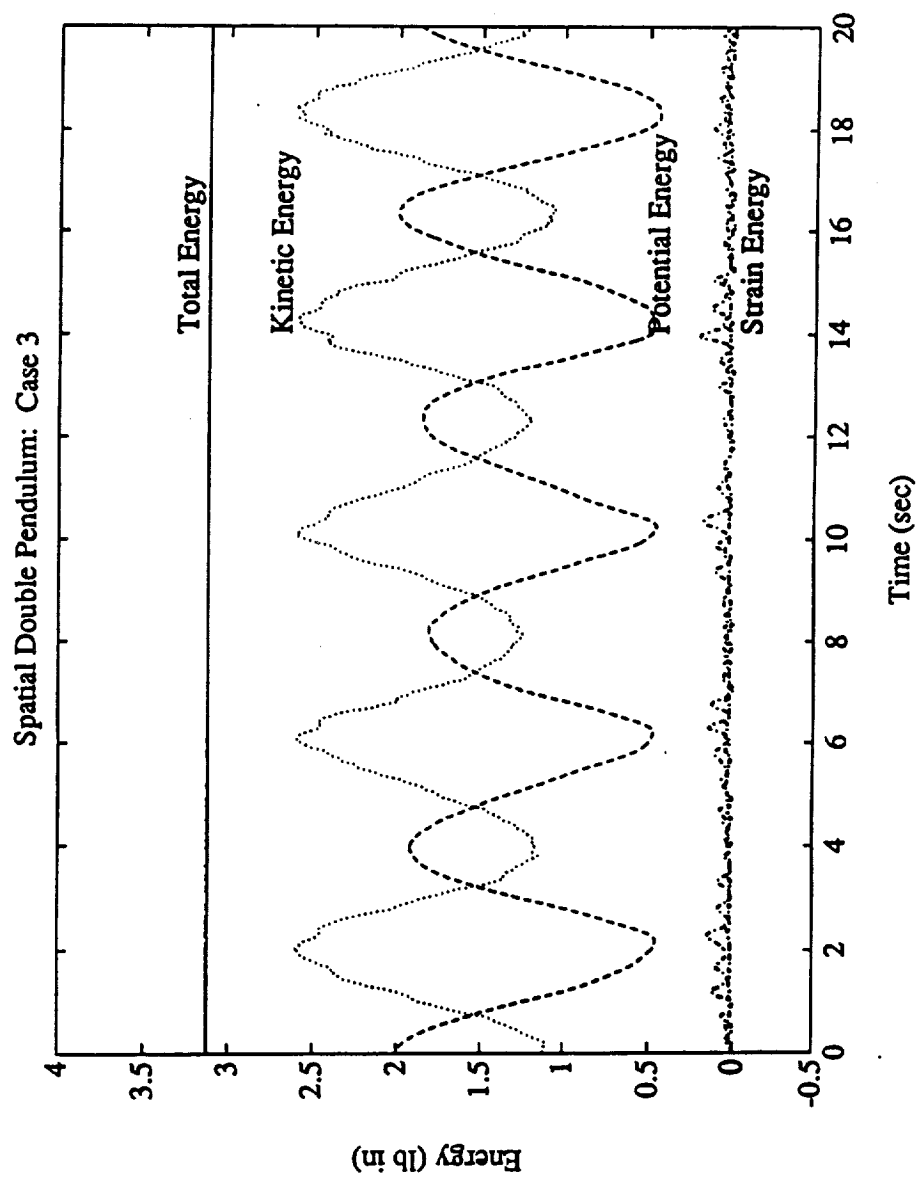


Figure 4.5e Spatial motion of pinned beam: energy history (3).

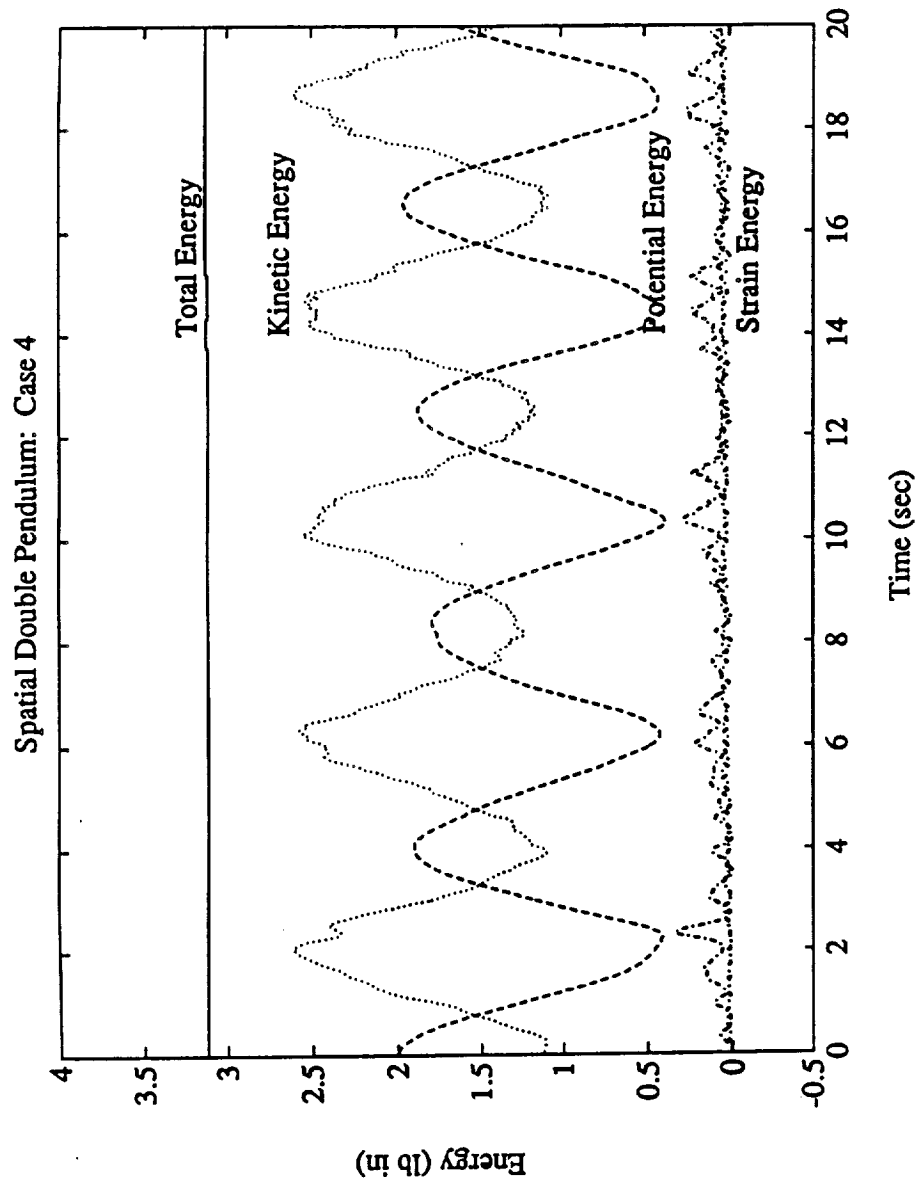


Figure 4.5f Spatial motion of pinned beam: energy history (4).

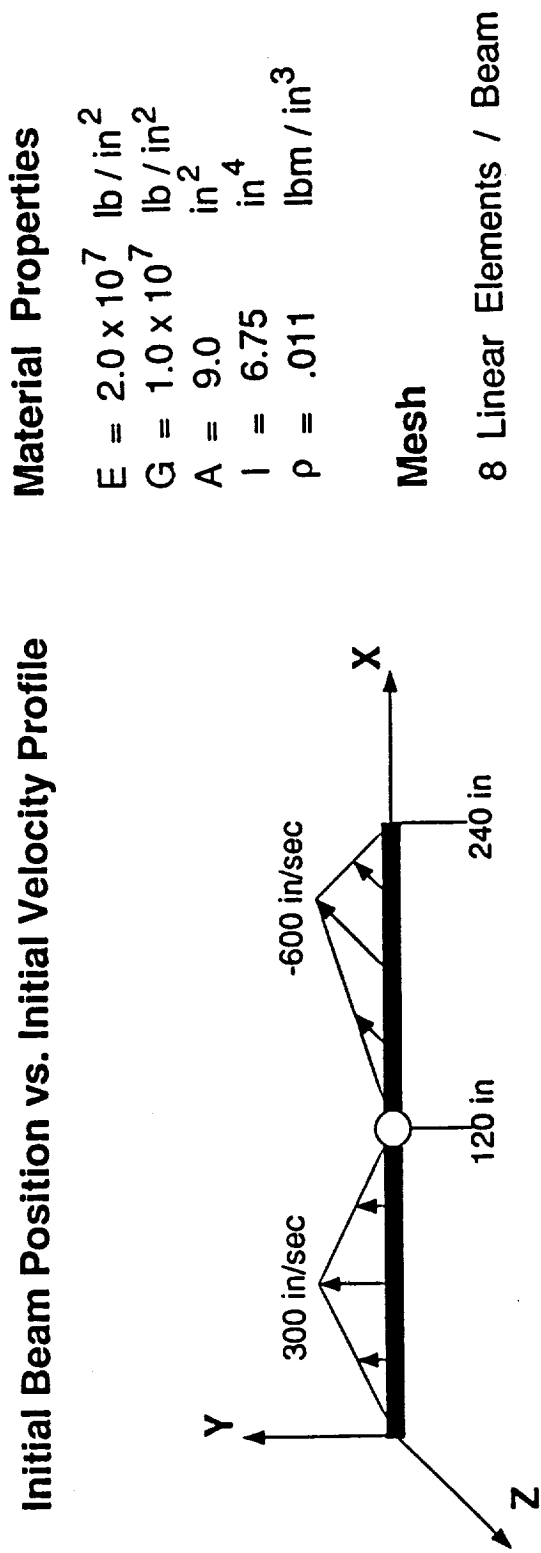


Figure 4.6a Spatial motion of double pendulum: problem data.

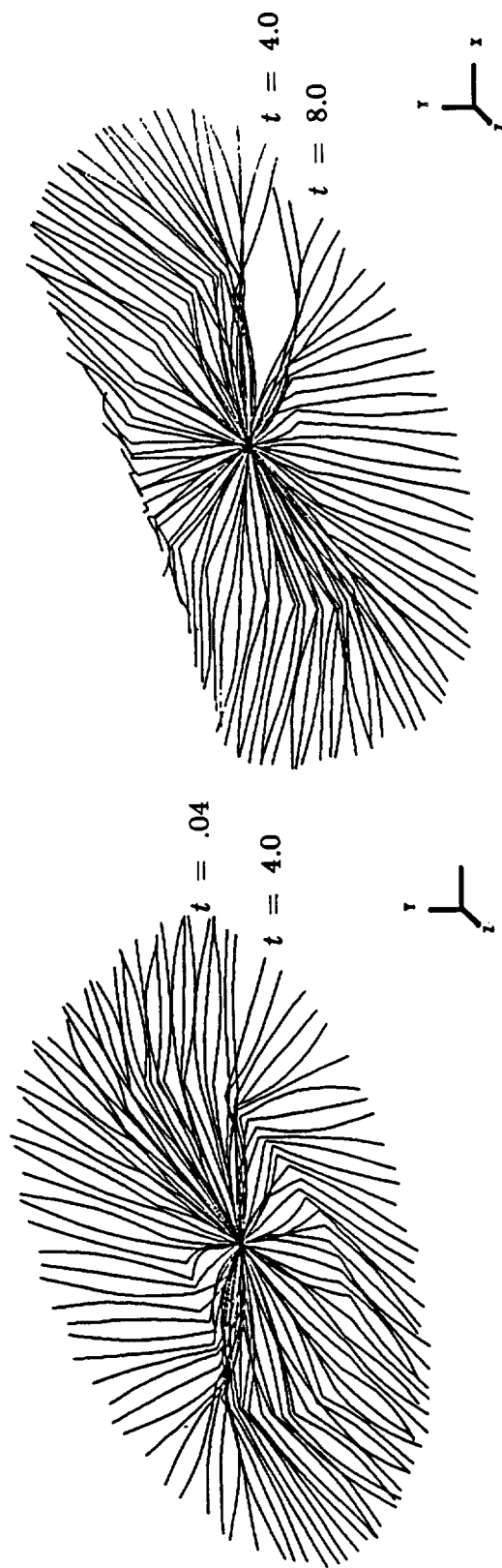


Figure 4.6b Spatial motion of double pendulum: motion history.

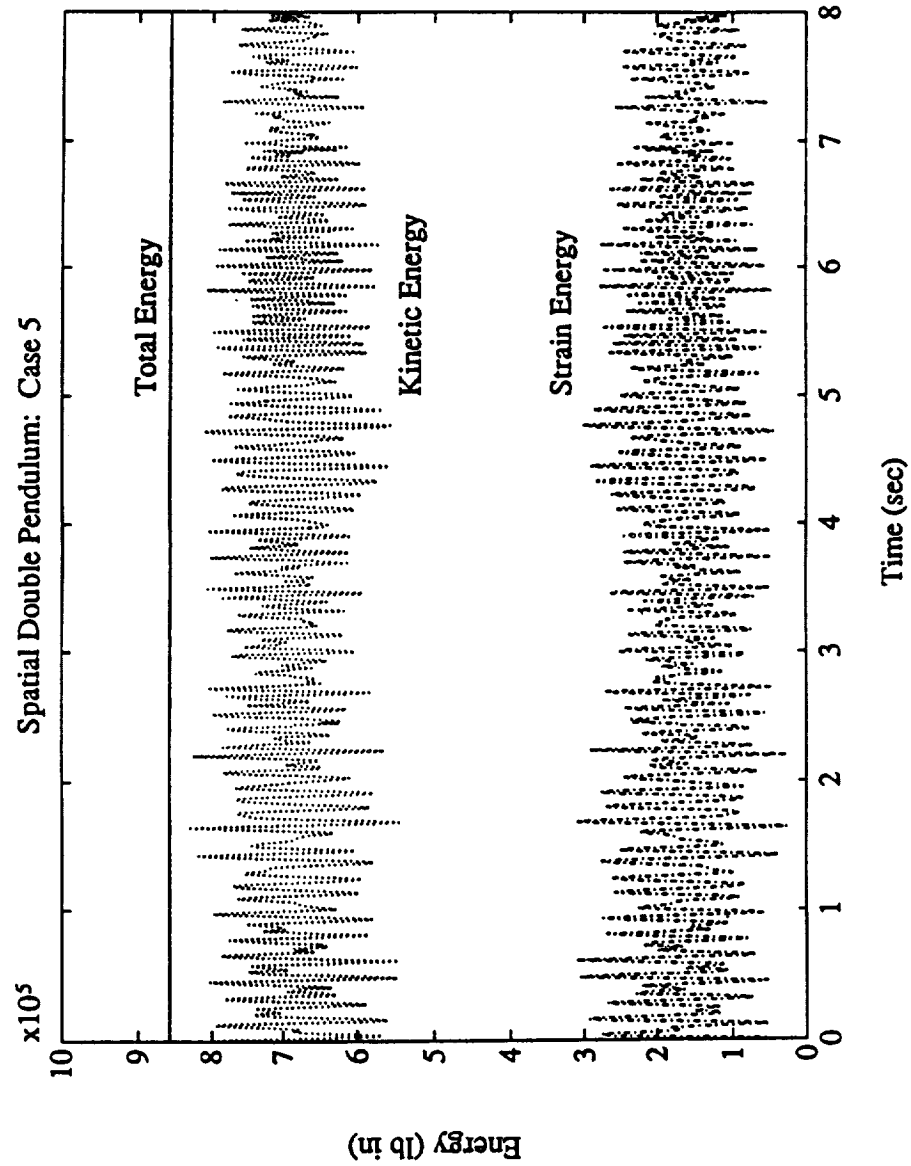


Figure 4.6c Spatial motion of double pendulum: energy history.

CHAPTER V

DEPLOYMENT DYNAMICS OF BEAM STRUCTURES

5.1 Introduction

The purpose of this chapter is to use the present spatial beam formulation to model the dynamics of the beam's deployment. Such a capability for simulating the extrusion of beam-like structures can offer a general utility to study various practical problems such as tethers, space assembly, hot rolling, and fluid jets. Much of the relevant literature addressing this type of problem has been motivated by space industry applications. Current spacecraft designs employ flexible deployable appendages such as antennae or solar arrays. The appendages, which are compactly stored during a launch phase, may be extended during the spacecraft's attitude acquisition phase. As the relatively long appendages tend to be deployed with relatively small extension rates, the transient effect of deployment may be felt over a long period of time and is critical to the mission success.

Initial works investigated the effect of appendage deployment on satellite control by modeling the appendages as point masses [101] and rigid bodies [102-103]. The deployment of flexible appendages from specific configurations of a spinning spacecraft was analyzed numerically in [104]. More general formulations for studying the effect of the deployment of beam-type appendages on the attitude stability of a satellite are given in [105-108], and a similar analysis for studying the deployment of plate-like structures is given in [109]. The above analyses employ appropriate modal coordinates to model the flexible deformations. As such, the classical vibrations approach

which employs a linear combination of spatial modal functions weighted by time-dependent generalized coordinates to model elastic deflections must be altered to account for the time-dependent spatial domain. As this approach may be somewhat questionable, an alternative method models the beam as a series of elastically connected rigid links, and then considers the links outside the rigid body at a given time in deriving equations of motion [110]. The equations of motion concerning the nonrotating dynamics of axially-moving strings [111-116], beams[117], and nonlinear elastica [118] have been formulated using an approach based on continuum mechanics. In the flavor of these last works, the present chapter analyzes the nonrotating dynamics of deployment.

An axially moving beam-like structure is somewhat similar to a flow problem. The deployment may be thought of as a moving boundary problem in which the spatial domain occupied by the continuum is a function of time. Moving boundary problems are common in fluid dynamics, as typical heat conduction or diffusion problems involve phase changes from solid, liquid, or vapour states at an interface whose position is an unknown function of time. The fluid dynamics community has generated a great deal of research on numerical solution techniques for moving boundary problems which has provided much insight for the present work.

A good account of numerical solution methods developed for moving boundary problems in heat flow or diffusion is given in [119-120]. In discretizing the changing spatial domain encountered in these problems, either a fixed or a variable grid method may be adopted. The fixed grid method maintains a constant spatial grid sizing throughout the simulation. When the nodes are fixed in space, the location of the moving boundary does

not necessarily coincide with a node. Special numerical techniques must then be incorporated to locate the position and model the physics of the boundary [121-122]. Alternative approaches avoid these complications arising from the unequal grid size near the moving boundary. In one method, the unequal interval is transferred to a more tractable region by moving the whole uniform grid system with the velocity of the moving boundary [123]. Another method varies the time step such that the boundary moves the distance of one fixed space mesh during that time [124-126]. Alternatively, a deforming numerical grid which maintains an equal number of variable length space intervals may be employed to solve moving boundary problems [127]. This approach has a greater intuitive appeal as the moving boundary always corresponds to a specific nodal point. When employing this approach, the grid deformation must theoretically be accounted for in a proper manner. Within the context of the finite element method, the grid deformation can be accounted for by making the finite element basis functions implicit functions of time [128]. In this case, the time derivatives of the approximate displacements acquire additional convective-type terms within dynamic analyses.

For dynamic analyses, space-time finite elements can be employed to formulate a time integration algorithm which accounts for the grid deformation within a variable grid method. Previous works in the literature have used this approach with success to solve both parabolic and hyperbolic problems such as the one and two-dimensional heat equation of the Stefan ice/water interface problem [129-130], the Euler equations of compressible flow [131], and the advection-diffusion problem [132]. To solve flow problems with time-varying boundaries in this manner, space-time variational

statements must first be defined. The simplest way to get the weak form of the governing equations is through the standard Galerkin finite element method [133-135]. However, the straightforward application of the Galerkin principle may result in a coupling of all the discrete steps in the time domain in the same manner that spatial nodal variables become coupled through a standard spatial finite element discretization. Obviously, this is highly undesirable for an efficient transient integration algorithm. To alleviate this problem, the discontinuous Galerkin method in time has been applied to space-time finite element formulations [136-138]. A more attractive method is to use Hamilton's Law as the variational source for finite element discretization procedures in the time domain [139-141]. In addition to leading to a step-by-step integration procedure, the use of a true variational law of mechanics as that of Hamiltonian as opposed to constructed principles as the general weighted residual methods provides a physical basis for the discretization procedure [139].

Given the above overview, the large deformation beam formulation presented in Chapter II is extended to model the axial deployment of the beam. The deployment is modeled by referring the motion variables to the changing spatial configuration of an undeformed beam extending with the prescribed deployment speed. Deforming finite elements are used to discretize this changing spatial volume, and the internal force formulation of Chapter II and computation of Chapter III are retained. Due to the changing spatial reference for the dynamic variables, the inertia operator acquires terms representing the convective rate of change of the variable in addition to those representing the local rate of change of the variable. To simplify the numerical treatment of the inertia operator, a Hamiltonian variational

formulation is introduced as the basis for a space-time finite element discretization procedure. This space-time discretization of the Hamiltonian formulation results in a transient integration scheme which accounts for the deforming spatial grid. In this manner, an effective computational method has been developed to model the deployment of present beam formulation.

The rest of the chapter will be organized as follows. Section 5.2 presents the variable spatial grid description of the beam kinematics. The coupling between the convective effects and the temporal differentiation within the inertia operator are discussed in detail. The Hamiltonian formulation of the moving boundary value problem is derived in Section 5.3. The space-time discretization of the resulting Hamiltonian is carried out in Section 5.4, and care is exercised to annihilate unwanted spurious mechanisms in the discrete equations of motion. The computer implementation of the present approach and preliminary results on a planar inverse-spaghetti problems is illustrated in Section 5.5.

5.2 Deployment Kinematics

The problem under consideration, as shown below in Figure 5.1, is the axial extension of a beam-like structure from a stationary guide. As the beam extends from the guide, the spatial volume which deforms is constantly changing. To model this effect, the beam can be discretized by a growing number of finite elements of a fixed length or by an equal number of finite elements growing in length. These two approaches are illustrated in Figure 5.2. It is seen that in the first approach, a special element of varying length must be used at either the boundary or the free end. This inconsistency is avoided in the second approach as the grid points are equally spaced.

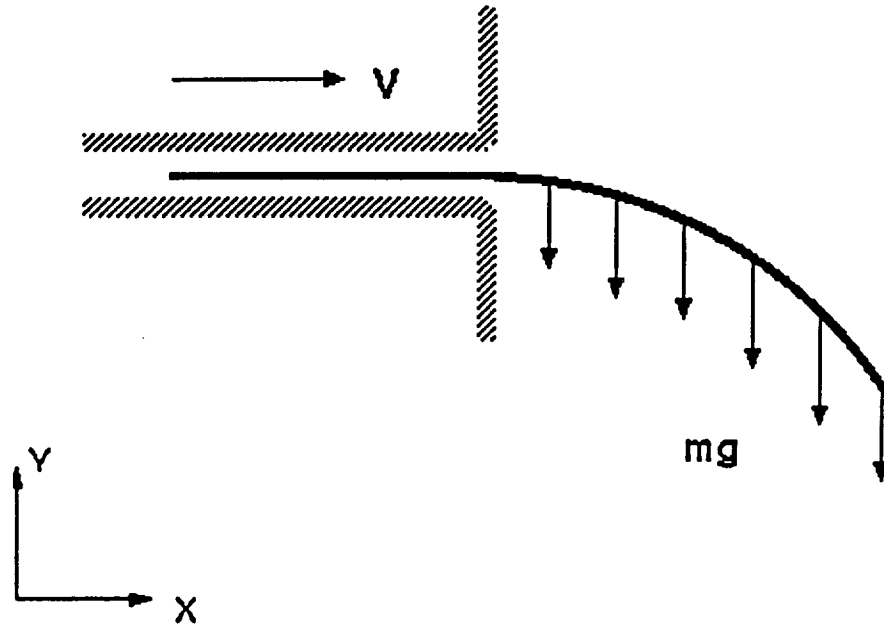


Figure 5.1 Axial deployment subject to gravity.

Conceptually, this variable or moving grid approach is more appealing, and it can readily be adopted into the present beam formulation. Theoretically and computationally, it remains to properly account for the effects of grid deformation. To this end, the kinematics of the beam deployment are described as follows.

The present formulation is based on the use of an inertial reference for the beam kinematics. As detailed in Chapter II, the beam configuration is completely characterized using a position vector locating the neutral axis of the beam from the inertial origin and an additional reference frame which orients the cross-section from the inertial frame. To retain this concept and model the deployment of the beam, the displacement variables locating the

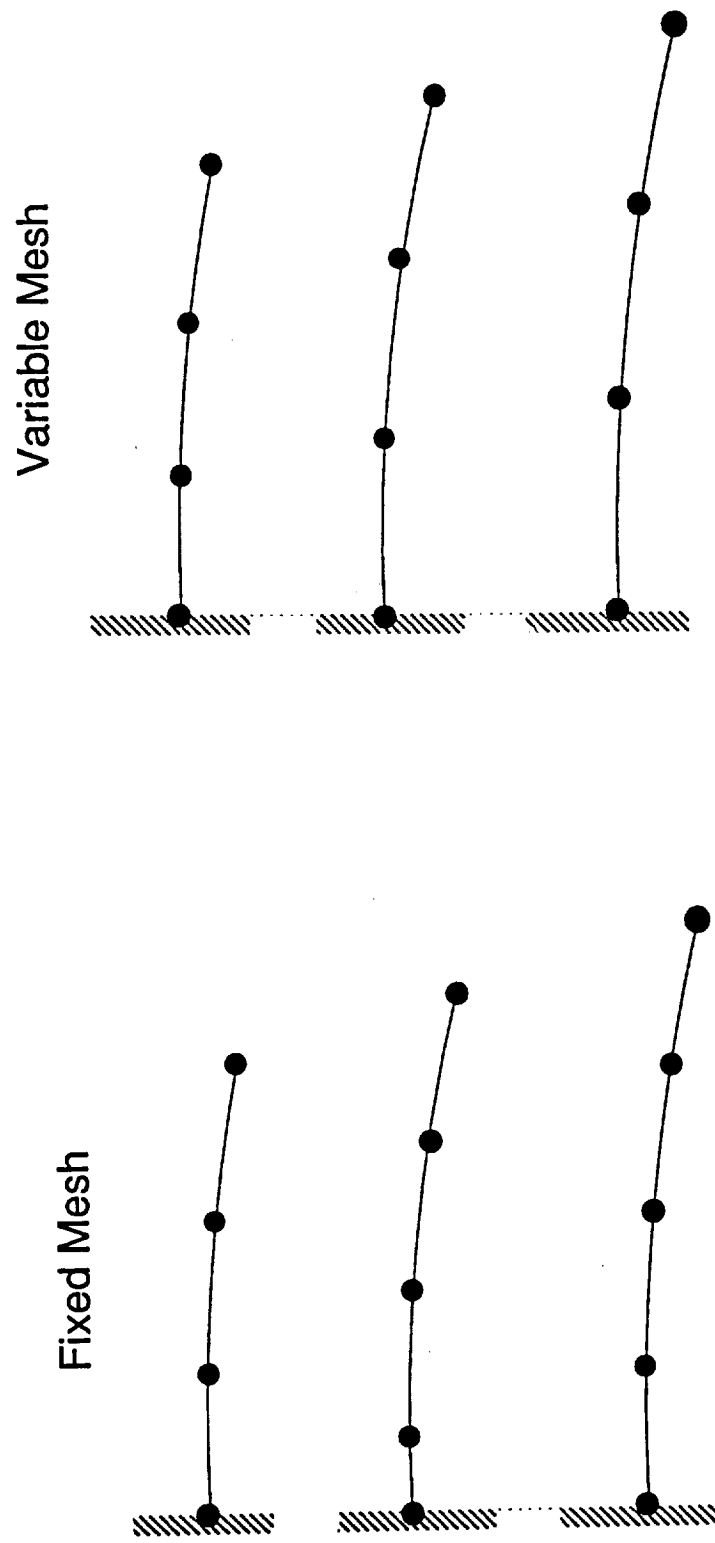


Figure 5.2 Fixed vs. Variable Grid Approaches

neutral axis are measured from a set of moving nodes which represent the position of a phantom beam rigidly moving from the guide in a prescribed manner. As shown in below in Figure 5.3,

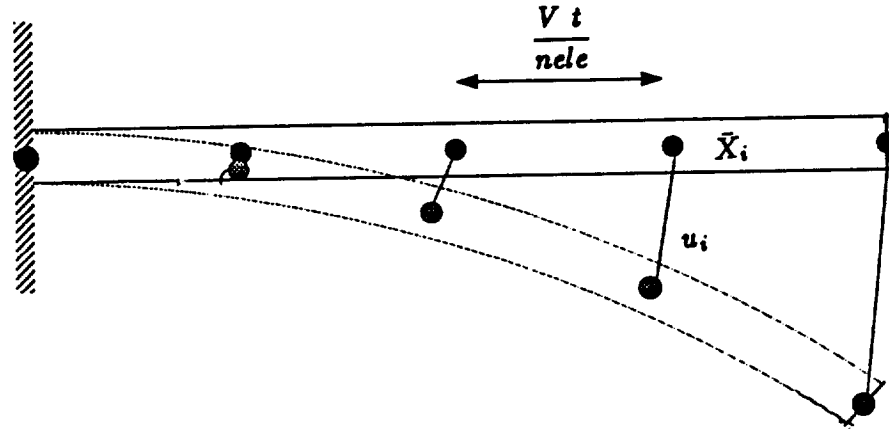


Figure 5.3 Deployment kinematics.

the position vector \mathbf{r} locating an arbitrary point within the changing spatial configuration occupied by the beam is described as

$$\mathbf{r} = \{ \bar{X}(t) + u \}^T \mathbf{e} + \ell^T \mathbf{b} . \quad (5.2.1)$$

In the above equation, $\bar{X}(t)$ represents time-dependent inertial coordinates of the phantom beam neutral axis. In reference to a particular moving node i , the position vector is given as

$$\mathbf{r}_i = \{ \bar{X}_i(t) + u_i \}^T \mathbf{e} + \ell^T \mathbf{b}_i . \quad (5.2.2)$$

The location of the moving reference nodes $\bar{X}_i(t)$ are determined by spatially dividing the length corresponding to a rigid deployment with an equal number of elements. If the prescribed deployment speed is a constant value

of V , the total length of the rigid phantom beam at time t is $V t$. The moving reference nodes are equally positioned between the free end and the boundary, and the position and velocity of the nodes can be prescribed as

$$\bar{X}_i(t) = \frac{(i-1)}{nele} V t \quad (5.2.3)$$

$$\frac{d\bar{X}_i}{dt} \equiv \bar{V}_i(t) = \frac{(i-1)}{nele} V \quad (5.2.4)$$

where $nele$ represents the fixed number of deforming elements. The kinematic relation (5.2.2) is thus an Eulerian description as material points of the beam are not specifically tracked.

As the displacement variables are measured from a moving reference, the material time derivative definition must be introduced to obtain the velocities and accelerations of a material particle. The definition of the material time derivative is given as [45]

$$\frac{D}{Dt} \equiv \frac{\partial}{\partial t} + v_j \frac{\partial}{\partial x_j} \quad (5.2.5)$$

where x_j are the inertial coordinates of a spatial point within the deformed beam configuration, and v_j are the instantaneous velocity coordinates at that point. For use within the present beam formulation, this definition must be transformed such that the spatial derivative is taken with respect to the convected coordinates ξ_i . This convected coordinate definition is given as

$$\frac{D}{Dt} \equiv \frac{\partial}{\partial t} + v_j T_{ij} \frac{\partial}{\partial \xi_i} \quad (5.2.6)$$

where the rotational tensor T_{ij} maps the inertial coordinates to the convected coordinates. It is recalled that the convected reference frame was introduced in Chapter II to obtain a more physically effective deformation

description. As the internal force is computed from the convected spatial coordinates, the transformation (5.2.6) is introduced to achieve a consistent computation of the inertia force. For the particular Eulerian description (5.2.1), the appropriate material time derivative becomes

$$\frac{D}{Dt} = \frac{\partial}{\partial t} + V^* \frac{\partial}{\partial \xi} \quad (5.2.7)$$

$$V^* = T_{11} v_1 + T_{12} v_2 + T_{13} v_3 \quad (5.2.8)$$

as the translational variables and the cross-section orientation are solely functions of the neutral-axis length coordinate ξ . To complete this definition, an expression for the instantaneous velocity v_i is obtained from the kinematic definition (5.2.2). From this definition, the spatial coordinates are given as

$$x_i = \bar{X}_i + u_i + R_{ji} \ell_j \quad (5.2.9)$$

where R_{ji} is the rotational tensor corresponding to the cross-section orientation. The instantaneous velocity of this point becomes

$$v_i = \bar{V}_i + \dot{u}_i + R_{ji} \tilde{\omega}_{jk} \ell_k \quad (5.2.10)$$

$$\bar{V}_i = \frac{d \bar{X}_i}{dt} , \quad \dot{u}_i = \frac{\partial u_i}{\partial t} . \quad (5.2.11)$$

From this expression, the velocity V^* of (5.2.8) can be written as

$$V^* = \dot{u}^* + \dot{\Theta}^{*T} \ell \quad (5.2.12)$$

where

$$\dot{u}^* = T_{1j} (\bar{V}_j + \dot{u}_j)$$

$$\dot{\Theta}^{*T} = \{ 0 , S_{11} \omega_3 - S_{31} \omega_1 , S_{21} \omega_1 - S_{11} \omega_2 \}$$

correspond to the translational and rotational contributions respectively as derived from (5.2.8) and (5.2.10).

The velocity and acceleration of a material particle can now be derived by applying (5.2.6) to the Eulerian description (5.2.1). For rotating coordinate systems, the definitions of the time and space derivatives for the body fixed components of a given vector are given as

$$\frac{\partial^e}{\partial t} = \frac{\partial^b}{\partial t} + \tilde{\omega} \quad , \quad \tilde{\omega} = - \frac{d\mathbf{R}}{dt} \mathbf{R}^T \quad (5.2.13)$$

$$\frac{\partial^e}{\partial \xi} = \frac{\partial^b}{\partial \xi} + \tilde{\kappa} \quad , \quad \tilde{\kappa} = - \frac{d\mathbf{R}}{d\xi} \mathbf{R}^T \quad . \quad (5.2.14)$$

The velocity of a material particle thus becomes

$$\begin{aligned} \frac{D \mathbf{r}}{Dt} = & \mathbf{e}^T \left[(\bar{V} + \dot{u}) + V^* \frac{\partial^e u}{\partial \xi} \right] + \\ & \mathbf{b}^T \left[\tilde{\omega} + V^* \tilde{\kappa} \right] \ell \end{aligned} \quad (5.2.15)$$

and likewise the acceleration

$$\begin{aligned} \frac{D^2 \mathbf{r}}{Dt^2} = & \mathbf{e}^T \left[\frac{\partial^{e^2} u}{\partial t^2} + 2 V^* \frac{\partial^{e^2} u}{\partial t \partial \xi} + V^{*2} \frac{\partial^{e^2} u}{\partial \xi^2} + \right. \\ & \left. \frac{\partial^e u}{\partial \xi} \left(\frac{\partial V^*}{\partial t} + V^* \frac{\partial V^*}{\partial \xi} \right) \right] + \\ & \mathbf{b}^T \left[\frac{\partial^b \tilde{\omega}}{\partial t} + \tilde{\omega} \tilde{\omega} + \right. \\ & V^* \left(\frac{\partial^b \tilde{\omega}}{\partial \xi} + \frac{\partial^b \tilde{\kappa}}{\partial t} + \tilde{\omega} \tilde{\kappa} + \tilde{\kappa} \tilde{\omega} \right) + \\ & V^{*2} \left(\frac{\partial^b \tilde{\kappa}}{\partial \xi} + \tilde{\kappa} \tilde{\kappa} \right) + \\ & \left. \frac{\partial V^*}{\partial t} \tilde{\kappa} + V^* \frac{\partial V^*}{\partial \xi} \tilde{\kappa} \right] \ell \quad . \end{aligned} \quad (5.2.16)$$

The equations of motion as derived from the stated beam kinematic description will be discussed next.

5.3 Hamiltonian Equations of Motion

The beam formulation presented in Chapter II is based on the well-known Cauchy equilibrium equations of motion for a solid continuum. The principal of virtual work, which is a spatial variational form of the partial differential equations of motion, is given as

$$\delta F^I + \delta F^S = \delta F^E + \delta F^T \quad (5.3.1)$$

where the inertia operator δF^I , the internal force operator δF^S , the external force operator δF^E , and the traction operator δF^T are identified from (2.3.1). Due to the beam kinematic assumptions, the traction operator is identically equal to zero and will henceforth be neglected. This variational form provides a basis for the implementation of spatial finite element approximation methods to lead the partial differential equations of motion to a set of ordinary differential equations in time. Standard numerical integration techniques can then be employed to obtain a solution to the equations at discrete time levels.

For the deployment problem, a variational form of the temporal operators is considered such that a finite element discretization in time can be applied simultaneously with the discretization in space. As the principle of virtual work is used as the basis for the spatial discretization, Hamilton's Law is used as a variational source for this space-time finite element discretization. Hamilton's law is deduced from an integration of the principle of virtual work over an arbitrary time interval given as [98]

$$\int_{t_1}^{t_2} \delta F^I dt + \int_{t_1}^{t_2} \delta F^S dt = \int_{t_1}^{t_2} \delta F^E dt \quad (5.3.2)$$

An integration by parts is then performed on the inertia term

$$\int_{t_1}^{t_2} \delta F^I dt = \int_{t_1}^{t_2} \int_{\vartheta} \rho \ddot{r}_i \delta r_i d\vartheta dt \quad (5.3.3)$$

to lead the equation (5.3.2) to the form

$$\begin{aligned} \int_{t_1}^{t_2} \int_{\vartheta} \{ \rho \dot{r}_i \delta \dot{r}_i - \sigma_{ij} \delta \varepsilon_{ij} - \delta r_i f_i \} d\vartheta dt = \\ \left[\int_{\vartheta} \rho \dot{r}_i \delta r_i d\vartheta \right] \Big|_{t_1}^{t_2} \end{aligned} \quad (5.3.4)$$

A well-known form of the above variational statement is obtained by requiring that the arbitrary virtual changes δr_i vanish at the time limits t_1 and t_2 as

$$\delta r_i (t_1) = \delta r_i (t_2) = 0$$

With this assumption, the boundary term on the right-hand side of (5.3.4) can then be neglected such that

$$\int_{t_1}^{t_2} (\delta T + \delta \bar{W}) dt = 0$$

where T represents the kinetic energy and $\delta \bar{W}$ represents the virtual work of the applied and internal forces. This interpretation is known as Hamilton's principle. In general though, one can treat $r_i(t_1)$ and $r_i(t_2)$ as undetermined quantities. The distinction between Hamilton's Law and Hamilton's principle is thus whether these temporal boundary terms are retained or neglected.

This distinction between Hamilton's Law and Hamilton's principle becomes important in the numerical approximation of the variational statements. Although the boundary term is often seen as irrelevant in deriving the equations of motion, it is important for numerical solution techniques.

The boundary term must be retained to achieve correct approximate solutions from a Hamiltonian variational statement. Early works which implemented a space-time discretization of Hamilton's principle resulted in an inconsistent treatment of initial data [133-135,142]. In contrast, the initial conditions can be properly incorporated into the variational formulation of Hamilton's Law. Additionally, when Hamilton's Law is used as the variational statement, C_0 continuous approximating functions may be employed such that an attractive step-by-step integration procedure results [139-140].

To interpret the well-known Hamilton's Law for the present deployment problem, an integration by parts must be performed on the inertia term

$$\int_{t_1}^{t_2} \delta F^I dt = \int_{t_1}^{t_2} \int_{\vartheta(t)} \rho \frac{D^2 r_i}{Dt^2} \delta r_i d\vartheta dt \quad (5.3.5)$$

which contains the material time derivative definition (5.2.6). The proper interchange of the time derivative and a time dependent spatial volume integral is given by the Reynolds transport theorem as [45]

$$\frac{D}{Dt} \int_{\vartheta(t)} \rho F d\vartheta = \int_{\vartheta(t)} \rho \frac{D F}{Dt} d\vartheta ,$$

where ρ is the mass density and F is an arbitrary function of the material. From this theorem, an integration by parts can be performed on (5.3.5) to yield

$$\begin{aligned} \int_{t_1}^{t_2} \delta F^I = & \left[\int_{\vartheta(t)} \rho \frac{D r_i}{Dt} \delta r_i d\vartheta \right] \Big|_{t_1}^{t_2} - \\ & \int_{t_1}^{t_2} \int_{\vartheta(t)} \rho \frac{D r_i}{Dt} \frac{D \delta r_i}{Dt} d\vartheta dt . \end{aligned} \quad (5.3.6)$$

The interpretation of Hamilton's Law for Eulerian continuum formulations

is thus given as

$$\begin{aligned} \int_{t_1}^{t_2} \int_{\vartheta(t)} \left\{ \rho \frac{D r_i}{Dt} \frac{D \delta r_i}{Dt} - \sigma_{ij} \delta \varepsilon_{ij} - \delta r_i f_i \right\} d\vartheta dt = \\ \left[\int_{\vartheta(t)} \rho \frac{D r_i}{Dt} \frac{D \delta r_i}{Dt} d\vartheta \right] \Big|_{t_1}^{t_2} . \end{aligned} \quad (5.3.7)$$

The above variational statement provides an attractive source for a concurrent space-time discretization procedure for the present deployment problem. The complex acceleration expression (5.2.16) need not be explicitly considered as the temporal weak form requires only the velocity expressions. In addition, consistency with the internal force operator is achieved as the spatial derivatives contained within the inertia are reduced to first order. Finally, the deforming spatial grid which has been introduced to model the changing spatial volume occupied by the beam will be taken into account automatically.

To complete the formulation, an expression for the inertia operator is derived by incorporating the kinematic expressions into (5.3.6); the details of the derivation are given in Appendix A. By neglecting coupling terms caused by the rotational contribution $\dot{\Theta}^{*T} \ell$ within the velocity V^* given in (5.2.12), the interior term of the inertia operator becomes

$$\begin{aligned} \delta F_i^I &\equiv \int_{t_1}^{t_2} \int_v \rho \frac{D r_i}{Dt} \frac{D \delta r_i}{Dt} d\vartheta dt \\ &= \int_{t_1}^{t_2} \int_{\xi} \left\{ (\bar{V} + \dot{u}) + \dot{u}^* \frac{\partial u}{\partial \xi} \right\}^T m \left\{ \frac{\partial \delta u}{\partial t} + \dot{u}^* \frac{\partial \delta u}{\partial \xi} \right\} \\ &\quad + \left\{ \omega^T + \dot{u}^* \kappa^T \right\} J \left\{ \delta \omega + \dot{u}^* \delta \kappa \right\} d\xi dt . \end{aligned} \quad (5.3.8)$$

In this expression,

$$m = \int_A \rho dA , \quad J = \int_A \rho \tilde{\ell} \tilde{\ell}^T dA$$

represents the beam mass per unit length and cross-sectional inertia properties, and

$$\begin{aligned}\delta\omega &= \frac{\partial \delta\alpha}{\partial t} + \tilde{\omega} \delta\alpha \\ \delta\kappa &= \frac{\partial \delta\alpha}{\partial \xi} + \tilde{\kappa} \delta\alpha \quad .\end{aligned}$$

represent the angular velocity and curvature variations, respectively. Likewise, the resulting expression for the boundary term of the inertia operator becomes

$$\begin{aligned}\delta F_b^I &\equiv \left[\int_{\vartheta(t)} \rho \frac{D r_i}{Dt} \delta r_i d\vartheta \right] \Big|_{t_1}^{t_2} \\ &= \left[\int_{\xi(t)} \left\{ m \left\{ (\bar{V} + \dot{u}) + \dot{u}^* \frac{\partial u}{\partial \xi} \right\}^T \delta u \right. \right. \\ &\quad \left. \left. + \left\{ \omega^T + \dot{u}^* \kappa^T \right\} J \delta\alpha \right\} d\xi \right] \Big|_{t_1}^{t_2} .\end{aligned}\quad (5.3.9)$$

These expressions (5.3.8) and (5.3.9) are much more tractable to handle numerically than the acceleration term given earlier in (5.2.16).

To complete (5.3.7), the nonlinear internal force operator, as derived in Chapter II, is given as

$$\int_{t_1}^{t_2} \delta F^S = \int_{t_1}^{t_2} \int_{\xi} \{ \delta u^T \quad \delta \alpha^T \} [B]^T \left\{ \begin{matrix} N_\gamma \\ M_\kappa \end{matrix} \right\} d\xi dt \quad , \quad (5.3.10)$$

and likewise the external force operator is given as

$$\int_{t_1}^{t_2} \delta F^E = \int_{t_1}^{t_2} \int_{\xi(t)} \delta r_i f_i d\xi dt \quad . \quad (5.3.11)$$

5.4 Space-Time Discretization

In conventional finite element models, the displacement field u is approximated with a linear combination of spatial interpolation functions

and time-dependent nodal displacements as given by (3.3.1). This concept can be modified to account for mesh deformation by making the spatial interpolation an implicit function of time. Thus when node motion is allowed, the appropriate spatial approximation is given as

$$u(\xi, t) \simeq \sum_{I=1}^{npe} N_I(\xi(t)) u_I(t) \quad . \quad (5.4.1)$$

For a simultaneous discretization in time, the nodal displacements are approximated in the same manner as a linear combination of temporal interpolation functions and nodal values at discrete time steps as

$$u_I(t) \simeq \sum_{J=1}^{npe} N_J(t) u_I^{t_J} \quad . \quad (5.4.2)$$

From (5.4.1) and (5.4.2), the space-time discretization is given as

$$u \simeq \hat{u} = \sum_{I=1}^{npe} \sum_{J=1}^{npe} N_I(\xi) N_J(t) u_I^{t_J} \quad . \quad (5.4.3)$$

In this expression, the value $u_I^{t_J}$ corresponds to the value of u at the spatial node I and time t_J . The nodal value is thus the displacement with respect to the node $\bar{X}_I(t_j)$ whose position is prescribed throughout the simulation as a function of the deployment speed.

5.4.1 Discrete Equations of Motion

The space-time discretizations of the inertia, internal force, and external force operators within Hamilton's Law (5.3.7) are given as follows. The following analysis is specialized to the case of planar motion where the appropriate degrees of freedom become

$$u = \{ u_1, u_2, \theta \}$$

corresponding to two translational displacements which locate the neutral axis and a single angle of rotation which orients the body-fixed reference frame. These three degrees of freedom can be treated in the same manner. The inertia expression reduces to the form

$$\delta F_i^I = \int_{t_1}^{t_2} \int_{\xi(t)} \frac{D \delta u^T}{Dt} M \frac{D u}{Dt} \quad (5.4.4)$$

$$\delta F_b^I = \left[\int_{\xi(t)} \frac{D \delta u^T}{Dt} M \delta u d\xi \right] \Big|_{t_1}^{t_2} \quad (5.4.5)$$

where

$$M \equiv \text{Diag} \{ m, m, J \} .$$

This expression is evaluated by substituting the approximations

$$\begin{aligned} \frac{D \hat{u}}{Dt} &= \sum_{I=1}^{npe} \sum_{J=1}^{npe} \left[N_I(\xi) \frac{d N_J(t)}{dt} + \dot{u}^* N_J(t) \frac{d N_J(\xi)}{d\xi} \right] u_I^{t_J} \\ \frac{D \delta \hat{u}}{Dt} &= \sum_{I=1}^{npe} \sum_{J=1}^{npe} \left[N_I(\xi) \frac{d N_J(t)}{dt} + \dot{u}^* N_J(t) \frac{d N_J(\xi)}{d\xi} \right] \delta u_I^{t_J} \end{aligned}$$

into (5.4.4) and (5.4.5). The result for the interior term is written as

$$\delta F_i^I = \{ \delta u^{t_1} \delta u^{t_2} \} \begin{bmatrix} A_{11} & A_{12} \\ A_{21} & A_{22} \end{bmatrix} \begin{Bmatrix} u^{t_1} \\ u^{t_2} \end{Bmatrix} \quad (5.4.6)$$

where the spatial element kernels constituting the A matrices are given in Appendix B. Likewise, the boundary terms of the inertia operator, evaluated as

$$\delta F_b^I = \int_{\xi(t_2)} \frac{D \hat{u}(t_2)}{Dt} \cdot \delta \hat{u}(t_2) d\xi - \int_{\xi(t_1)} \frac{D \hat{u}(t_1)}{Dt} \cdot \delta \hat{u}(t_1) d\xi ,$$

is approximated using

$$\begin{aligned} \frac{D \hat{u}(t_1, t_2)}{Dt} &= \sum_{J=1}^{npe} N_J(\xi) \dot{u}_J^{t_1, t_2} + \dot{u}^{*t_1, t_2} \frac{d N_J(\xi)}{d\xi} u_J^{t_1, t_2} \\ \delta \hat{u}(t_1, t_2) &= \sum_{J=1}^{npe} N_J(\xi) \delta u_J^{t_1, t_2} \end{aligned}$$

where it is reiterated that

$$\begin{aligned} u &= (u_1, u_2, \theta) \\ \dot{u}^{*t_2} &= T_{11} (\bar{V}_1 + \dot{u}_1^{t_2}) + T_{12} (\bar{V}_2 + \dot{u}_2^{t_2}) . \end{aligned}$$

The discrete form of (5.4.5) is given as

$$\delta F_b^I = \{ \delta u^{t_1} \delta u^{t_2} \} \left\{ \begin{bmatrix} B_1 & 0 \\ 0 & B_2 \end{bmatrix} \begin{Bmatrix} \dot{u}^{t_1} \\ \dot{u}^{t_2} \end{Bmatrix} + \begin{bmatrix} C_1 & 0 \\ 0 & C_2 \end{bmatrix} \begin{Bmatrix} u^{t_1} \\ u^{t_2} \end{Bmatrix} \right\} \quad (5.4.7)$$

where the spatial kernels B_1 , B_2 , C_1 , and C_2 are also given in Appendix B.

The discrete form of the linear internal force operator is given as

$$\int_{t_1}^{t_2} \delta F^S dt = \{ \delta u^{t_1} \delta u^{t_2} \} \frac{h}{4} \begin{bmatrix} K & K \\ K & K \end{bmatrix} \begin{Bmatrix} u^{t_1} \\ u^{t_2} \end{Bmatrix} \quad (5.4.8)$$

where K is the linear Timoshenko beam stiffness matrix and h is the time step between t_1 and t_2 . This linear discretization is presented to illustrate the general flow of the algorithm; the extension of the algorithm incorporating the nonlinear internal force is discussed in Section 5.4.3. Finally, the external force is discretized as

$$\int_{t_1}^{t_2} \delta F^E dt = \{ \delta u^{t_1} \delta u^{t_2} \} \frac{h}{2} \begin{Bmatrix} f^{t_1} + f^{t_2} \\ f^{t_1} + f^{t_2} \end{Bmatrix} \quad (5.4.9)$$

In all the above discretizations, the double integration over the changing spatial domain and the arbitrary time interval has been performed using reduced integration methods. The reduced integration methods were first chosen as a similar application implementing a space-time discretization of Hamilton's Law concluded that the reduced integration methods resulted in unconditional stability of the transient integration algorithm. In contrast, the full integration methods resulted in a conditional stability of the

transient integration algorithm [141]. A discrete Fourier analysis, presented in Section 5.4.2, concludes that the reduced integration gives a consistent approximation of the original partial differential equations of motion.

From the discretizations (5.4.6 - 5.4.9), the transient integration algorithm is given as follows. The discrete equations of motion arising from the space-time procedure are written as

$$\begin{bmatrix} A_{11} & A_{12} \\ A_{21} & A_{22} \end{bmatrix} \begin{Bmatrix} u^{t_1} \\ u^{t_2} \end{Bmatrix} - \frac{h}{4} \begin{bmatrix} K & K \\ K & K \end{bmatrix} \begin{Bmatrix} u^{t_1} \\ u^{t_2} \end{Bmatrix} = \begin{Bmatrix} f_{rhs}^{t_1} \\ f_{rhs}^{t_2} \end{Bmatrix} \quad (5.4.10)$$

$$\begin{Bmatrix} f_{rhs}^{t_1} \\ f_{rhs}^{t_2} \end{Bmatrix} = \begin{Bmatrix} B_1 \dot{u}^{t_1} + C_1 u^{t_1} - \frac{h}{2} (f^{t_1} + f^{t_2}) \\ B_2 \dot{u}^{t_2} + C_2 u^{t_2} - \frac{h}{2} (f^{t_1} + f^{t_2}) \end{Bmatrix} \quad (5.4.11)$$

for the linear system. Given the initial conditions u^{t_1} and \dot{u}^{t_1} , the first block of the above equations can be solved for u^{t_2} as

$$\left\{ A_{12} - \frac{h}{4} K \right\} u^{t_2} = - \left\{ A_{11} - \frac{h}{4} K \right\} u^{t_1} + f_{rhs}^{t_1} . \quad (5.4.12)$$

It can be shown from the explicit expression of A_{12} given in Appendix B that the left-hand side matrix in the above equation is positive definite. Thus from a solution to (5.4.12) for u^{t_2} , the second block equation can then be solved for \dot{u}^{t_2} as

$$B_2 \dot{u}^{t_2} = \left\{ A_{21} - \frac{h}{4} K \right\} u^{t_1} + \left\{ A_{22} - \frac{h}{4} K - C_2 \right\} u^{t_2} + \frac{h}{2} (f^{t_1} + f^{t_2}) .$$

Again, it can be seen that B_2 is also positive definite. These solutions u^{t_2} and \dot{u}^{t_2} form the initial conditions for the next time step, and thus the time finite elements result in a step-by-step integration formula.

5.4.2 Consistency Analysis

A discrete Fourier analysis provides a mechanism for examining the consistency of the discrete equations of motion with respect to the original partial differential equations [143-144]. The strong form of the partial differential equations of motion are given as

$$\frac{\partial^2 u}{\partial t^2} + 2 \bar{V} \frac{\partial^2 u}{\partial x \partial t} + \hat{V}^2 \frac{\partial^2 u}{\partial x^2} = 0 \quad . \quad (5.4.13)$$

As the main desire is to analyze the characteristics of the inertia operator, the following approximations have been made in the above equation. The convective velocity V^* has been approximated by the deployment speed \bar{V} , and only axial vibrations have been retained such that $\hat{V}^2 = \bar{V}^2 + c^2$ where c^2 represents the elastic wave speed E / ρ .

The traditional Fourier analysis seeks a general harmonic wave solution to the above equation of the form

$$u = u_o e^{i (w t - k x)} \quad (5.4.14)$$

where w is the circular frequency, k the wave number, and i the imaginary number $i = \sqrt{-1}$. The substitution of (5.4.14) into (5.4.13) yields the characteristic equation

$$\{ -w^2 + 2 \bar{V} k w - \hat{V}^2 k^2 \} u_o = 0 \quad . \quad (5.4.15)$$

The fundamental relation between the frequency and the wave number as dictated by this characteristic equation is thus given by

$$w^* = (\bar{V} \pm c^*) k^* \quad (5.4.16)$$

where non-dimensional parameters

$$w^* = wh \quad , \quad k^* = kh \quad , \quad \bar{V}^* = \frac{\bar{V}h}{\ell} \quad , \quad c^* = \frac{ch}{\ell}$$

have been introduced for an arbitrary step-size h and element length ℓ , respectively.

For the discrete equations of motion, the difference equations are obtained by assembling the spatial nodes of two interior beam elements with two sequential steps in time. The spatial nodes, designated as $j - 1$, j , $j + 1$, are spaced a distance ℓ apart, and the time nodes, designated as $i - 1$, i , $i + 1$, are spaced a time step of h apart such that $u_j^{t_i} \rightarrow u_{j,i}$. For the finite element equations resulting from the reduced integration of the variational equations, the difference equations become

$$\begin{aligned} & \frac{\ell}{4h} \left[u_{j+1,i+1} - 2u_{j+1,i} + u_{j+1,i-1} + 2u_{j,i+1} - 4u_{j,i} + \right. \\ & \quad \left. 2u_{j,i-1} + u_{j-1,i+1} - 2u_{j-1,i} + u_{j-1,i-1} \right] + \\ & \frac{2\bar{V}}{4} \left[u_{j+1,i+1} - u_{j-1,i+1} - u_{j+1,i-1} + u_{j-1,i-1} \right] + \\ & \hat{V}^2 \frac{h}{4\ell} \left[u_{j+1,i+1} - 2u_{j,i+1} + u_{j-1,i+1} + 2u_{j+1,i} - 4u_{j,i} + \right. \\ & \quad \left. 2u_{j-1,i} + u_{j+1,i-1} - 2u_{j,i-1} + u_{j-1,i-1} \right] \\ & = 0 \quad . \end{aligned} \tag{5.4.17}$$

Likewise, the difference equations for a fully integrated version become

$$\begin{aligned} & \frac{\ell}{6h} \left[u_{j+1,i+1} - 4u_{j+1,i} + u_{j+1,i-1} + 2u_{j,i+1} - 8u_{j,i} + \right. \\ & \quad \left. 2u_{j,i-1} + u_{j-1,i+1} - 4u_{j-1,i} + u_{j-1,i-1} \right] + \\ & \frac{2\bar{V}}{4} \left[u_{j+1,i+1} - u_{j-1,i+1} - u_{j+1,i-1} + u_{j-1,i-1} \right] + \\ & \hat{V}^2 \frac{h}{6\ell} \left[u_{j+1,i+1} - 4u_{j,i+1} + u_{j-1,i+1} + 2u_{j+1,i} - 8u_{j,i} + \right. \end{aligned}$$

$$\begin{aligned}
 & 2 u_{j-1,i} + u_{j+1,i-1} - 4 u_{j,i-1} + u_{j-1,i-1} \Big] \\
 & = 0 \quad . \quad (5.4.18)
 \end{aligned}$$

To compare the characteristics of the difference equations to the characteristics of the continuum equation given in (5.4.15), a harmonic solution to the difference equations of the form

$$u_{j,i} = u_0 e^{i(wt - kx)}$$

is sought. By substituting the harmonic solution into the difference equations (5.4.17) and (5.4.18), the characteristic equations of the discrete cases become

$$\begin{aligned}
 \left\{ 1 - \frac{\ell^2}{4} \bar{k}^2 \right\} \bar{w}^2 - 2V \frac{\sin k\ell}{\ell} \frac{\sin wh}{h} \\
 + \hat{V}^2 \left\{ 1 - \frac{h^2}{4} \bar{w}^2 \right\} \bar{k}^2 = 0 \quad (5.4.19)
 \end{aligned}$$

for the reduced integration version (5.4.17) and

$$\begin{aligned}
 \left\{ \frac{2}{3} \left(1 - \frac{\ell^2}{4} \bar{k}^2 + \frac{1}{3} \hat{V}^2 \frac{h^2}{\ell^2} \right) \bar{w}^2 - 2V \frac{\sin k\ell}{\ell} \frac{\sin wh}{h} - \right. \\
 \left. \hat{V}^2 \left\{ \frac{2}{3} \left(1 - \frac{h^2}{4} \bar{w}^2 + \frac{1}{3} \frac{\ell^2}{h^2 \hat{V}^2} \right) \bar{w}^2 \right. \right. \\
 \left. \left. + \frac{4}{3} \left\{ \frac{1}{h^2} + \frac{\hat{V}^2}{\ell^2} \right\} \right\} = 0 \quad (5.4.20)
 \end{aligned}$$

for the fully integrated version (5.4.18) where

$$\bar{k} = \frac{\sin \frac{k\ell}{2}}{\frac{\ell}{2}}, \quad \bar{w} = \frac{\sin \frac{w\ell}{2}}{\frac{w}{2}}$$

for both cases.

It is now observed from a careful comparison of the characteristic equation for the continuum case (5.4.15) to those for the discrete cases

(5.4.19) and (5.4.20), the latter corresponding to the full integration scheme results in an inconsistent representation. Spurious mechanisms emanate from nonphysical rigid-body motions. The possibility of introducing spurious mechanism by the preceding finite element discretization can be determined from the solution of the above equations with $\bar{w} = 0$. The reduced integration characteristic equation (5.4.19) reduces to

$$\bar{k}^2 = 0 \Rightarrow k = \frac{2\pi n}{\ell} \quad n = 0, 1, 2, \dots \quad (5.4.21)$$

for this analysis. As the highest admissible deformation mode shape admitted by linear shape functions is π / ℓ , the only potential solution of (5.4.19) is $k = 0$. This solution coincides with the correct rigid-body mode solution of the continuum characteristic equation (5.4.16). The latter case of full integration leads to

$$\frac{1}{3} \frac{\ell^2}{h^2 \hat{V}^2} \bar{k}^2 + \frac{4}{3} \left\{ \frac{1}{h^2} + \frac{\hat{V}^2}{\ell^2} \right\} = 0$$

which does not admit a physically valid solution. It is also noted that the representation (5.4.20) does not converge in the limit to the true characteristic equation (5.4.15), whereas the representation (5.4.19) does have this property. Finally, the dispersion relation of the reduced integration difference equations can be derived as

$$\tan \frac{w^*}{2} = (\bar{V}^* \pm c^*) \tan \frac{k^*}{2}$$

to be compared to the true dispersion relation (5.4.16). This is done below in Figure 5.4 where it is seen the approximation is valid for the range $k^* < \frac{\pi}{2}$. The reduced integration version is thus the consistent discretization of the variational equations of motion.

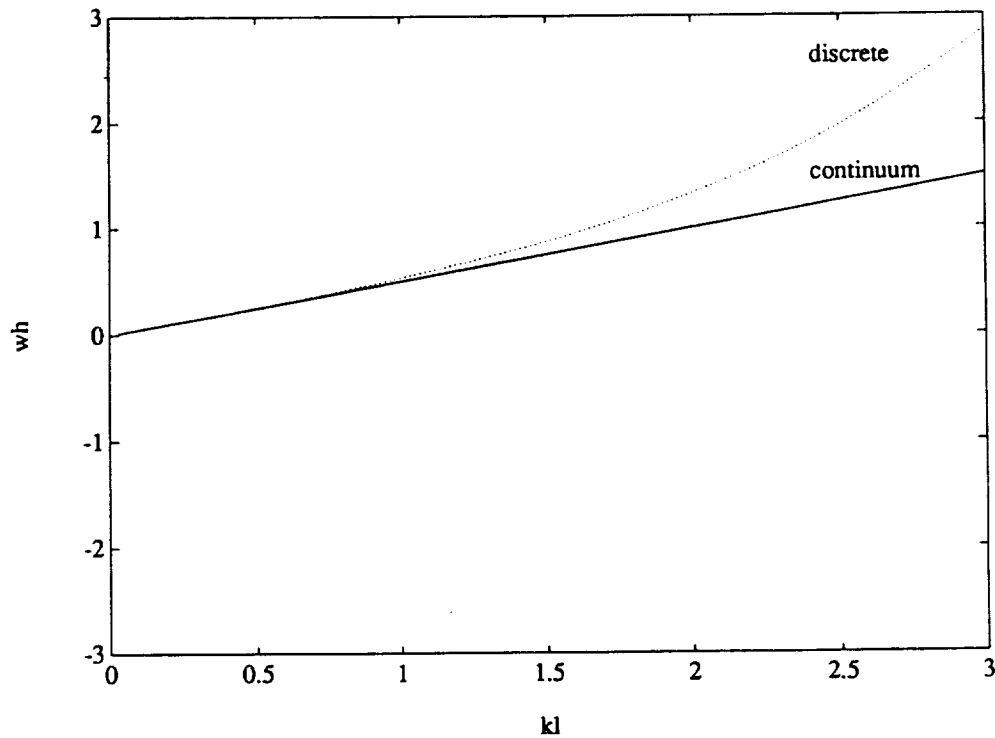


Figure 5.4 Dispersion relations.

5.4.3 Nonlinear Solution Strategy

To include the nonlinear force term within the procedure, the equations

$$\begin{bmatrix} A_{11} & A_{12} \\ A_{21} & A_{22} \end{bmatrix} \begin{Bmatrix} u^{t_1} \\ u^{t_2} \end{Bmatrix} - \int_{t_1}^{t_2} \int_{\vartheta(t)} [B]^T \sigma d\vartheta dt = \begin{Bmatrix} f_{rhs}^{t_1} \\ f_{rhs}^{t_2} \end{Bmatrix}$$

are solved via the Newton-Rhapson iteration technique. The displacement u^{t_2} is obtained first by iteratively solving a nonlinear version of (5.4.10). To

this end, a solution to the following residual equation

$$\begin{aligned} r &= A_{11} u^{t_1} + A_{12} u^{t_2} - \int_{t_1}^{t_2} \int_v [B]^T \sigma d\vartheta dt - f_{rhs}^{t_1} \\ &= 0 \end{aligned} \quad (5.4.22)$$

is obtained by iterating about the linearized set of equations

$$E_{(k+1)} \Delta u^{t_2}_{(k+1)} = -r_{(k+1)} \quad (5.4.23)$$

The above equations are solved at the $(k+1)^{th}$ iteration for incremental displacements Δu^{t_2} which update the solutions obtained at the k^{th} iteration via

$$u_{(k+1)}^{t_2} = u_{(k)}^{t_2} + \Delta u^{t_2} \quad .$$

The iterative procedure is started with $u_{(0)}^{t_2} = u^{t_1}$ and continued until a convergence criterion is reached. The solution matrix E introduced in (5.4.23) is obtained from (5.4.22) as

$$E = A_{12} - \frac{h}{4} (K_G + K_M)$$

where K^G and K^M correspond to the material and geometric stiffness matrices of the nonlinear internal force.

To complete the procedure, an evaluation of the time integral of the internal force within the residual (5.4.22) is necessary. Using a reduced integration interpretation, this is given as

$$\int_{t_1}^{t_2} \delta F^S dt = \{ \delta u^{t_1} \delta u^{t_2} \} \frac{h}{2} \left\{ \begin{matrix} S \left(\frac{1}{2} (u^{t_1} + u^{t_2}) \right) \\ S \left(\frac{1}{2} (u^{t_1} + u^{t_2}) \right) \end{matrix} \right\}$$

where the internal force is evaluated using an average of the displacements between the two time steps.

It is important to note that in the moving node formulation the displacement coordinates u^n and u^{n+1} are defined with respect to different spatial grids; the coordinates u^n are defined from the nodes \bar{X}^n whereas the coordinates u^{n+1} are defined from the nodes \bar{X}^{n+1} . Therefore, prior to the computation of the displacement average for the evaluation of the internal force, the coordinates u^n must be extrapolated to the grid \bar{X}^{n+1} . In addition, the internal force computation discussed in Chapter III was based on an incremental procedure in which the current stress state was obtained by updating a past stress state with an increment of stress. This stress increment is a function of the displacement increment Δu between a current configuration u and the past configuration u^n as

$$\Delta u = u^{n+1} - u^n .$$

To incorporate this concept within the moving node formulation, the displacement increment must be also be computed from variables defined on a consistent grid.

To this end, an extrapolation of the variables u^n to the grid \bar{X}^{n+1} must be defined in a manner consistent with the present internal force formulation. The stress update remains unaffected by the extrapolation of u^n if the constant elemental strain states of the past configuration are represented without alteration. A consistent extrapolation thus must retain the orientation of the elemental convected reference frames. By retaining the convected reference frame orientation as determined from the original translational coordinates x^n for the extrapolated displacements $x^{n'}$, the deformed position of the beam neutral axis can equivalently be described

with either coordinates as

$$\begin{aligned} x^n &= \bar{X}^n + u^n \\ x^{n'} &= \bar{X}^{n+1} + u^{n'} \end{aligned}$$

Figure 5.5 below illuminates the above concept. For a given element bounded by nodes i and $i+1$, the a_1 axis of the convected reference frame is determined from

$$\frac{x_{i+1} - x_i}{\ell}, \quad \ell = \|x_{i+1} - x_i\|.$$

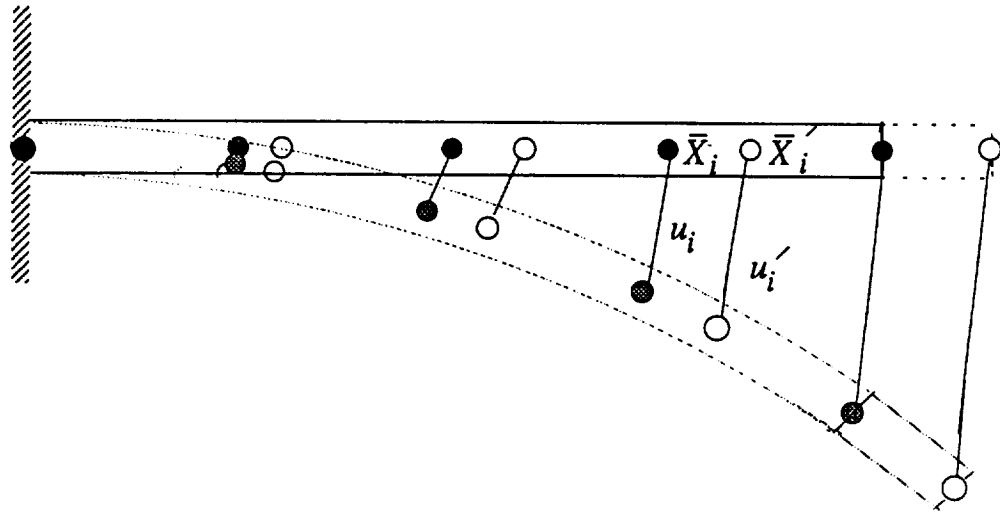


Figure 5.5 Extrapolation of displacement coordinates.

To retain the orientation of the element convected frame, the extrapolations must be such that

$$\frac{x'_{i+1} - x'_i}{\ell'} = \frac{x_{i+1} - x_i}{\ell} \quad (5.4.24)$$

Given a constant deployment velocity V , the nodal positions \bar{X}_i are automatically prescribed such that the length between two nodes

$$\ell_X = \bar{X}_{i+1} - \bar{X}_i = \frac{V t}{nele}$$

is a function of time as given by (5.2.3). It is easily seen that, starting from the first node which remains fixed at the boundary of the guide as

$$\bar{X}_1^n = \bar{X}_1^{n+1} = \bar{X}'_1 ,$$

the rest of the nodes for $i = 2, nele + 1$ can be generated as

$$\begin{aligned} \bar{X}'_{i+1} &= \bar{X}'_i + \ell'_X \\ &= \bar{X}'_i + \frac{\ell'_X}{\ell_X} (\bar{X}_{i+1} - \bar{X}_i) . \end{aligned}$$

If the extrapolated displacements are generated from previous values in the same sequential manner for nodes $i = 2, nele + 1$ as

$$\begin{aligned} u'_1 &= u_1 \\ u'_{i+1} &= u'_i + \frac{\ell'_X}{\ell_X} (u_{i+1} - u_i) , \end{aligned}$$

it is easily shown the condition (5.4.24) is satisfied. The position of the deformed neutral axis and thus the strain state is unaltered by the extrapolation. The rotational variables are extrapolated in the same manner such that a constant curvature state is retained without alteration. These extrapolations are performed on variables prior to an internal stiffness computation and are otherwise not a part of the integration algorithm itself.

5.5 Results

The computational techniques, namely the space-time finite element integration algorithm combined with the internal force computation discussed in Chapter III, have been implemented into a Fortran 77 software package. The software was first verified by repeating planar examples reported in Chapter IV using a fixed node reference. The formulation was then tested on an analysis of a sheet of paper issuing from a rigid horizontal guide into a uniform gravitational field and compared to results reported in [118]. In work of [118], the nonlinear equations of motion of an elastica that moves out of a horizontal guide at a constant velocity are shown to depend on two parameters, namely a dimensionless weight-to-stiffness ratio $\mu = mg\ell^4 / EI$ and a dimensionless velocity $\nu = V\ell\sqrt{m\ell / EI}$. In these expressions, m is the mass per unit area of the paper, g is the acceleration of gravity, ℓ is the length of the paper, EI the bending stiffness, and V the constant velocity of the paper ejection. The analysis was performed with $\mu = 50$ and $\nu^2 = 100, 50, 20, 10$ corresponding to $V = 92, 65, 41, 20$ in/sec respectively. The trajectories of the beam tip for the various deployment speeds are shown in Figure 5.6 and compared to the static shape of a fully extended cantilevered beam with given properties such that $\mu = 50$. The results are comparable to those reported in [18]. Figure 5.7 gives an animated history of the beam deformations throughout various stages of the deployment. The deformation shapes are again compared to the static shape.

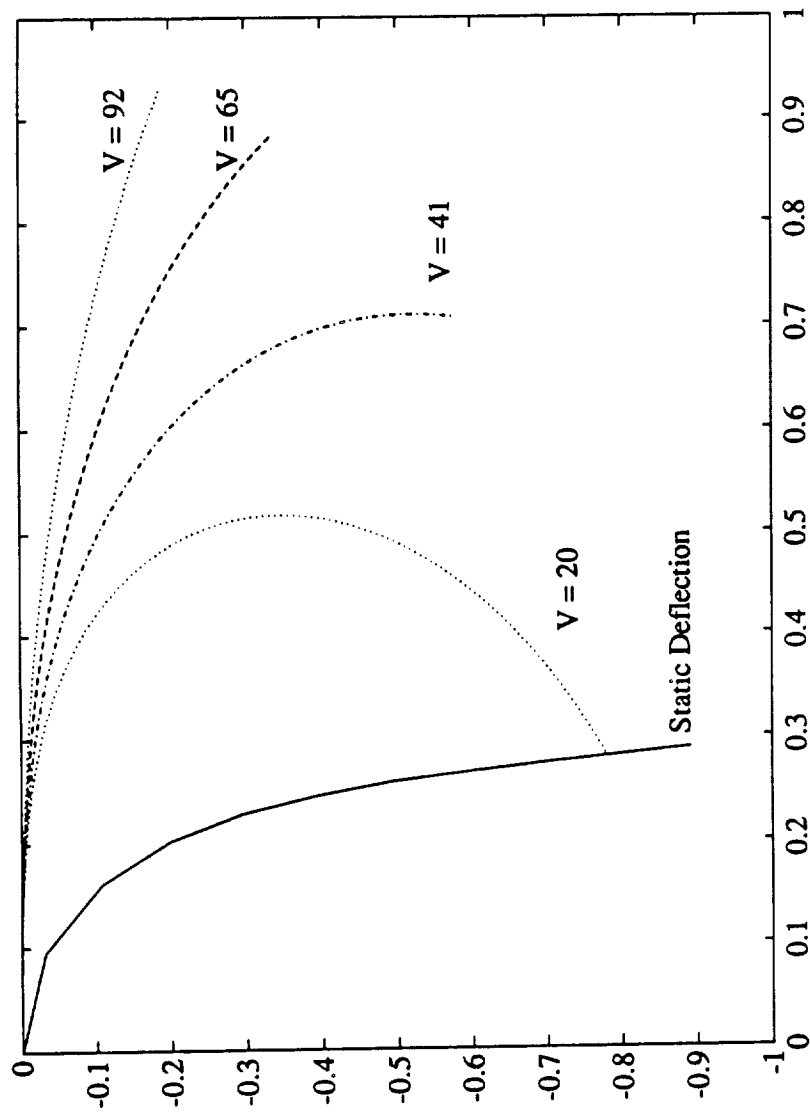


Figure 5.6 End orbits for various deployment speeds (V).

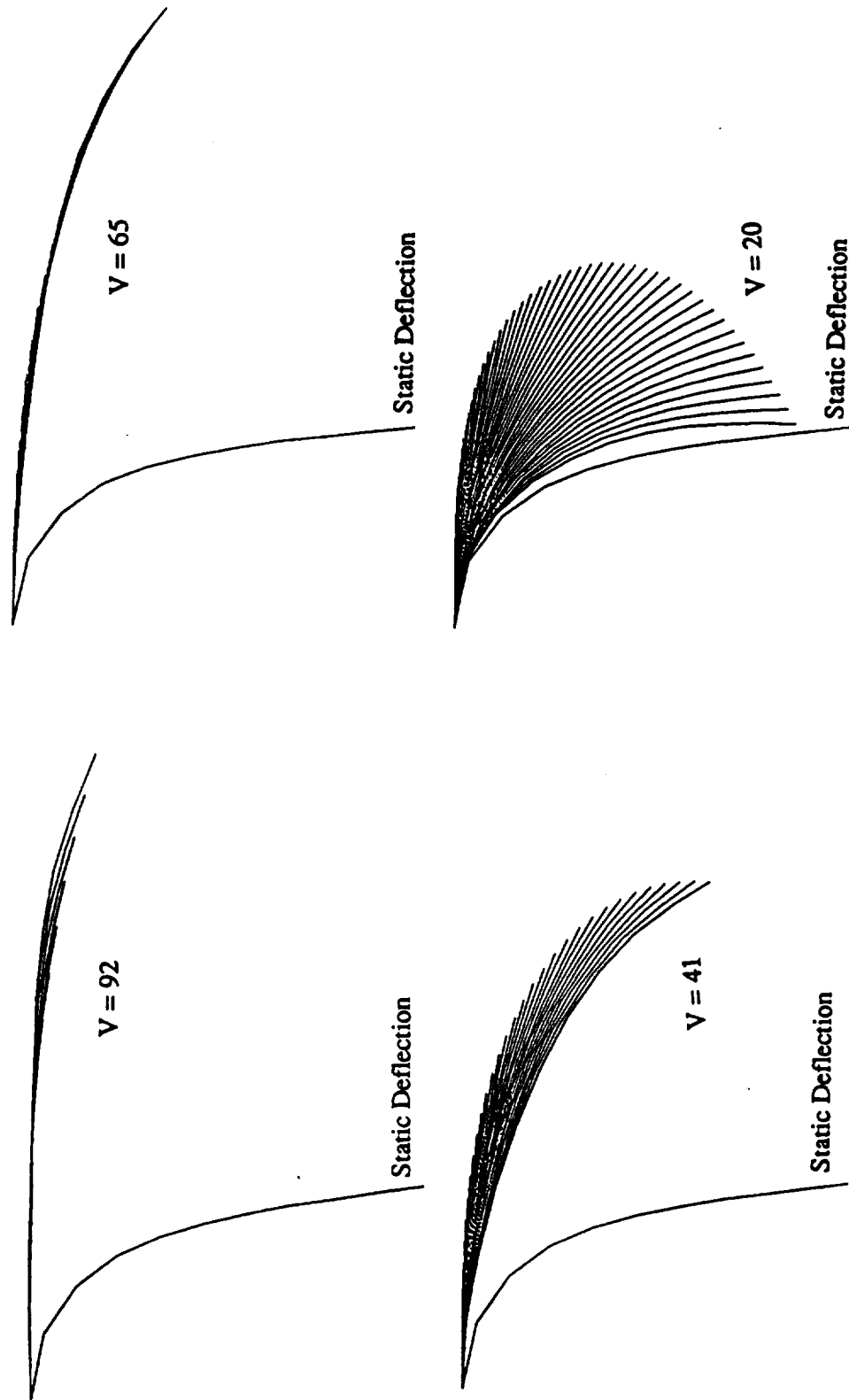


Figure 5.7 Motion history for various deployment speeds (V).

5.6 Concluding Remarks

An effective computational method has been developed for the modeling of beam deployment which retains the advantages of the present beam formulation. A deforming spatial grid has been introduced to model the changing spatial volume. Due to the changing spatial reference for the dynamic variables, the inertia operator acquires terms representing the convective rate of change of the variable in addition to those representing the local rate of change of the variable. A variational formulation is presented in Hamiltonian form to simplify the numerical treatment of the inertia operator. A space-time discretization of the Hamiltonian formulation is implemented which accurately accounts for the deforming spatial grid in the transient integration scheme. Reduced integration techniques were used to analyze the required integrations over both the space and time domains; a discrete Fourier analysis concluded that this discretization resulted in a consistent approximation to the governing partial differential equations of motion. To effect the moving node formulation within the present internal force computational procedure, the solutions of a past configuration are appropriately extrapolated to the grid representing the current configuration. The results obtained from the present computational procedure agree with those reported in [118].

The next chapter summarizes the work presented in this dissertation.

CHAPTER VI

CONCLUSIONS

6.1 Summary of Work

The present thesis work has focused on the dynamic analysis of three-dimensional elastic beams which experience large rotational and large deformational motions. A realistic mathematical model of a spatial flexible beam was developed as an integral kernel of a general multibody dynamics methodology. The model accounts for both large rotations and large deformations as typically experienced by a flexible component within an articulated structure. Computational solution techniques were then derived and implemented which enhance and exploit various features inherent in the formulation. The resulting methodology provides a tool to study the effects of component flexibility on the performance of multibody systems.

To model the spatial dynamics of highly flexible beams, the beam motion is described using an inertial reference for the translational displacements and a body-fixed reference for the rotational quantities. Finite strain rod theories are then defined in conjunction with the beam kinematic description. The resulting strain measures account for the effects of stretching, bending, torsion, and transverse shear deformations, and thus model potential deformations of typically lightweight and highly flexible space structure appendages. In addition, due to the kinematic description of the beam motion, the form of the equations of motion are similar to that of rigid body dynamics. As such, these equations can be solved with numerical solution procedures developed for general multibody dynamic systems. Another ad-

vantage of the present formalism is the use of a convected coordinate representation of the Cauchy stress tensor and a conjugate strain definition to model the beam deformation. This is in contrast to many finite-deformation analysis which typically adopt the Piola-Kirchoff stress tensor to model the deformation. As such, the stress/strain representation of the present formulation coincides with the actual strains measured by sensors rotating with and operating on the deformed structure. An easy interface is thus possible with control-type applications such as vibration suppression and slewing maneuvers.

The numerical treatment of the beam formalism is considered in detail in the present thesis. A computational procedure for the internal force has been derived from the continuum formulation. As the formulation is based on an inertial reference for the beam dynamics, the degrees of freedom of the flexible component contain information of both rigid and flexible deformation motions without distinction. The rigid motions must not influence the strain computation. To this end, a unique computation which exploits characteristics of the strain formulation as well as finite rotation theory was derived to filter out the rigid body motions embedded within the degrees of freedom. The procedure was proven to remain invariant to arbitrary finite rigid rotations of the beam while accurately modeling the beam strain.

The present internal force computation was successfully interfaced with multibody dynamic solution procedures. As a consequence of the present beam formulation, the structure of the equations of motion is identical for both rigid and flexible components of an arbitrary multibody configuration. The following numerical solution procedures, which have been

developed and successfully implemented in the present work, are thus applicable for both the rigid and flexible components of the articulated structure. An interlaced application of the central difference algorithm is used to integrate the translational coordinates and the angular velocity vector. Given the solution for the angular velocity, an implicit algorithm is used to discretize the Euler parameter/angular velocity kinematical relation to obtain the corresponding angular orientation. The constraint conditions, which are augmented to the formulation via Lagrange multipliers, are enforced via a separate procedure which implicitly integrates an alternative stabilized companion differential equation for the Lagrange multipliers. The numerical techniques were originally tested on multirigid body systems and then successfully extended to models incorporating the present beam formulation. The combined developments of the objective internal force computation with the dynamic solution procedures result in the computational preservation of total energy for undamped systems. This distinct feature has been demonstrated in several examples.

The final development presented in this thesis is the modeling of the dynamics of deployment/retrieval of the beam formulation. To model the deployment, a moving spatial grid is employed as a reference for the dynamic variables. This reference corresponds to the configuration of a deployed beam as if it were rigid. The introduction of this moving spatial reference leads to complexities in the beam inertia operator. For this reason, a Hamiltonian variational formulation is employed to simplify the numerical treatment of the inertia operator. Space-time finite elements are used to discretize the Hamiltonian formulation, resulting in a transient integration scheme which accurately accounts for the deforming spatial grid. The

methodology is successfully interfaced with the internal force computational formalism, thus retaining the large rotation/large deformation modeling capabilities of the present work.

The major contributions of this work are summarized as follows:

- a) A formulation for the spatial motion of flexible beams has been developed based on physically applicable strain definitions representative of those measured from actual sensors located and operating on a rotating flexible structure.
- b) A numerical procedure for the accurate computation of the internal force has been developed from the continuum formulation and proven to be invariant to arbitrary rigid motions of the beam.
- c) Multibody dynamic solution procedures have been developed and applied to models of articulated structures incorporating the present beam formulation.
- d) The dynamics of deployment/retrieval have been modeled by incorporating a moving node reference for the present beam formulation and a space-time discretization of the corresponding Hamiltonian variational statement.
- e) The computational procedures developed to simulate the dynamics of multibody systems with flexible beam components have been implemented into a software testbed, providing a mechanism for dynamic analysis of space structures, robot assemblies, and similar applications.

6.2 Directions for Further Research

Accurate numerical simulations of flexible multibody systems can

be utilized to facilitate interdisciplinary research. The techniques used in designing control schemes for robotic type applications can be enhanced with this simulation capability. As the implementation of a maneuvering strategy developed from rigid models is not guaranteed to be successful, it is important to determine to what extent the flexibility affects the robot performance.

A potential application for this type of simulation capability is the *in-space construction facility* being developed for the construction, maintenance, and repair of future massive space structures. The main body of the crane is designed to carry the structural components to be assembled. A mobile transporter which controls an attached remote manipulator system moves along the crane arm to provide fine positioning and delicate readjustment tasks required of the assembly process. Limited numerical experiments which have been performed on flexible models of the space crane suggest that the development of control strategies and maneuvering speeds need be further addressed, and the effect of flexibility on the tip positioning accuracy need be determined. Control strategies that work when the system configurations change in a manner effecting rapidly varying frequency responses must be developed for the successful operation of the space crane.

To effect on-board adaptive control strategies, real-time software simulation capabilities must also be developed. To this end, parallel algorithms that address the highly nonlinear equilibrium equations augmented with complex kinematic and control constraints must be derived and implemented within current multi-processor technologies.

In addition to applications involving robotics and control, another area of research is the prediction of conditions which lead the present beam

model to unstable motion. The influence of the deployment of flexible appendages on the spacecraft attitude stability may be parameterized in terms of the deployment velocity and the orbital angular velocity. In addition, it should be explored whether the present computational procedure can predict the onset of chaotic motion within the nonlinear beam model due to a change in certain input conditions. In general, the present flexible beam computational methodology provides a tool for further analysis of many engineering operations.

REFERENCES

1. Ashley, H., "Observation on the Dynamic Behavior of Flexible Bodies in Orbit," *AIAA J.* **5** (1967) 460-469.
2. Grotte, P.B., J.C. McMunn, and R. Gluck, "Equations of Motion of Flexible Spacecraft," *J. of Spacecraft and Rockets* **8** (1971) 561-567.
3. Canavin, J.R. and Likins, P.W., "Floating Reference Frames for Flexible Spacecraft," *J. of Spacecraft* (1977) 724-732.
4. De Veubeke, B.F., "The Dynamics of Flexible Bodies," *Int J. Engng. Sci.* **14** (1976) 895-913.
5. McDonough, T.B., "Formulation of the Global Equations of Motion of a Deformable Body," *AIAA J.* **14** (1976) 656-660.
6. Kane, T. and Levinson, D., "Simulation of Large Motions of Nonuniform Beams in Orbit: Part II - The Unrestrained Beam," *J. Astronautical Sciences* **29** (1981) 245-275.
7. Cavin, R.K. and Dusto, A.R., "Hamilton's Principle: Finite-Element Methods and Flexible Body Dynamics," *AIAA J.* **15** (1977) 1684-1690.
8. Agrawal, O.P. and Shabana, A.A., "Dynamic Analysis of Multibody Systems using Component Modes," *Computers & Structures* **21** (1985) 1303-1312.
9. Agrawal, O.P. and Shabana, A.A., "Application of Deformable-Body Mean Axis to Flexible Multibody System Dynamics," *Comp. Meth. Appl. Mech. Engrg.* **56** (1986) 217-245.
10. Yoo, W.S. and Haug, E.J., "Dynamics of Flexible Mechanical Systems using Vibration and Static Correction Modes," *J. Mechanisms, Transmissions, and Automation in Design* **108** (1986) 315-322.
11. Yoo, W.S. and Haug, E.J., "Dynamics of Articulated Structures, Part I: Theory and Part II: Computer Implementation and Applications," *J. of Structure Mechanics* **14** (1986) 105-126 and 177-189.
12. Bodley, C., Devers, A., Park, A., and Frisch, H., "A Digital Computer Program for Dynamic Interaction Simulation of Controls and Structures (DISCOS)," NASA Technical Paper 1219, (1978).

13. Song, J.O. and Haug, E.J., "Dynamic Analysis of Planar Flexible Mechanisms," *Comp. Meth. Appl. Mech. Engrg.* **24** (1980) 359-381.
14. Laskin, R.A., Likins, P.W., and Longman, R.W., "Dynamical Equations of a Free-Free Beam Subject to Large Overall Motions," *J. Astronautical Sciences* **31** (1983) 507-528.
15. Kane, T.R., Ryan, R.R., and Banerjee, A.K., "Dynamics of a Cantilever Beam Attached to a Moving Base," *J. Guidance, Control, and Dynamics* **10** (1987) 139-151.
16. Bakr, E.M. and Shabana, A.A., "Geometrically Nonlinear Analysis of Multibody Systems," *Computers & Structures* **23** (1986) 739-751.
17. Christensen, E.R. and Lee, S.W., "Nonlinear Finite Element Modeling of the Dynamics of Unrestrained Flexible Structures," *Computers & Structures* **23** (1986) 819-829.
18. Wempner, G., "Finite Elements, Finite Rotations and Small Strains of Flexible Shells," *Int. J. Solids and Structures* **5** 117-153.
19. Belytschko, T. and Hsieh, B.J., "Nonlinear Transient Finite Element Analysis with Convected Coordinates," *Int. J. Num. Meth. Eng.* **7** (1973) 255-271.
20. Belytschko, T., Schwer, L., and Klein, M.J., "Large Displacement, Transient Analysis of Space Frames," *Int. J. Num. Meth. Eng.* **11** (1977) 65-84.
21. Belytschko, T., and Glaum, L.W., "Applications of Higher Order Rotational Stretch Theories to Nonlinear Finite Element Analysis," *Computers & Structures* **10** (1979) 175-182.
22. Housner, J., "Convected Transient Analysis for Large Space Structures Maneuver and Deployment," Proc. the 25th Structures, Structural Dynamics and Materials Conference, AIAA Paper No. 84-1023, (1984) 616-629.
23. Housner, J.M., Wu, S.C., and Chang, C.W., "A Finite Element Method for Time Varying Geometry in Multibody Structures," Proc. the 29th Structures, Structural Dynamics and Materials Conference, April 1988, AIAA Paper No. 88-2234.
24. Bathe, K.J., and Bolourchi, S., "Large Displacement Analysis of Three-Dimensional Beam Structures," *Int. J. Num. Meth. Eng.* **14** (1979) 961-986.

25. Dvorkin, E.N., Onate, E., and Oliver, J., "On a Non-Linear Formulation for Curved Timoshenko Beam Elements Considering Large Displacement/Rotation Increments," *Int. J. Num. Meth. Eng.* **26** (1988) 1597-1613.
26. Surana, K.S. "Geometrically Non-Linear Formulation for Two Dimension Curved Beam Elements," *Computers & Structures* **17** (1983) 105-114.
27. Surana, K.S., and Sorem, R.M., "Geometrically Non-Linear Formulation for Three Dimensional Curved Beam Elements with Large Rotations," *Int. J. Num. Meth. Eng.* **28** (1989) 43-73.
28. Rankin, C.C., and Brogan, F.A., "An Element Independent Corotational Procedure for the Treatment of Large Rotations," *J. Pressure Vessel Technology* **108** (1986) 165-174.
29. Rankin, C.C., and Nour-Omid, B., "The Use of Projectors to Improve Finite Element Performance," *Computers & Structures* **30** (1988) 257-267.
30. Wu, S.C. and Haug, E.J., "Geometric Nonlinear Substructuring for Dynamics of Flexible Mechanical Systems," *Int. J. Num. Meth. Engrg.* **26** (1988) 2211-2226.
31. Simo, J.C., "A finite strain beam formulation. Part I: The three dimensional dynamic problem," *Comp. Meth. Appl. Mech. Engrg.* **49** (1985) 55-70.
32. Simo, J.C. and Vu-Quoc, L., "A Three-Dimensional Finite Strain Rod Model. Part II: Computational Aspects," *Comp. Meth. Appl. Mech. Engrg.* **58** (1986) 79-116.
33. Simo, J.C. and Vu-Quoc, L., "Finite-Strain Rods Undergoing Large Motions," *Comp. Meth. Appl. Mech. Engrg.* **66** (1988) 125-161.
34. Cardona, A. and Geradin, M., "A Beam Finite Element Nonlinear Theory with Finite Rotations," *Int. J. Num. Meth. Eng.* **26** (1988) 2403-2438.
35. Iura, M. and Atluri, S.N., "On a Consistent Theory, and Variational Formulation of Finitely Stretched and Rotated 3-D Space-Curved Beams," *Computational Mechanics* (4) (1989) 73-88.
36. Iura, M. and Atluri, S.N., "Dynamic Analysis of Finitely Stretched and Rotated Three-Dimensional Space-Curved Beams," *Computers & Structures* **29** (1988) 875-889.

37. Antman, S.S., "Kirchhoff Problem for Nonlinearly Elastic Rods," *Quat. J. Appl. Math* XXXII 3 (1974) 221-240.
38. Reissner, E., "On One-Dimensional Finite-Strain Beam Theory: the Plane Problem," *J. Appl. Math. and Phys. (ZAMP)* 23 (1972) 795-804.
39. Reissner, E., "On a One-Dimensional Large-Displacement Finite-Strain Beam Theory," *Studies in Applied Mathematics* 52 (1973) 87-95.
40. Reissner, E., "On Finite Deformations of Space-Curved Beams," *ZAMP* 132 (1981) 734-744.
41. Wempner, G., *Mechanics of Solids with Applications to Thin Bodies*, Sijthoff & Noordhoff, The Netherlands (1981).
42. Danielson, D.A., and Hodges, D.H., "Nonlinear Beam Kinematics by Decomposition of the Rotation Tensor," *J. Appl. Mech.* 54 (1987) 258-262.
43. Danielson, D.A., and Hodges, D.H., "A Beam Theory for Large Global Rotation, Moderate Local Rotation, and Small Strain," *J. Appl. Mech.* 55 (1988) 179-184.
44. Park, K.C., Chiou, J.C., and Downer, J.D., "Explicit-Implicit Staggered Procedure for Multibody Dynamics Analysis," *J. Guidance, Control, and Dynamics* 13 (1990) 562-570.
45. Malvern, L.E., *Introduction to the Mechanics of a Continuous Medium*, Prentice-Hall, Inc., Englewood Cliffs, N. J., (1969).
46. Eringen, A.C., *Mechanics of Continua*, Robert E. Krieger Publishing Co., Huntington, N.Y., (1980).
47. Goldstein, H., *Classical Mechanics*, 2nd ed., Addison-Wesley (1980).
48. Moore, E.N., *Theoretical Mechanics*, Wiley & Sons (1983).
49. Truesdell, C., "The Simplest Rate Theory of Pure Elasticity," *Comm. Pure Appl. Math.* 8 (1955) 123-132.
50. Stanley, G.S., "Continuum-Based Shell Elements," PhD Thesis, Stanford University, 1985.
51. Dienes, J.K., "On the Analysis of Rotation and Stress Rate in Deforming Bodies," *Acta Mechanica* 32 (1979) 217-232.

52. Rubinstein, R. and Atluri, S.N., "Objectivity of Incremental Constitutive Relations over Finite Time Steps in Computational Finite Deformation Analysis," *Comp. Meth. Appl. Mech. Engrg.* **36** (1983) 277-290.
53. Flanagan, D.D., and Taylor, L.M., "An Accurate Numerical Algorithm for Stress Integration with Finite Rotations," *Comp. Meth. Appl. Mech. Engrg.* **62** (1987) 305-320.
54. Argyris, J.H., Dunne, P.C., Scharpf, D.W., "On Large Displacement-Small Strain Analysis of Structures with Rotational Degrees of Freedom," *Comp. Meth. Appl. Mech. and Eng.* **14** (1978) 401-451.
55. Argyris, J., "An Excursion into Large Rotations," *Comp. Meth. Appl. Mech. Eng.* **32** (1982) 85-155.
56. Cardonna, A., "An Integrated Approach to Mechanism Analysis," PhD Thesis, University of Liege, (1989).
57. Simmonds, J.G., and Danielson, D.A., "Nonlinear Shell Theory with Finite Rotation and Stress Function Vectors," *J. Appl. Mech.* **39** (1972) 1085-1090.
58. Geradin, M., and Cardona, A., "Kinematics and Dynamics of Rigid and Flexible Mechanisms using Finite Elements and Quaternion Algebra," *Computational Mechanics* **4** (1989) 115-135.
59. Wehage, R.A., "Quaternions and Euler Parameters. A Brief Exposition," in *Computer Aided Analysis and Optimization of Mechanical System Dynamics* E.J. Haug, ed., Springer-Verlag, (1984).
60. Spring, K.W., "Euler Parameters and the use of Quaternion Algebra in the Manipulation of Finite Rotations: A Review," *Mechanism and Machine Theory* **21** (1986) 365-373.
61. Nikravesh, P.E., "Spatial Kinematic and Dynamic Analysis with Euler Parameters," in *Computer Aided Analysis and Optimization of Mechanical System Dynamics* E.J. Haug, ed., Springer-Verlag, (1984).
62. Nikravesh, P.E., Wehage, R.A., and Kwon, O.K., "Euler Parameters in Computational Kinematics and Dynamics. Part 1," *J. Mechanisms, Transmissions, and Automation in Design* **107** (1985) 358-365.
63. Geradin, M., "Finite Element Approach to Kinematic and Dynamic Analysis of Mechanisms using Euler Parameters," in *Numerical Methods for Nonlinear Problems II*, C. Taylor et al., ed., Pineridge Press, Swansea, U.K. (1984).

64. Zienkiewicz, O.C., 1977, *The Finite Element Method*, 3rd ed., McGraw Hill Book Company, Ltd, London.
65. Stuelpnagel, J., "On the Parametrization of the Three-Dimensional Rotation Group," *SIAM Review* 6 (1964) 422-430.
66. Nour-Omid, B., and Rankin, C.C., "Finite Rotation Analysis and Consistent Linearization using Projectors," To be Submitted: *Comp. Meth. Appl. Mech. Eng.* (1990).
67. Spurrier, R.A., "Comment on 'Singularity-Free Extraction of a Quaternion from a Direction-Cosine Matrix'," *Journal of Spacecraft and Rockets* 15 (1978) 255.
68. Geradin, M., Robert, G., and Buchet, P., "Kinematic and Dynamic Analysis of Mechanisms: A Finite Element Approach Based on Euler Parameters," in: *Finite Element Methods for Nonlinear Problems* (P. Bergan, ed.), Berlin, Heidelberg, New York, Springer, (1986).
69. Likins, P., "Dynamic Analysis of a System of Hinge-Connected Rigid Bodies with Nonrigid Appendages," *Internat. J. Solids and Structures* 9 (1973) 1473-1487.
70. Hooker, W., "Equations of Motion for Interconnected Rigid and Elastic Bodies: A Derivation Independent of Angular Momentum," *Celestial Mech.* 11 (1975) 337-359.
71. Ho, J., "Direct Path Method for Flexible Multibody Spacecraft Dynamics," *J. Spacecraft and Rockets* 14 (1977) 102-110.
72. Hughes, P., "Dynamics of a Chain of Flexible Bodies," *J. Astronaut. Sci.* 27 (1979) 359-380.
73. Singh, R.P., VanderVoort, R.J., Likins, P.W., "Dynamics of Flexible Bodies in Tree Topology - A Computer-Oriented Approach," *J. Guidance, Control, and Dynamics* 8 (1985) 584-590.
74. Kim, S., and Haug, E.J., "A Recursive Formulation for Flexible Multibody Dynamics, Part I: Open-Loop Systems," *Comp. Meth. Appl. Mech. Engrg.* 71 (1988) 293-314.
75. Bae, D.S., and Haug, E.J., "A Recursive Formulation for Constrained Mechanical System Dynamics: Part II, Closed Loop Systems," *Mech. Structures and Machines* 15 (1987) 481-506.
76. Ider, S.K. and Amirouche, F.M.L., "Nonlinear Modeling of Flexible Multibody Systems Dynamics Subjected to Variable Constraints," *Journal of Applied Mechanics* 56 (1989) 444-450.

77. Shabana, A.A. and Wehage, R.A., "A Coordinate Reduction Technique for Dynamic Analysis of Spatial Substructures with Large Angular Rotations," *J. Struct. Mech.* **11** (1983) 401-431.
78. Walton, W.C. and Steeves, E.C., "A New Matrix Theorem and its Application for Establishing Independent Coordinates for Complex Dynamical Systems with Constraints," NASA TR-R326 (1984).
79. Mani, N.K., Haug, E.J., and Atkinson, K.E., "Application of Singular Value Decomposition for Analysis for Mechanical System Dynamics," *Journal of Mechanisms, Transmissions, and Automation in Design* **82** (1985) 82-87.
80. Singh, R.P., and Likins, P.W., "Singular Value Decomposition for Constrained Dynamical Systems," *J. App. Mech.* **52** (1985) 943-948.
81. Wehage, R.A. and Haug, E.J., "Generalized Coordinate Partitioning for Dimension Reduction in Analysis of Constrained Dynamic Systems," *ASME J. of Mech. Design* **104** (1982) 247-255.
82. Kamman, J.W., and Huston, R.L., "Dynamics of Constrained Multibody Systems," *Journal of Applied Mechanics* **51** (1984) 899-903.
83. Amirouche, F.M.L., Jia, T., and Ider, S.K., "Recursive Householder Transformation for Complex Dynamical Systems with Constraints," *Journal of Applied Mechanics*
84. Ider, S.K. and Amirouche, F.M.L., "Coordinate Reduction in the Dynamics of Constrained Multibody Systems - A New Approach," *Journal of Applied Mechanics* **55** (1988) 899-904.
85. Kim, S.S., and Vanderploeg, M.J., "QR Decomposition for State Space Representation of Constrained Mechanical Dynamic Systems," *J. of Mechanisms, Transmissions, and Automation in Design* **10** (1986) 183-188.
86. Petzold, L., "Differential/Algebraic Equations are not ODEs," *SIAM J. Sci. Stat. Comp.* **3** (1982) 367-384.
87. Gear, C.W., "Simultaneous Numerical Solution of Differential/Algebraic Equations," *IEEE Trans. Circuit Theory* **CT-18** (1971) 89-95.
88. Orlandea, N., Chace, M.A., and Calahan, D.A., "A Sparsity Oriented Approach to the Dynamic Analysis and Design of Mechanical Systems, Parts I and II," *ASME J. Engng. Ind.* **99** (1977) 773-784.
89. Baumgarte, J.W., "Stabilization of Constraints and Integrals of Motion in Dynamical Systems," *Comp. Meth. Appl. Mech. Engr.* **1** (1972) 1-16.

90. Baumgarte, J.W., "A New Method of Stabilization for Holonomic Constraints," *Journal of Applied Mechanics* **50** (1983) 869-870.
91. Park, K.C., and Chiou, J.C., "Evaluation of Constraint Stabilization Procedures for Multibody Dynamical Systems," *Proc. the 28th Structures, Structural Dynamics and Materials Conference*, Part 2A, Monterey, CA, AIAA Paper No. 87-0927 (1987) 769-773.
92. Park, K.C., and Chiou, J.C., "Stabilization of Computational Procedures for Constrained Dynamical Systems," *Journal of Guidance, Control and Dynamics* **11** (1988) 365-370.
93. Park, K.C., and Felippa, C.A., "Partitioned Analysis of Coupled Systems," in *Computational Methods for Transient Analysis*, T. Belytschko and T.J.R. Hughes (eds.), Elsevier Pub Co., (1983) 157-219.
94. Park, K.C., Chiou, J.C., and Downer, J.D., "A Computational Procedure for Large Rotational Motions in Multibody Dynamics," *Proc. the 29th Structures, Structural Dynamics and Materials Conference*, Part 3, Williamsburg, VA, AIAA Paper No. 88-2416 (1988) 1593-1601.
95. Gantmacher, F.R., *The Theory of Matrices*, 2, Chelsea Publication Co., New York, 1959, 190-196.
96. Rubinstein, R. and Atluri, S.N., "Objectivity of Incremental Constitutive Relations over Finite Time Steps in Computational Finite Deformation Analyses," *Comp. Meth. App. Mech. Eng.* **36** (1983) 277-290.
97. Hughes, T.J.R., and Winget, J., "Finite Rotation Effects in Numerical Integration of Rate Constitutive Equations Arising in Large-Deformation Analysis," *Int. J. Num. Meth. Eng.*, **15** (1980) 1862-1867.
98. Lanczos, L., *The Variational Principles of Mechanics*, 4th ed., University of Toronto Press, 1970.
99. Chiou, J.C., "Constraint Treatment Techniques and Parallel Algorithms for Multibody Dynamic Analysis," PhD Thesis, University of Colorado, 1990.
100. Vu-Quoc, L., "Dynamics of Flexible Structures Performing Large Overall Motions: A Geometrically-Nonlinear Approach," PhD Thesis, University of California, Berkeley, 1986.
101. Cloutier, G.J., "Dynamics of Deployment of Extendible Booms from Spinning Space Vehicles," *J. Spacecraft and Rockets* **5** (1968) 547-552.

102. Sellappan, R. and Bainum, P.M., "Dynamics of Spin-Stabilized Spacecraft During Deployment of Telescoping Appendages," *J. Spacecraft and Rockets* 13 (1976) 605-610.
103. Bowers, E.J. and Williams, C.E., "Optimization of RAE Satellite Boom Deployment Timing," *J. Spacecraft and Rockets* 7 (1970) 1057-1062.
104. Cherchas, D.B., "Dynamics of Spin-Stabilized Satellites during Extension of Long Flexible Booms," *J. Spacecraft and Rockets* 8 (1971) 802-804.
105. Lips, K.W., and Modi, V.J., "Transient Attitude Dynamics of Satellites with Deploying Flexible Appendages," *Acta Astronautica* 5 (1978) 797-815.
106. Lips, K.W., and Modi, V.J., "Three-Dimensional Response Characteristics for Spacecraft with Deploying Flexible Appendages," *J. Guidance and Control* 4 (1981) 650-656.
107. Tsuchiya, K., "Dynamics of a Spacecraft During Extension of Flexible Appendages," *J. Guidance, Control, and Dynamics* 6 (1983) 100-103.
108. Jankovic, M.S., "Comments on 'Dynamics of a Spacecraft during Extension of Flexible Appendages'," *J. Guidance, Control, and Dynamics* 7 (1984) 128.
109. Ibrahim, A.E. and Misra, A.K., "Attitude Dynamics of a Satellite During Deployment of Large Plate-Type Structures," *J. Guidance, Control, and Dynamics* 5 (1982) 442-447.
110. Banerjee, A.K., and Kane, T.R., "Extrusion of a Beam from a Rotating Base," *J. Guidance, Control, and Dynamics* 12 (1989) 140-146.
111. Carrier, G.F., "The Spaghetti Problem," *Am. Math. Monthly* 56 (1949) 669-672.
112. Sack, R.A., "Transverse Oscillations in Traveling Strings," *British Journal of Applied Physics* 5 (1954) 224-226.
113. Archibald, F.R. and Emslie, A.G., "The Vibration of a String Having a Uniform Motion Along Its Length," *J. Applied Mechanics* 25 (1958) 347-348.
114. Swope, R.D. and Ames, W.F., "Vibration of a Moving Threadline," *J. Franklin Institute* 275 (1963) 36-55.
115. Mote, C.D., Jr. "On the Nonlinear Oscillation of an Axially Moving String," *J. Appl. Mech.* 33 (1966) 463-464.

116. Ames, W.F., Lee, S.Y., and Zaiser, J.N., "Non-linear Vibration of a Traveling Threadline," *Int. J. Non-Linear Mechanics* **3** (1968) 449-469.
117. Tabarrok, B., Leech, C.M., and Kim, Y.I., "On the Dynamics of an Axially Moving Beam," *J. Franklin Institute* **297** (1974) 201-220.
118. Mansfield, L. and Simmonds, J.G., "The Reverse Spaghetti Problem: Drooping Motion of an Elastica Issuing from a Horizontal Guide," *J. Appl. Mech.* **54** (1987) 147-150.
119. Ockendon, J.R. and Hodgkins, W.R., eds. *Moving Boundary Problems in Heat Flow and Diffusion*, Clarendon Press, Oxford, (1975).
120. Crank, J., *Free and Moving Boundary Problems*, Clarendon Press, Oxford, (1984).
121. Crank, J., *Q.J. Mech. Appl. Math.* **10** (1957) 220-231.
122. Crank, J. and Gupta, R.S., "A Moving Boundary Problem Arising from the Diffusion of Oxygen in Absorbing Tissue," *J. Inst. Maths. Applics.* **10** (1972) 19-33.
123. Crank, J. and Gupta, R.S., "A Method for Solving Moving Boundary Problems in Heat Flow using Cubic Splines or Polynomials," *J. Inst. Maths. Applics.* **10** (1972) 296-304.
124. Douglas, J., and Gallie, T.M., "On the Numerical Integration of a Parabolic Differential Equation Subject to a Moving Boundary Condition," *Duke Math. J.* **22** (1955) 557-571.
125. Gupta, R.S. and Kumar, D., "A Modified Variable Time Step for the Stefan Problem," *Comp. Meth. Appl. Mech. Eng* **23** (1980) 101-109.
126. Marshall, G., "A Front Tracking Method for One-Dimensional Moving Boundary Problems," *SIAM J. Sci. Stat. Comput.* **7** (1986) 252-263.
127. Murray, W.D., and Landis, F., "Numerical and Machine Solutions of Transient Heat-Conduction Problems Involving melting or Freezing: Part I – Method of Analysis and Sample Solutions," *J. of Heat Transfer* **81** (1959) 106-112.
128. Lynch, D.R. and Gray, W.G., "Finite Element Simulation of Flow in Deforming Regions," *J. Comp. Physics* **36** (1980) 135-153.
129. Bonnerot, R. and Jamet, P., "A Second Order Finite Element Method for the One-Dimensional Stefan Problem," *Int. J. Num. Meth. Eng.* **8** (1974) 811-820.

130. Bonnerot, R., Jamet, P., "Numerical Computation of the Free Boundary for the Two-Dimensional Stefan Problem by Space-Time Finite Elements," *J. Comput. Phys.* **25** (1977) 163-181.
131. Jamet, P., and Bonnerot, R., "Numerical Solution of the Euler Equations of Compressible Flow by a Finite Element Method Which Follows the Free Boundary and the Interfaces," *J. Comput. Phys.* **18** (1975) 21-25.
132. Nguyen, H. and Reynen, J., "A Space-Time Least-Square Finite Element Scheme for Advection-Diffusion Equations," *Comp. Meth. Appl. Mech. Eng.* **42** (1984) 331-342.
133. Oden, J.T., "A General Theory of Finite Elements II. Applications," *Int J. Num. Meth. Eng.* **1** (1969) 247-259.
134. Argyris, J.H., and Scharph, D.W., "Finite Elements in Time and Space," *Nuclear Engineering and Design* **10** (1969) 456-464.
135. Fried, I., "Finite-Element Analysis of Time-Dependent Phenomena," *AIAA J.* **7** (1969) 1170-1173.
136. Jamet, P., "Galerkin-Type Approximations which are Discontinuous in Time for Parabolic Equations in a Variable Domain," *SIAM J. Numer. Anal.* **15** (1978) 912-928.
137. Hughes, T.J.R., and Hulbert, G.M., "Space-time Finite Element Methods for Elastodynamics: Formulations and Error Estimates," *Comp. Meth. App. Mech. Eng.* **66** (1988) 339-363.
138. Bar-Yoseph, P., "Space-Time Discontinuous Finite Element Approximations for Multi-Dimensional Nonlinear Hyperbolic Systems," *Computational Mechanics* **5** (1989) 145-160.
139. Simkins, T.E., "Finite Elements for Initial Value Problems in Dynamics," *AIAA J.* **19** (1981) 1357-1362.
140. Borri, M., Lanz, M., and Mantagazza, P., "Comment on 'Time Finite Element Discretization of Hamilton's Law of Varying Action'," *AIAA J.* **23** (1985) 1457-1458.
141. Borri, M., Ghiringhelli, G.L., Lanz, M., Mantegazza, P., and Merlini, T., "Dynamic Response of Mechanical Systems by a Weak Hamiltonian Formulation," *Computers & Structures* **20** (1985) 495-508.
142. Baruch, J., and Riff, R., "Hamilton's Principle, Hamilton's Law - 6th Correct Formulations," *AIAA J.* **23** (1982) 687-692.

143. Park, K.C., and Flaggs, D.L., "A Fourier Analysis of Spurious Mechanisms and Locking in the Finite Element Method," *Comp. Meth. Appl. Mech. Eng.* **46** (1984) 68-81.
144. Flaggs, D.L., "Symbolic Analysis of the Finite Element Method in Structural Mechanics," PhD Thesis, Stanford University, (1988).

APPENDIX A

It is desired to obtain an expression for the variational operator

$$\delta F_i^I = \int_{t_1}^{t_2} \int_{v(t)} \rho \frac{D \mathbf{r}}{Dt} \cdot \frac{D \delta \mathbf{r}}{Dt} dv dt \quad (\text{A.1})$$

corresponding to the inertial operator of the Hamiltonian formulation. The velocity of a material particle was given in (5.2.15) as

$$\begin{aligned} \frac{D \mathbf{r}}{Dt} = & \mathbf{e}^T \left[(\bar{V} + \dot{u}) + V^* \frac{\partial^e u}{\partial \xi} \right] + \\ & \mathbf{b}^T \left[\tilde{\omega} + V^* \tilde{\kappa} \right] \ell \end{aligned} \quad (5.2.15)$$

where V^* is the neutral-axis or ξ component of the instantaneous velocity of a spatial point as defined in (5.2.8). The virtual displacements $\delta \mathbf{r}$ are defined as a set of infinitesimally small displacements of purely kinematic nature that are consistent with the system constraints at a given instant of time. Therefore, for the deployment problem $\delta \mathbf{r}$ is defined for a specific instant of the moving reference where \bar{X} is held fixed and the definition (2.2.10c)

$$\delta \mathbf{r} = \delta u^T \mathbf{e} + \ell^T \delta \tilde{\alpha}^T \mathbf{b}$$

remains valid. The following expression is thus obtained

$$\begin{aligned} \frac{D \delta \mathbf{r}}{Dt} = & \mathbf{e}^T \left[\delta u + V^* \frac{\partial^e \delta u}{\partial \xi} \right] + \\ & \mathbf{b}^T \left[\frac{\partial \delta \tilde{\alpha}}{\partial t} + \tilde{\omega} \delta \tilde{\alpha} + V^* \frac{\partial \delta \tilde{\alpha}}{\partial \xi} + V^* \tilde{\kappa} \delta \tilde{\alpha} \right] \ell \end{aligned}$$

by applying the material time derivative operator (5.2.7) including the rotating coordinate transformations (5.2.13 - 5.2.14) to the virtual displacement

definition. With this information, (A.1) can now be evaluated as

$$\begin{aligned}
\delta F_i^I = & \int_{t_1}^{t_2} \int_{v(t)} \\
& \left\{ (\bar{U} + \dot{u}) + V^* \frac{\partial u}{\partial \xi} \right\}^T \left\{ \frac{\partial \delta u}{\partial t} + V^* \frac{\partial \delta u}{\partial \xi} \right\} + \\
& \left\{ \omega^T + V^* \kappa^T \right\} \tilde{\ell} \tilde{\ell}^T \left\{ \delta \omega + V^* \delta \kappa \right\} + \\
& \left\{ (\bar{U} + \dot{u}) + V^* \frac{\partial u}{\partial \xi} \right\}^T \mathbf{R}^T \left\{ \delta \omega + V^* \delta \kappa \right\} \ell + \\
& \ell^T \left\{ \omega^T + V^* \kappa^T \right\} \mathbf{R} \left\{ \frac{\partial \delta u}{\partial t} + V^* \frac{\partial \delta u}{\partial \xi} \right\} dv dt
\end{aligned}$$

where the well known expressions

$$\begin{aligned}
\delta \omega &= \frac{\partial \delta \alpha}{\partial t} + \tilde{\omega} \delta \alpha \\
\delta \kappa &= \frac{\partial \delta \alpha}{\partial \xi} + \tilde{\kappa} \delta \alpha
\end{aligned}$$

have been introduced. The above is integrated throughout constant cross-sectional area coordinates represented by ℓ . Typically, the last two terms of the above expression which are linear in ℓ vanish as an integration is performed over symmetrical cross-sections. In this case however, V^* is also a function of ℓ

$$V^* = \dot{u}^* + \dot{\Theta}^{*T} \ell$$

as derived in (5.2.12), and additional terms are generated. The final expression is given as

$$\begin{aligned}
\delta F_i^I = & \int_{t_1}^{t_2} \int_{\xi} \\
& \left\{ (\bar{V} + \dot{u}) + \dot{u}^* \frac{\partial u}{\partial \xi} \right\}^T m \left\{ \frac{\partial \delta u}{\partial t} + \dot{u}^* \frac{\partial \delta u}{\partial \xi} \right\} + \\
& \left\{ \omega^T + \dot{u}^* \kappa^T \right\} J \left\{ \delta \omega + \dot{u}^* \delta \kappa \right\} + \\
& (\dot{\Theta}_2^{*2} J_2 + \dot{\Theta}_3^{*2} J_3) \frac{\partial u^T}{\partial \xi} \frac{\partial \delta u}{\partial \xi} +
\end{aligned}$$

$$\begin{aligned}
& \frac{\partial \delta u^T}{\partial t} \mathbf{R}^T \tilde{\kappa} \ell^* + \frac{\partial \delta u^T}{\partial \xi} \mathbf{R}^T \tilde{\omega} \ell^* + \\
& \frac{\partial \delta u^T}{\partial \xi} \mathbf{R}^T \tilde{\kappa} 2 \dot{u}^* \ell^* + \\
& (\bar{V} + \dot{u})^T \mathbf{R}^T \left(\frac{\partial \delta \tilde{\alpha}}{\partial \xi} + \tilde{\kappa} \delta \tilde{\alpha} \right) \ell^* + \\
& \frac{\partial u^T}{\partial \xi} \mathbf{R}^T \left(\frac{\partial \delta \tilde{\alpha}}{\partial t} + \tilde{\omega} \delta \tilde{\alpha} \right) \ell^* + \\
& \frac{\partial u^T}{\partial \xi} \mathbf{R}^T \left(\frac{\partial \delta \tilde{\alpha}}{\partial \xi} + \tilde{\kappa} \delta \tilde{\alpha} \right) 2 \dot{u}^* \ell^* d\xi dt
\end{aligned}$$

where

$$m = \int_A \rho dA, \quad \mathbf{J} = \text{Diag}\{J_1, J_2, J_3\} = \int_A \rho \tilde{\ell} \tilde{\ell}^T dA$$

represents the beam mass per unit length and cross-sectional inertia properties and

$$\ell^* = \{0, \dot{\Theta}_2^* J_2, \dot{\Theta}_3^* J_3\}^T.$$

In the same manner, the boundary term is evaluated as

$$\begin{aligned}
\delta F_b^I = & \left[\int_{\xi} \right. \\
& \left\{ (\bar{V} + \dot{u}^*) + \dot{u}^* \frac{\partial u}{\partial \xi} \right\}^T m \delta u + \left\{ \omega^T + \dot{u}^* \kappa^T \right\} J \delta \alpha + \\
& \left. \frac{\partial u^T}{\partial \xi} \mathbf{R}^T \delta \tilde{\alpha} \ell^* + \ell^{*T} \tilde{\kappa}^T \mathbf{R} \delta u d\xi \right] \Big|_{t_1}^{t_2}.
\end{aligned}$$

It is seen that the convective velocity V^* gives rise to a slight coupling between the translational and rotational degrees of freedom. For the present analysis, we will neglect the effect of $\dot{\Theta}^{*T} \ell$ within the convective velocity V^* .

APPENDIX B

The space-time discretization of the inertia operator within Hamilton's Law was given in (5.4.4) as

$$\delta F_i^I = \{ \delta u^{t_1} \delta u^{t_2} \} \begin{bmatrix} A_{11} & A_{12} \\ A_{21} & A_{22} \end{bmatrix} \begin{Bmatrix} u^{t_1} \\ u^{t_2} \end{Bmatrix}$$

for the interior term and

$$\delta F_b^I = \{ \delta u^{t_1} \delta u^{t_2} \} \left\{ \begin{bmatrix} B_1 & 0 \\ 0 & B_2 \end{bmatrix} \begin{Bmatrix} \dot{u}^{t_1} \\ \dot{u}^{t_2} \end{Bmatrix} + \begin{bmatrix} C_1 & 0 \\ 0 & C_2 \end{bmatrix} \begin{Bmatrix} u^{t_1} \\ u^{t_2} \end{Bmatrix} \right\}$$

was given in (5.4.7) for the boundary term. In the above terms, the A , B , and C matrices have been derived using both full and reduced integration techniques in analyzing the integrations of the changing spatial domain and the arbitrary time interval inherent in the formulation. The results are given below in terms of individual spatial finite element kernels to be assembled across the spatial domain via the manner standard of finite elements.

The A matrices are given explicitly as

$$\begin{aligned} A_{11} &= \frac{1}{h} M_1 - M_2^S + h_1^* M_3 \\ A_{12} &= -\frac{1}{h} M_1 + M_2^A + h_2^* M_3 \\ A_{21} &= -\frac{1}{h} M_1 + M_2^{A^T} + h_2^* M_3 \\ A_{22} &= \frac{1}{h} M_1 + M_2^S + h_1^* M_3 . \end{aligned}$$

The spatial element kernels as derived from reduced integration techniques are given as

$$\begin{aligned} M_1 &= \frac{\rho A \ell}{4} \begin{bmatrix} 1 & 1 \\ 1 & 1 \end{bmatrix}, \quad M_2^S = \rho A \frac{\dot{u}_a^*}{2} \begin{bmatrix} -1 & 0 \\ 0 & 1 \end{bmatrix} \\ M_2^A &= \rho A \frac{\dot{u}_a^*}{2} \begin{bmatrix} 0 & -1 \\ 1 & 0 \end{bmatrix}, \quad M_3 = \frac{\rho A}{\ell} \dot{u}_a^{*2} \begin{bmatrix} 1 & -1 \\ -1 & 1 \end{bmatrix} \end{aligned}$$

where

$$\dot{u}_a^* = \frac{(\dot{u}_1^* + \dot{u}_2^*)}{2}$$

is the average nodal velocity \dot{u}^* for a given element. The same kernels integrated exactly are given as

$$\begin{aligned} M_1 &= \frac{\rho A \ell}{6} \begin{bmatrix} 2 & 1 \\ 1 & 2 \end{bmatrix} \\ M_2^S &= \frac{\rho A}{4} \begin{bmatrix} -\frac{4}{3}\dot{u}_1^* - \frac{2}{3}\dot{u}_2^* & \frac{\dot{u}_1^*}{3} - \frac{\dot{u}_2^*}{3} \\ \frac{\dot{u}_1^*}{3} - \frac{\dot{u}_2^*}{3} & \frac{2}{3}\dot{u}_1^* + \frac{4}{3}\dot{u}_2^* \end{bmatrix} \\ M_2^A &= \rho A \frac{\dot{u}_a^*}{2} \begin{bmatrix} 0 & -1 \\ 1 & 0 \end{bmatrix} \\ M_3 &= \frac{\rho A}{\ell} \dot{u}_a^{*2} \begin{bmatrix} 1 & -1 \\ -1 & 1 \end{bmatrix} \end{aligned}$$

Finally, the factors

$$\begin{aligned} h_1^* &= \frac{1}{3}, \quad \frac{1}{4} \\ h_2^* &= \frac{1}{6}, \quad \frac{1}{4} \end{aligned}$$

correspond to the exact vs. reduced integration analysis respectively. With this information, the difference equations (5.4.14) and (5.4.15) to be analyzed with the discrete Fourier procedure are easily derived.

Likewise, the spatial kernels of the boundary term are defined as

$$\begin{aligned} B_1 &= B(-\ell^{t_1}), \quad C_1 = C(\dot{u}^*), \quad C_2 = C(T_{1j} \bar{V}_j) \\ B_2 &= \begin{bmatrix} B(\ell^{t_2}) + \Delta u_1^{t_2} T_{11} D & \Delta u_1^{t_2} T_{11} D & 0 \\ \Delta u_2^{t_2} T_{11} D & B(\ell^{t_2}) + \Delta u_2^{t_2} T_{12} D & 0 \\ \Delta \theta^{t_2} T_{11} D & \Delta \theta^{t_2} T_{12} D & B(\ell^{t_2}) \end{bmatrix} \end{aligned}$$

where

$$\Delta u_i = \frac{u_{i_2} - u_{i_1}}{\ell}$$

and the matrices are defined as

$$\begin{aligned} B &= \frac{\rho A \ell}{4} \begin{bmatrix} 1 & 1 \\ 1 & 1 \end{bmatrix} \\ C &= \rho A \frac{\dot{u}_a^*}{2} \begin{bmatrix} -1 & 1 \\ -1 & 1 \end{bmatrix} \\ D &= \frac{1}{4} \begin{bmatrix} 1 & 1 \\ 1 & 1 \end{bmatrix} \end{aligned}$$

for the reduced integration evaluation and

$$\begin{aligned} B &= \frac{\rho A \ell}{6} \begin{bmatrix} 2 & 1 \\ 1 & 2 \end{bmatrix} \\ C &= \frac{\rho A}{6} \begin{bmatrix} -2\dot{u}_1^* - u_2^* & 2\dot{u}_1^* + u_2^* \\ -\dot{u}_1^* - 2u_2^* & \dot{u}_1^* + 2u_2^* \end{bmatrix} \\ D &= \frac{1}{6} \begin{bmatrix} 2 & 1 \\ 1 & 2 \end{bmatrix} \end{aligned}$$

for the exact integration evaluation.

